THE UNIVERSITY OF CHICAGO

DIETARY GLUTEN PERMANENTLY RESHAPES THE TISSUE-RESIDENT $\gamma\delta$ INTRAEPITHELIAL T CELL COMPARTMENT IN CELIAC DISEASE

A DISSERTATION SUBMITTED TO
THE FACULTY OF THE DIVISION OF THE BIOLOGICAL SCIENCES
AND THE PRITZKER SCHOOL OF MEDICINE
IN CANDIDACY FOR THE DEGREE OF
DOCTOR OF PHILOSOPHY

COMMITTEE ON IMMUNOLOGY

BY
TOUFIC MAYASSI

CHICAGO, ILLINOIS
DECEMBER 2018

CONTENTS

LIST OF FIGURES

LIST OF TABLES

ACKNOWLEDGMENTS

I am very grateful to have had the opportunity to obtain my PhD from the University of Chicago and more importantly from the lab of Bana Jabri. The past six years have been the some of the most challenging of my life but easily the most rewarding. I have grown not only scientifically but also emotionally and as a person.

I would first like to thank the patients and their families for being so generous to allow us to obtain the samples that were needed for our study. We were able to accomplish this by working with a long list of physicians who also were generous with their time such as Stefano Gaundalini, Sonia Kupfer, Carol Semrad, Hilary Jericho, Ranjana Gokhale, Robert Kavitt, Edwin McDonald, Atsushi Sakuraba, Joel Pekow, Neil Sangupta, and Sushila Dalal. In the same vein, I would like to thank the long list of people who have helped consent patients over the years including Kathryn Lesko, Ian Lawrence, Mathew Dimaano, Nicholas DiNardi, Diane McKiernan, Sarbani Adhikari, Fengshi Dong, and Lisa Martin. The work put forward in my thesis would not have been possible without contributions from all the people listed above.

During my time in Bana Jabri's lab I have had the chance to work with a long list of great collaborators both inside and outside of our lab. Within the lab, I would like to thank Cezary Ciszewski, Jagoda Rokicka, Dustin Shaw, Marlies Meisel, Reinhard Hinterleitner, Romain Bouziat, Vu Dinh, Sangman Kim, Zachary Earley, Mathew Zurenski, Jordan Ernest, and Jill Voss. Outside of the lab I would like to thank David Price, Kristin Ladell, James McLaren, Aaron Dinner, Herman Gudjonson, Jamie Rossjohn, Hugh Reid, Mai Tran, Luis Barreiro, Jean-Christophe Grenier, Frits Koning, Vincent Van unen, Cisca Wijmenga, Yang Li, Raul Aguirre-Gamboa, Maria Zorro, Erin Adams, and Adrienne Luoma. Each collaboration was unique and presented its own challenge thus allowing me to grow.

The thesis committee is a critical part of any PhD and my committee played a critical role in challenging me to be at my best over the years. I would like to thank my chair Fotini Gounari and the other members of my committee including Albert Bendelac, Pete Savage, and Yoav Gilad. Each brought their own set of expertise to the table and they were not shy to criticize the project which helped prepare me for any challenges I faced while giving talks at conferences or in responding to reviewers during the peer review process.

Next, I want to thank my classmates Isabel Ishizuka, Kevin Lei, Douglas Kline, and Jeffery Bunker. We challenged each other everyday in class and stood by each others sides during the highs and lows. I will remain friends with them for life and hope they can achieve all their dreams in their future endeavors.

During the process of writing my thesis I have engaged in a back and forth with two individuals that helped me navigate the forest that is the literature on lymphocyte trafficking as well as the less trivial aspects to explain within my data set. These two individuals are my friend and fellow classmate Steven Erickson and my mentor's mentor Delphine Guy-Grand. I am grateful to both for the time they invested in listening to my ideas and in particular to Delphine for answering my questions and collecting literature to help guide me towards the relevant papers.

I am also grateful to the various members of the lab that I have grown close to over the past 6 years. This includes and is not limited to Sangman Kim, Romain Bouziat, Reinhard Hinterleitner, Marlies Meisel, and Cezary Ciszewski. They made coming to lab everyday fun and intersting and have helped me grow as a person and I look forward to our continued friendship.

My family helped prepare me for graduate school and I am eternally indebted to my parents Mohamad Mayassi and Mirna Mayassi for the sacrifices they made to help me achieve my goals.

It is comforting when you know that no matter how bad things get you still have a family that is waiting to pick you up. To my brother Adham Mayassi and my sister Fatin Mayassi, I hope that I have been the role model you needed as your older brother and I hope you get to live out all your dreams. I love you all and here is to our health and togetherness as a family.

Last but not least, I would like to thank my mentor Bana Jabri. A PhD is about the journey between a mentor and his or her student. Bana has been the complete mentor. She has helped me grow as a scientist and as a human. She gave me confidence in my own ideas very early on and never let me hesitate to question or challenge hers. She was fully committed to the project and there was never a time when she was unavailable to meet. I know this is only the beginning of our journey and I look forward to the next chapter.

ABSTRACT

Tissue-resident lymphocytes play a key role in immune surveillance, but it remains unclear how these inherently stable cell populations respond to chronic inflammation. In the setting of celiac disease (CeD), where exposure to dietary antigen can be controlled, gluten-induced inflammation triggered a profound depletion of naturally-occurring Vγ4$^+$/Vδ1$^+$ intraepithelial lymphocytes (IELs) with innate cytolytic properties and specificity for the butyrophilin-like (BTNL) molecules BTNL3/BTNL8. Creation of a new niche with reduced expression of BTNL8 and loss of Vγ4$^+$/Vδ1$^+$ IELs was accompanied by the expansion of gluten-sensitive, interferon-γ-producing Vδ1$^+$ IELs bearing T cell receptors (TCRs) with a shared non-germline-encoded motif that failed to recognize BTNL3/BTNL8. Exclusion of dietary gluten restored BTNL8 expression but failed to reconstitute the Vγ4$^+$/Vδ1$^+$ gut signature among TCR$\gamma\delta^+$ IELs. Collectively, these data demonstrate that chronic inflammation permanently reconfigures the tissue-resident TCR$\gamma\delta^+$ IEL compartment, thus the paradigm of tissue-resident lymphocyte stability needs revisiting.

CHAPTER 1

INTRODUCTION

1.1 Tissue-resident lymphocytes

The study of tissue-resident lymphocytes has garnered heightened interest in recent years as it has become clear that understanding immune responses at barrier surfaces and in tissues is critical to better defining the mechanisms by which host immunity is maintained during homeostatic and non-homeostatic states. This has of course been heavily influenced by the microbiota boom which has further highlighted the need to better understand tissue-resident lymphocyte biology as these cells have been increasingly shown to play an integral part in the crosstalk between the host and associated microbes[1].

In order to better understand the challenges that face the tissue-resident field one must first become acquainted with how tissue-residency is defined, grasp the complexity of the heterogeneity of cell types that can establish tissue-residency, and finally integrate what has been shown in support of the long-lived stable nature of tissue-resident lymphocytes.

1.1.1 Characteristics of a tissue-resident lymphocyte

Lymphocytes can be broadly separated into two pools with one encompassing cells found circulating in lymph, blood, and secondary lymphoid organs and the second encompassing cells found in non-lymphoid tissues where tissue-resident lymphocytes are maintained. At its simplest, a tissue-resident lymphocyte is a cell that does not emigrate from the tissue upon entry from the circulation, a process that involves the successful integration of tissue specific cues such as the up-regulation of the integrin CD103 in response to TGF-β[2], which allows for adherence to epithelia via interaction with E-cadherin[3], as well as the modulation of S1PR1 expression either via transcriptional regulation[4] or indirectly via the up-regulation of

the lymphocyte activation marker CD69[2,5] which antagonizes S1PR1[6], therefore; inhibiting egress into either blood or lymph. The lack of egress of tissue-resident lymphocytes has been demonstrated with parabiosis experiments in mice showing parabiotic pairs very infrequently exchange lymphocytes at tissue sites whereas circulating lymphocytes are readily exchanged[7–10]. Consequently, tissue-resident lymphocytes are maintained by self-renewal in tissues as opposed to being replenished from the periphery[8,10,11].

Cells circulating in lymph, blood, and secondary lymphoid organs serve as a reservoir from which immune responses can be generated in response to future insults at distal sites whereas cells already situated in the tissue are capable of exerting their effector functions locally. The capacity to perform effector functions locally[10–15] is the most relevant feature of the tissue-resident lymphocyte compartment as it arms the host with body wide immune capacity at barrier sites such as the skin and intestine.

1.1.2 Tissue-resident lymphocyte subsets

The tissue-resident lymphocyte compartment is complex and composed of unique cell types whose distribution varies by tissue[16] as well as by species[17,18]. Generally speaking, tissue-resident lymphocytes include T cell receptor (TCR)$\gamma\delta^+$ T cells, TCR$\alpha\beta^+$ CD4$^+$ T cells, TCR$\alpha\beta^+$ CD8$^+$ T cells, and innate lymphocytes (ILCs). These cell types can be further subdivided into three categories: (i) innate lymphocytes which encompass NK cells, lymphoid tissue inducer cells (LTi), and the helper ILC subsets ILC1, ILC2, ILC3 (ii) unconventional/innate-like T cells which encompass NKT cells, mucosal associated invariant T (MAIT) cells, TCR$\gamma\delta^+$ T cells, and TCR$\alpha\beta^+$ CD8$\alpha\alpha^+$ T cells (iii) tissue-resident memory (T_{RM}) T cells which encompass classical TCR$\alpha\beta^+$ CD4$^+$ and TCR$\alpha\beta^+$ CD8$\alpha\beta^+$ T cells. These cell types all have unique developmental requirements and their tissue-residence is governed by different signals. For instance, the establishment of tissue-resident TCR$\gamma\delta^+$ T

cells in mice depends on the expression of butyrophilin-like (Btnl) molecules such as Skint 1 in the skin[19] and Btnl1 and Btnl6 in the small intestine[20] while TCR$\alpha\beta^+$ CD8$\alpha\alpha^+$ T cells are thought to receive their instructions in the thymus en route to establishing residence in the small intestinal epithelium[21]. These two cell types are considered innate or naturally occurring tissue-resident lymphocytes in that they are not dependent on exposure to external stimuli such as the microbiota or dietary antigen to develop residence[20,22]. Alternatively, T_{RM} T cells are considered adaptive or induced tissue-resident memory in that they are generated in response to exogenous triggers such as the microbiota or specific infections[14,23] and therefore undergo classical priming and activation in secondary lymphoid organs prior to trafficking into tissues whereby their tissue-residence is established by an integration of a complex array of local signals which are still being fully elucidated. It is then critical to distinguish between naturally occurring and induced tissue-resident cells as the rules that govern the nature of tissue-residence for the two different classes of cells are different and therefore their maintenance and future participation in immune-responses will be different.

Additionally, the ligands to which different classes of tissue-resident lymphocytes respond to are unique and sample different elements of the tissue environment. For instance, NK cells via their diverse NK receptors can respond to a slew of self-ligands induced in response to tissue stress[24,25], TCR$\gamma\delta^+$ T cells respond to Btnl molecules which are self-ligands expressed in the mouse small intestine[20], NKT cells respond to CD1 molecules presenting lipid moieties[26,27], MAIT cells respond to MR1 molecules presenting bacterial derived vitamin metabolites[28,29], and T_{RM} T cells can respond to major histocompatibility complex (MHC) molecules presenting foreign peptides[23].

Interestingly, in light of the diverse routes to tissue-residence, there is a significant level of redundancy in the functional output of tissue-resident lymphocytes. For instance, TCR$\alpha\beta^+$ T cells, TCR$\gamma\delta^+$ T cells, MAIT cells, and ILC1s all have the capacity to produce IFN-γ[15].

This redundancy is most likely in place to ensure robust immune responses at barrier sites, however; whether a hierarchy exists between various cell subsets and the relative contributions of each subset to a given immune response are still questions that need to be answered. A better understanding of the role of various tissue-resident lymphocytes in tissue-immunity will depend on a clear understanding of the nature of the triggering signal and consequently the subset that is best suited to respond to it.

1.1.3 Stability and longevity of tissue-resident lymphocytes

In addition to lacking the capacity for re-circulation, tissue-resident lymphocytes are thought to be stable, long-lived populations[1,15,30]. This model of stability would have to accommodate the persistence of tissue-resident lymphocytes in the face of constant insults at barrier surfaces such as the gut and skin capable of generating new T_{RM} T cells. Furthermore, pre-existing T_{RM} T cells would have to resist displacement during secondary responses by newly generated T_{RM} T cells. These assumptions were recently tested in two studies focusing on inducible T_{RM} T cells generated in response to virus infection[10,11]. The combined results from these two studies demonstrated that T_{RM} T cells generated against a given antigen do not displace T_{RM} T cells previously generated against a non-related antigen[11] and recall responses are dominated by pre-existing T_{RM} T cells generated during the initial insult[10,11]. As for the majority of studies investigating T_{RM} T cells, the two studies described above focused on acute infection/inflammation models so it remains to be determined how stable T_{RM} T cells as well as naturally occurring tissue-resident lymphocytes are in the face of chronic inflammation such as can be the case in autoimmune disease in humans.

In the absence of antigen specific models it is more difficult to intimately study the stability and longevity of specific members of the naturally occurring tissue-resident compartment. In a study focused on studying the persistence of skin resident T_{RM} T cells generated in

response to cutaneous herpes simplex virus (HSV) infection, it was noted that HSV specific T_{RM} T cells displaced naturally occurring dendritic epidermal TCR$\gamma\delta^+$ T cells (DETCs) exclusively at the site of infection[12]. This result suggests infectious insults may alter the local composition of tissue-resident lymphocytes with long-term implications for the host.

1.2 Intraepithelial lymphocytes

1.2.1 Categorizing the tissue-resident IEL compartment

T cells within the IEL compartment are distinct from peripheral lymphocytes 17,18 and have been categorized primarily based on ontogeny into the naturally occurring (Type B) IELs and the adaptively induced (Type A) IELs[31,32]. Naturally occurring IEL are composed of TCR$\gamma\delta^+$ T cells as well as the unique mouse subset of TCR$\alpha\beta^+$CD8$\alpha\alpha^+$ T cells. Naturally occurring IELs are tissue resident lymphocytes that seed the tissue early in life and independently of microbial colonization of the gut[20,22,33,34] whereas adaptively induced IEL are classical TCR$\alpha\beta^+$CD8$\alpha\beta^+$ and TCR$\alpha\beta^+$CD4$^+$ T cells that are generated in response to local tissue insults[35] and gain residence within the IEL compartment not unlike tissue resident memory cells[15]. To that end both naturally occurring and adaptively induced IELs were shown to be stable tissue resident populations with little to no capacity to recirculate in the periphery in parabiosis experiments[7]. Finally, both human and mouse IELs express the tissue resident hallmark marker CD103[36,37] and have a cytolytic effector profile characterized by expression of the lymphocyte activation marker CD69 as well as granzyme and perforin cytolytic granules[38–40].

1.2.2 Regional composition of the intraepithelial lymphocyte compartment in human vs. mouse

The intestine is classically separated into two anatomically distinct regions starting proximally at the small intestine defined by the duodenum, jejunum, and ileum, followed by the large intestine defined by the colon[16]. IELs can be found along the full length of the intestinal tract with the density of IEL relative to intestinal epithelial cells (IEC) being higher in the small intestine relative to the colon[41,42]. These IELs are composed of T cells and innate lymphoid cells (ILCs). In an attempt to provide a resource, we present primary data side by side on the intraepithelial T cell compartments of both human and murine small intestine (duodenum) and large intestine (colon) (Fig. 1.2.2).

The intraepithelial T cell compartment in human is composed of TCR$\gamma\delta^+$, TCR$\alpha\beta^+$CD8$\alpha\beta^+$, and TCR$\alpha\beta^+$CD4$^+$ (Fig. 1.2.2). In addition to the 3 subsets above, the murine intraepithelial T cell compartment contains the naturally occurring TCR$\alpha\beta^+$CD8$\alpha\alpha^+$ IEL (Fig. 1.2.2). The proportions of these subsets and how they vary across the intestine between human and mouse is summarized in Figure 1.2.2. The human small and large intestine is dominated by TCR$\alpha\beta^+$ IELs. In contrast, the mouse small intestine has a more or less equal distribution of TCR$\gamma\delta^+$ and TCR$\alpha\beta^+$ IELs with a shift toward TCR$\alpha\beta^+$ IELs in the colon[41,42]. Interestingly, TCR$\gamma\delta^+$ IELs increase proportionally from the small to large intestine in human while decreasing proportionally from small to large intestine in mouse (Fig. 1.2.2). Amongst TCR$\alpha\beta^+$ IELs, TCR$\alpha\beta^+$CD4$^+$ IELs are a minor population in the small intestine but increase proportionally in the large intestine in both mouse[41–43] and human[44] (Fig. 1.2.2). Of note, the population of TCR$\alpha\beta^+$CD4$^+$ IELs in the human colon is primarily CD103$^-$, a phenotype which has been described for IELs exposed to chronic antigen challenge[45], however; we cannot rule out contaminating CD103$^-$ cells from the lamina propria (Lp). A key difference is the sizeable proportion of the TCR$\alpha\beta^+$CD8$\alpha\alpha^+$ IELs in mouse, a

population which is seemingly absent in human (Fig. 1.2.2). The existence of this population in human has been speculated on 29 based on misinterpretation of data that failed to exclude TCR$\gamma\delta^+$ IELs, which can express CD8$\alpha\alpha$, from the analysis[46,47]. Additionally, a recent report showing a TCR$\alpha\beta^+$CD8α^+/CD8β-dim population in human intestine[48] attempted to extend this observation to suggest the existence of TCR$\alpha\beta^+$CD8$\alpha\alpha^+$ IELs in human, however; the data suggests the same cell may express both CD8$\alpha\alpha^+$ and CD8$\alpha\beta^+$ dimers, a cell type that would not phenocopy the bonafide TCR$\alpha\beta^+$CD8$\alpha\alpha^+$ IELs found in mouse. Finally, the TCR$\alpha\beta^+$ CD8/CD4 double negative population which is enriched in the mouse colon[41,43] and considered to be similar in nature to TCR$\alpha\beta^+$CD8$\alpha\alpha^+$ IELs[21,49] as well as the TCR$\alpha\beta^+$CD4$^+$CD8α^+ IELs[50] whose inflammatory potential is modulated in the intestine via the upregulation of Runx3 and downregulation of ThPOK[51,52] are both still poorly characterized in human. Single cell *ex vivo* transcriptional profiling of these subsets will help establish the extent to which these populations exist in human and whether or not they play a role in health or disease.

The physiological significance of the difference in distribution of various T cell subsets across the gut is still to be determined. Nonetheless, a complex array of local signals may play a role in shaping each compartment locally as can be appreciated from a study comparing the small and large intestine IEL compartments in neonatal mice vs. adult mice[34]. It is well accepted that the microbial burden in the colon is higher than that in the small intestine, however; the mucus layer produced in the colon is thicker and keeps the microbiota farther from the hosts epithelial cells than in the small intestine[53,54]. Furthermore, the impact of the microbiota on adaptively induced IELs is well established as these cells decrease drastically in absolute numbers in germ-free mice[20,22,33]. Additionally, food is primarily absorbed in the small intestine therefore providing a unique pool of antigens that may impact IELs in the small intestine that are absent in the large intestine.

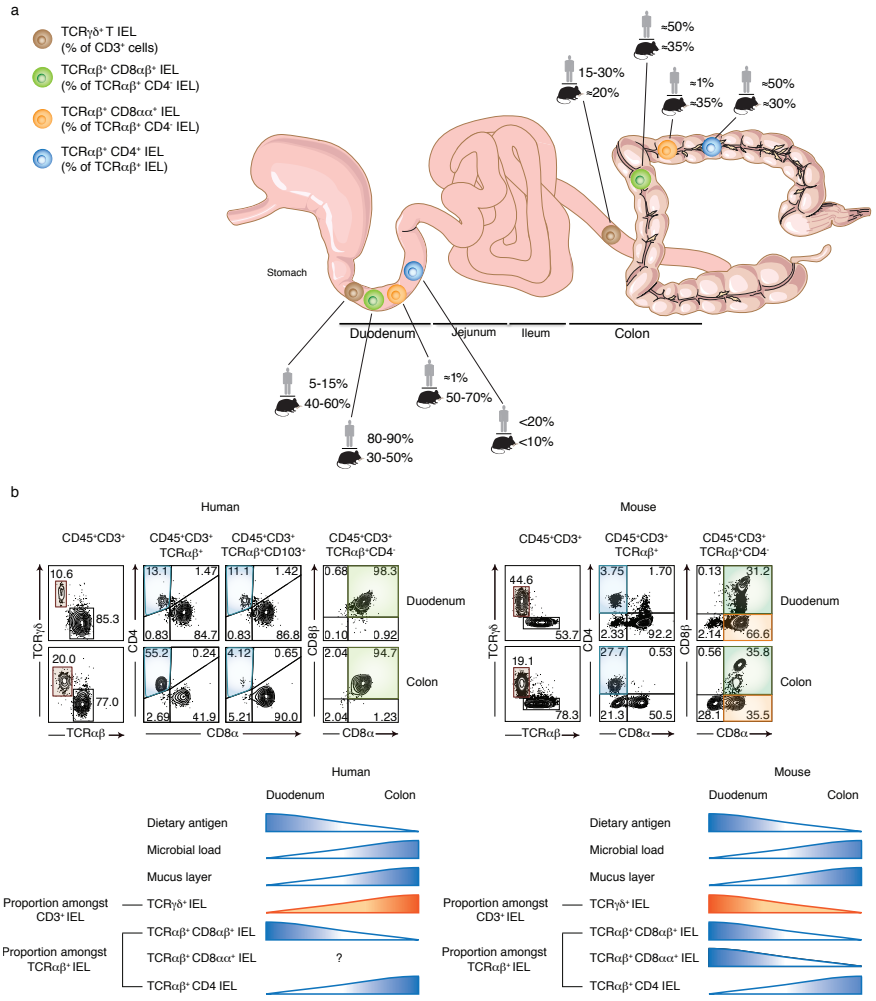

Figure 1.1: Regional composition of the intraepithelial lymphocyte compartment
A summary of the regional distribution of intraepithelial lymphocyte (IEL) subsets in human and mouse. We compare here the proportion of T cell subsets between the small intestine (duodenum) and large intestine (colon; right colon in human) while highlighting key differences between human and mouse. Human data is from healthy adults and mouse data is from 8-week old C57BL/6 specific pathogen free (SPF) mice from our colony at the University of Chicago. (**a**) The proportion of TCR$\gamma\delta^+$ IEL amongst CD3$^+$ IEL is summarized for human and mouse in duodenum and colon. The proportion of TCR$\alpha\beta^+$CD8$\alpha\beta^+$ and TCR$\alpha\beta^+$CD8$\alpha\alpha^+$ amongst TCR$\alpha\beta^+$CD4$^-$ IEL and TCR$\alpha\beta^+$CD4$^+$ IEL amongst TCR$\alpha\beta^+$ IEL is summarized for human and mouse in duodenum and colon. Ranges are based on published data in addition to our own unpublished data. (**b**) Freshly isolated IEL[55] were stained with fluorescently labeled antibodies against CD45, CD3, TCR$\gamma\delta$, TCR$\alpha\beta$, CD4, CD8α, CD8β, and CD103 (human only). Top: representative flow cytometry contour plots with outliers and large dots are shown for the indicated populations (pre-gate indicated above plot) for human (left) or mouse (right) duodenum and colon. Bottom: the proportion of a given cell subset is summarized between the duodenum and colon for both human and mouse. For example, the proportion of TCR$\gamma\delta^+$ IEL amongst CD3$^+$ IEL in human is lower in the duodenum relative to the colon. The comparisons are made directly between the duodenum and colon, therefore, the linear depiction of increases/decreases in proportions between the two segments are meant for simplicity and not to illustrate the progression across the other segments of the gut.

1.3 TCR$\gamma\delta^+$ IELs

The modern era of investigating TCR$\gamma\delta^+$ T cells began in the mid 1980s with the characterization of the γ-chain genes[56] and subsequent identification of the $\gamma\delta$ TCR itself[57]. Since then, immunologists have been trying to understand the function and roles of these enigmatic T cells in immune responses. The preferential localization of TCR$\gamma\delta^+$ T cells in tissues such as the intestinal epithelium has complicated the investigation of these cells, particullary in humans where access to tissues can be challenging. Having attended the 6th International $\gamma\delta$ T Cell Conference, the field as a whole is still struggling to find a consensus on the best models, methods, and even terminology to use when referring to different γ-chains after 30 years. Nonetheless, there has been a regained interest in studying TCR$\gamma\delta^+$ T cells in recent years, which can be attributed to a new appreciation for the roles of innate-like/tissue-resident lymphocytes in immunity.

1.3.1 TCR$\gamma\delta^+$ IEL TCR repertoire

Although they are classified as innate-like[15], $\gamma\delta$ T cells still have a critical feature that sets them apart from ILCs and that is their TCR. Therefore, to fully understand the biology of these cells one must carefully study the nature of the TCR repertoire. For starters, a unique feature of the $\gamma\delta$ TCR repertoire is that the expression of particular γ or δ genes is associated with enrichment in particular tissues. For example, almost all TCR$\gamma\delta^+$ T cells found in murine skin express a Vγ5Vδ1$^+$ TCR[58] and the majority of murine small intestine IELs express Vγ7$^+$ TCRs[20]. Similarly, in humans the majority of TCR$\gamma\delta^+$ T cells found in the blood are Vγ9Vδ2$^+$ and there is a preference for Vδ1 and Vδ3 chain usage in the gut epithelium[59]. These observations suggest TCR$\gamma\delta^+$ T cells may be selected by tissue-specific ligands, a hypothesis given credence by the discovery that establishment of skin-resident DETC is dependent on Skint1[19] and establishment of the Vγ7$^+$ IEL niche in murine small intestine is dependent on Btnl1[20].

Studies investigating the TCR repertoire of TCR$\gamma\delta^+$ T cells in humans have primarily focused on the peripheral blood[60–64]. Collectively, these studies have demonstrated the peripheral TCR repertoire is clonal, stable, and private. In contrast, only a few studies have investigated the TCR repertoire of TCR$\gamma\delta^+$ T cells in tissues such as the intesine and skin in conjunction with peripheral blood[60–62]. The repertoire in all three compartments was reported to be clonal, there was no overlap between compartments or individuals, and, in support of the stable tissue-resident nature of these cells, the dominant clones in the small intestine could be found a year later upon a follow up biopsy[60]. Importantly, there has been no extensive study to date where both the γ and δ chains were sequenced from human tissue.

Characterizing alterations to the TCR repertoire in disease states can be used to gain insights into TCR$\gamma\delta^+$ T cell biology. A study investigating the TCR repertoire of human peripheral blood TCR$\gamma\delta^+$ T cells in patients with CMV reactivation post stem cell transplantation revealed a focusing of the repertoire suggestive of an adaptive immune like clonal expansion in response to CMV[63]. The nature of the $\gamma\delta$ TCR repertoire providing evidence for adaptive immunity was also suggested in a study showing the repertoire in human cord blood is polyclonal whereas the peripheral blood repertoire becomes increasingly clonal with time[64]. However, both studies failed to demonstrate retraction of expanded clones upon removal of the driving antigen as well as recall responses upon re-introduction of the antigen; two critical features of adaptive immunity. Conversely, investigation of the $\gamma\delta$ TCR repertoire in T-cell infiltrates from patients with psoriasis showed the repertoire to be polyclonal[65], which would be more in favor of a non-specific expansion and more in line with their characterization as innate-like T cells.

It is then likely that the TCR$\gamma\delta^+$ T cell compartment is heterogenous and capable of mounting specific, adaptive like immune responses as well as innate-like responses. A

more comprehensive characterization of the repertoire in tissues at steady state, during inflammation, and upon resolution of inflammation is still needed to fully understand the scope of TCR$\gamma\delta^+$ T cell immune responses.

1.3.2 TCR$\gamma\delta^+$ IEL specificity

An area of active research in the field is characterizing the nature of ligands that the recombined $\gamma\delta$ TCR can recognize. Janeway and Hayday hypothesized in 1988 that because of their prevalence at mucosal surfaces such as the intestinal epithelium that TCR$\gamma\delta^+$ T cells could play a role in tissue surveillance and potentially be capable of recognizing non polymorphic MHC class I molecules that were either constitutively expressed or induced under certain conditions[66]. Support for this hypothesis has come with the characterization of the crystal structure of a mouse $\gamma\delta$ TCR with the non-classical MHC T22[67] and of two human $\gamma\delta$ TCRs with the non-classical MHC CD1d molecule[68,69]. However, none of the TCRs implicated in crystal structures thus far are of IEL origin so it remains to be determined whether mouse and human IELs are restricted to these non-classical MHC class I molecules. In support of alternative ligands for TCR$\gamma\delta^+$ IELs, the butyrophilin-like molecules Skint1 and Btnl1 have been implicated in the selection of TCR$\gamma\delta^+$ IELs in murine skin[19] and intestine[20], respectively. These observations have also been extended to humans where it was shown that human colonic IELs respond to BTNL3 and BTNL8[20].

A host of other molecules with less concrete biochemical evidence have also been suggested as TCR$\gamma\delta^+$ T cell ligands, including soluble proteins, small peptides, phospholipids, and prenyl pyrophosphates[70]. Given the diversity of possible antigens and the length and variability of structural elements of the $\gamma\delta$ TCR such as the complimentary determining region 3 loop (CDR3), people have hypothesized that $\gamma\delta$ TCRs are closer to B cell receptors than they are to $\alpha\beta$ TCRs[71]. The evidence over the years has made it clear that there is no universal

ligand for the $\gamma\delta$ TCR and that the tissue localization and microenvironment will most likely dictate reactivity. Understanding the nature and diversity of TCRs expressed by TCR$\gamma\delta^+$ T cells in tissues in both health and disease will be critical to gaining further insights into antigen recognition patterns.

1.3.3 TCR$\gamma\delta^+$ IEL function

TCR$\gamma\delta^+$ IELs are situated at the barrier and therefore are suited to serve as part of the first line of defense[72], while maintaining tissue integrity[73]. Accordingly, TCR$\delta^{-/-}$ mice display higher burdens of bacteria in peripheral organs post infection with *Salmonella typhimurium*[74] and show increased epithelial cell damage post infection with *Eimeria vermiformis*[75], an observation that fits with the proposed role for TCR$\gamma\delta^+$ IELs in tissue repair mediated via secretion of keratinocyte growth factor (KGF)[76]. The exact mechanisms by which TCR$\gamma\delta^+$ IELs respond to insults are still being elucidated but intravital microscopy experiments have shown the TCR$\gamma\delta^+$ IEL compartment is highly motile[13,77,78], displaying dynamic microbial sensitive scanning of the intestinal epithelium[13] that is dependent on MyD88 signaling in epithelial cells[13,74], suggesting the function of TCR$\gamma\delta^+$ IELs is dictated by interactions with the tissue. Interestingly, TCR-Btnl1 interactions were not required for TCR$\gamma\delta^+$ IEL motility or sensing of bacterial infection[13], suggesting different signals may dictate the development/establishment of TCR$\gamma\delta^+$ IEL niches and their subsequent functions.

Establishing requirement for a given function of TCR$\gamma\delta^+$ IELs has been challenging due to the lack of models where IELs can be selectively ablated in addition to the redundancy in functional capacity between different IEL subsets as well as the multi-layered nature of the immune system. For instance, TCR$\alpha\beta^+$ IELs are the primary producers of IFN-γ in response to *Listeria monocytogenes* infection, but in β2-Microglobulin deficient mice, which lack adaptively induced TCR$\alpha\beta^+$CD8$\alpha\beta^+$ IELs, this response is compensated for

by the β2-Microglobulin independent TCR$\gamma\delta^+$ and TCR$\alpha\beta^+$CD8$\alpha\alpha^+$ IEL subsets[79]. For this reason, it has been important to first establish the functional capacity of different IEL cell types using unbiased approaches such as transcriptional profiling. Two such studies in mice[38,39] have shown that TCR$\gamma\delta^+$ IELs are in an activated yet resting state[31] characterized by high levels of transcript in the steady state for genes such as *GZMB*, *FASL* and *RANTES* while the expression of cytokines and growth factors such as IFN-γ and KGF was low[38], suggesting that only once activated during tissue stress would they produce KGF[76]. Such studies are lacking in human and the role of TCR$\gamma\delta^+$ IELs during homeostasis or pathology is still poorly understood.

1.4 Celiac disease

Celiac disease (CeD) is a T cell-mediated enteropathy with an autoimmune component that manifests in the small intestine of genetically susceptible individuals in response to gluten protein found in wheat, barley, and rye[80]. The critical events required for disease pathogenesis are the induction of a gluten-specific inflammatory T helper-1 (Th1) CD4 T cell response as well as the targeted killing of intestinal epithelial cells (IEC) by licensed TCR$\alpha\beta^+$CD8$\alpha\beta^+$ IELs resulting in villous atrophy[81]. These immunological events translate into a wide disease spectrum, ranging from potential CeD to refractory sprue[82].

1.4.1 Celiac disease as a human model to study dynamic immunological processes

Insight into the function of immune cells can be gained from disease states where the balance of normal events is disrupted. Studying immune cells at tissue surfaces in humans is challenging and greatly limited by access to and availability of tissues harboring the cells of interest. To that extent, CeD is a rare case where biopsies from the site of inflammation can be readily obtained without great harm to the patient. Most importantly, the disease driving

antigen gluten can be controlled, allowing for the study of cells from patients with ongoing inflammation and tissue destruction (active CeD) as well as from patients treated with a gluten free diet (GFD CeD), which results in cessation of inflammation and restoration of a relatively healthy mucosa[81]. In addition to active CeD and GFD-treated CeD, the events preceding the initiation of tissue destruction can be studied in patients with potential CeD, a state characterized by the presence of $CD4^+$ T cell-mediated intolerance to dietary gluten without histological evidence of villous atrophy[83,84]. Therefore, CeD offers the opportunity to asses how different stages of inflammation alter tissue-resident lymphocytes as well as the unique chance to address the lasting impact of chronic inflammation upon resolution of disease on a GFD.

1.4.2 TCR$\gamma\delta^+$ IEL in celiac disease

A hallmark of CeD is the increased number of IELs in the small intestine[85]. The increase is dominated by TCR$\gamma\delta^+$ and TCR$\alpha\beta^+$CD8$\alpha\beta^+$ IELs. Interestingly, the increase in IEL has been shown to be biased towards TCR$\gamma\delta^+$ IELs in that TCR$\gamma\delta^+$ IELs make up a larger proportion of total IELs in active CeD patients and interestingly TCR$\gamma\delta^+$ IELs remain elevated in GFD-treated CeD patients[86–88]. The TCR$\gamma\delta^+$ IEL compartment may expand locally from pre-existing clones already situated in the tissue in response to local cues, a model supported by Hayday[31], or alternatively may integrate newly generated IELs recruited from the periphery upon activation in gut-associated lymphoid tissues (GALT)[89] in response to a specific antigen. Of note, the increase is not simply associated with villous atrophy as other diseases with villous atrophy such as tropical sprue and severe food allergy do not show an increase in TCR$\gamma\delta^+$ IELs[88]. Data in support of either model are still lacking.

An active role for TCR$\gamma\delta^+$ IELs in the pathogenesis of CeD has been dismissed, because of the observation that they remain increased in patients on a GFD that have resolved

inflammation[87], in favor of them playing a role in regulating disease activity[90]. A comprehensive characterization of TCR$\gamma\delta^+$ IELs in healthy individuals, active CeD patients, and GFD-treated CeD patients is still lacking and once completed will help educate future hypothesis about both the origin of the expansion as well as the role of these cells in CeD pathogenesis.

CHAPTER 2

DIETARY GLUTEN PERMANENTLY RESHAPES THE TISSUE-RESIDENT $\gamma\delta$ INTRAEPITHELIAL T CELL COMPARTMENT IN CELIAC DISEASE

Toufic Mayassi[1,2], Kristin Ladell[3], Herman Gudjonson[4,5], James E. McLaren[3], Dustin G. Shaw[1,2], Mai Tran[6], Jagoda J. Rokicka[2], Ian Lawrence[2], Jean-Christophe Grenier[7], Vincent van Unen[8], Cezary Ciszewski[2], Matthew Dimaano[2], Hoda E. Sayegh[2], Vinod Kumar[9], Cisca Wijmenga[9], Ranjana Gokhale[10,11], Hilary Jericho[10,11], Carol E. Semrad[2,11], Stefano Guandalini[10,11], Aaron R. Dinner[4,5,12], Sonia S. Kupfer[2,10], Hugh H. Reid[6,13], Luis B. Barreiro[7], Jamie Rossjohn[3,6,13], David A. Price[3*], Bana Jabri[1,2,9,14*]

[1] *Committee on Immunology, University of Chicago, Chicago, IL, USA*

[2] *Department of Medicine, University of Chicago, Chicago, IL, USA*

[3] *Division of Infection and Immunity, Cardiff University School of Medicine, Cardiff, UK*

[4] *Institute for Biophysical Dynamics, University of Chicago, Chicago, IL, USA*

[5] *Department of Chemistry, University of Chicago, Chicago, IL, USA*

[6] *Infection and Immunity Program and Department of Biochemistry and Molecular Biology, Biomedicine Discovery Institute, Monash University, Clayton, Victoria, Australia*

[7] *Department of Genetics, CHU Sainte-Justine Research Center, Montreal, Quebec, Canada*

[8] *Department of Immunohematology and Blood Transfusion, Leiden University Medical Center, Leiden, Netherlands*

[9] *Department of Genetics, University of Groningen, University Medical Center Groningen, Groningen, Netherlands*

[10] *Section of Gastroenterology, Hepatology, and Nutrition, Department of Pediatrics, University of Chicago, Chicago, IL, USA*

[11] *University of Chicago Celiac Disease Center, University of Chicago, Chicago, IL, USA*

[12] *James Franck Institute, University of Chicago, Chicago, IL, USA*

[13]*Australian Research Council Centre of Excellence in Advanced Molecular Imaging, Monash University, Clayton, Victoria, Australia*

[14]*Department of Pathology, University of Chicago, Chicago, IL, USA*

[*]*Corresponding author*

Correspondence

[*]Bana Jabri, University of Chicago, Departments of Medicine, Pathology, and Pediatrics, 900 East 57th Street KCBD, Chicago, IL 60637, USA. Tel: (773) 834-8670. E-mail: bjabri@bsd.uchicago.edu

[*]David A Price, Division of Infection and Immunity, Cardiff University School of Medicine, Heath Park, University Hospital, Cardiff CF14 4XN, Wales, UK. Tel: (44) 29 2068 7002. E-mail: priced6@cardiff.ac.uk

2.1 Summary

Tissue-resident lymphocytes play a key role in immune surveillance, but it remains unclear how these inherently stable cell populations respond to chronic inflammation. In the setting of celiac disease (CeD), where exposure to dietary antigen can be controlled, gluten-induced inflammation triggered a profound depletion of naturally-occurring Vγ4$^+$/Vδ1$^+$ intraepithelial lymphocytes (IELs) with innate cytolytic properties and specificity for the butyrophilin-like (BTNL) molecules BTNL3/BTNL8. Creation of a new niche with reduced expression of BTNL8 and loss of Vγ4$^+$/Vδ1$^+$ IELs was accompanied by the expansion of gluten-sensitive, interferon-γ-producing Vδ1$^+$ IELs bearing T cell receptors (TCRs) with a shared non-germline-encoded motif that failed to recognize BTNL3/BTNL8. Exclusion of dietary gluten restored BTNL8 expression but failed to reconstitute the Vγ4$^+$/Vδ1$^+$ gut signature among TCR$\gamma\delta^+$ IELs. Collectively, these data demonstrate that chronic inflammation permanently reconfigures the tissue-resident TCR$\gamma\delta^+$ IEL compartment, thus the

paradigm of tissue-resident lymphocyte stability needs revisiting.

2.2 One sentence summary

Chronic inflammation driven by persistent antigenic challenge with dietary gluten permanently reshapes the tissue-resident TCR$\gamma\delta^+$ intraepithelial lymphocyte compartment in patients with celiac disease.

2.3 Introduction

The properties of tissue-resident lymphocytes have been investigated extensively in mice under steady state conditions and during the induction of local memory populations in response to acute infections[30]. In mice, the tissue-resident TCR$\alpha\beta^+$CD8$\alpha\beta^+$ pool is highly stable and responds to secondary antigenic challenge via local proliferation of pre-existing memory cells[10,11], which endure over time despite the accumulation of new tissue-resident populations driven by subsequent infections[11]. However, it remains unclear if chronic inflammation can permanently reconfigure the tissue resident T cell compartment. This question is particularly relevant to ongoing immune-mediated disorders, where clinical outcomes may depend on the potential for tissue healing[91] balanced against the specter of a permanent immunological scar[92]. Intraepithelial lymphocytes (IELs) expressing $\gamma\delta$ T cell receptors (TCRs)[93,94] are viewed as tissue-resident T cells[73] that play a key role in immune surveillance[66] via dynamic scanning of the intestinal epithelium[13]. In mice, studies have shown that TCR$\gamma\delta^+$ cells seed the intestine early in life, irrespective of microbial colonization or exposure to dietary antigen[20,22], and persist in situ as naturally-occurring[32] or type b IELs[31]. Moreover, the peripheral and intraepithelial TCR$\gamma\delta^+$ compartments are largely non-overlapping as a consequence of distinct migratory characteristics, especially a lack of recirculating IELs[7,78].

Celiac disease (CeD), an inflammatory disorder triggered and maintained in genetically susceptible individuals by dietary exposure to gluten[95,96], offers a dynamic setting to study human tissue-resident T cells in the context of chronic inflammation as exposure to the driving antigen can be controlled. Active disease is characterized histologically by flattening of the small intestinal villi[95] and immunologically by expanded populations of TCR$\gamma\delta^+$ IELs[86–88]. Strict adherence to a gluten-free diet (GFD) usually leads to resolution of the villous abnormalities, together with a decrease in the frequencies of gluten-specific TCR$\alpha\beta^+$ CD4$^+$ T cells in the lamina propria and cytolytic TCR$\alpha\beta^+$ CD8$^+$ IELs, which are consequently implicated in the pathogenesis of CeD[81]. In contrast, the TCR$\gamma\delta^+$ IEL expansions generally persist in situ, despite a lack of exposure to gluten[87]. Therefore, tissue-resident TCR$\gamma\delta^+$ IELs were proposed to function in regulating disease activity, potentially by suppressing the influx of circulating T cells[31] and/or by maintaining tissue integrity[97] rather than participating in the pathogenesis of CeD[87]. These propositions remain unsubstantiated, however, pending a detailed functional evaluation of TCR$\gamma\delta^+$ IELs in patients with CeD. We set out to address this knowledge gap and more fundamentally to determine the effects of chronic inflammation on human tissue-resident TCR$\gamma\delta^+$ IELs.

2.4 Results

2.4.1 Vδ1$^+$ T cells with hallmarks of tissue-resident lymphocytes are permanently expanded in CeD

To investigate the effects of antigen-induced inflammation on tissue-resident immune responses in the human gastrointestinal tract, we first performed a flow cytometric survey of TCR$\gamma\delta^+$ cells in donor-matched samples of peripheral blood lymphocytes (PBL) and IELs from healthy controls (n = 102), patients with active CeD (n = 66), and patients with an established diagnosis of CeD ameliorated by standard treatment with a GFD (n = 59) (Fig. 2.1). In line

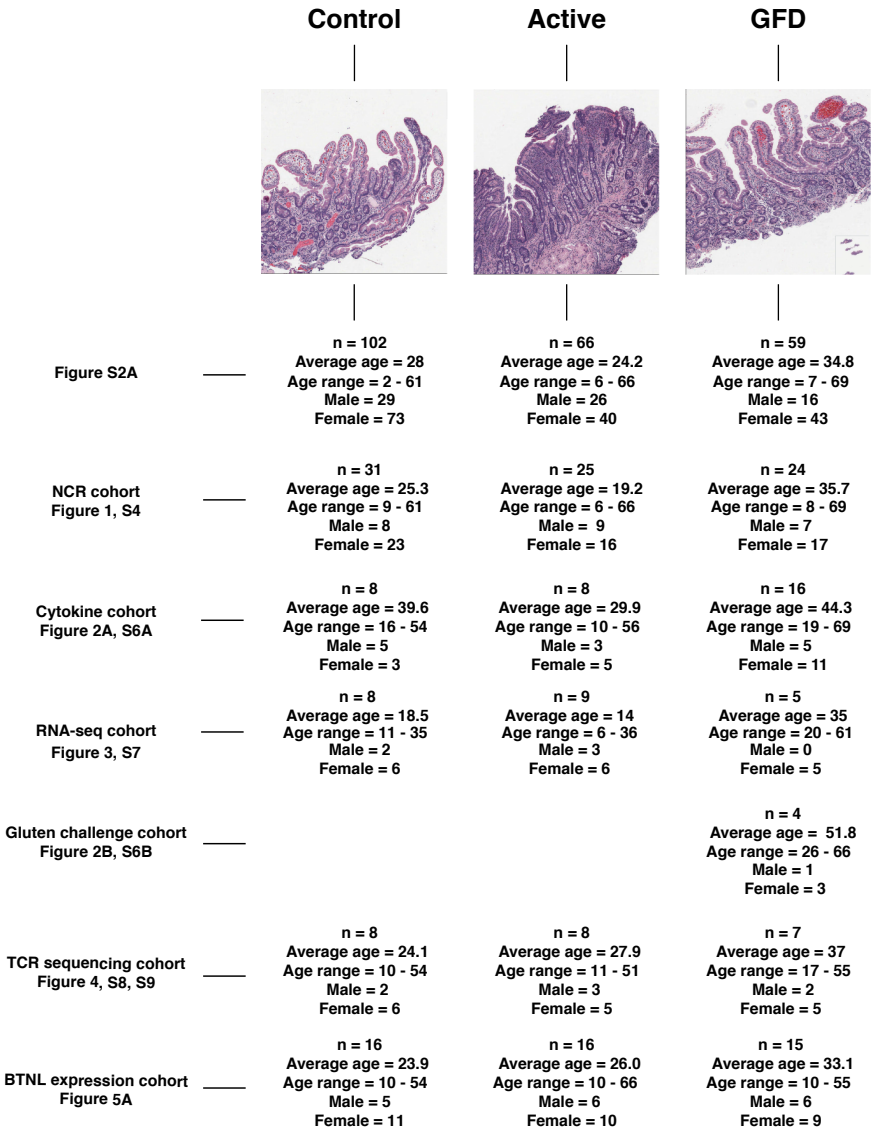

Figure 2.1: Cohort summary.
Cohort size, mean age, age range, and gender distribution summarized for the various datasets presented in this study.

with previous studies (19, 21), we found higher frequencies (Fig. 2.3A) and absolute numbers (Fig. 2.3B) of V$\delta1^+$ IELs in patients with CeD relative to healthy controls, irrespective of long-term adherence to a GFD (Fig. 2.3C). Moreover, V$\delta1^+$ T cells constituted a significantly higher fraction of all TCR$\gamma\delta^+$ IELs in patients with active CeD (Fig. 2.3D). A vast majority of V$\delta1^+$ IELs in healthy controls and patients with active or GFD-treated CeD expressed markers of tissue residency, namely CD69 and CD103 (1) (Fig. 2.3A). In addition, V$\delta1^+$

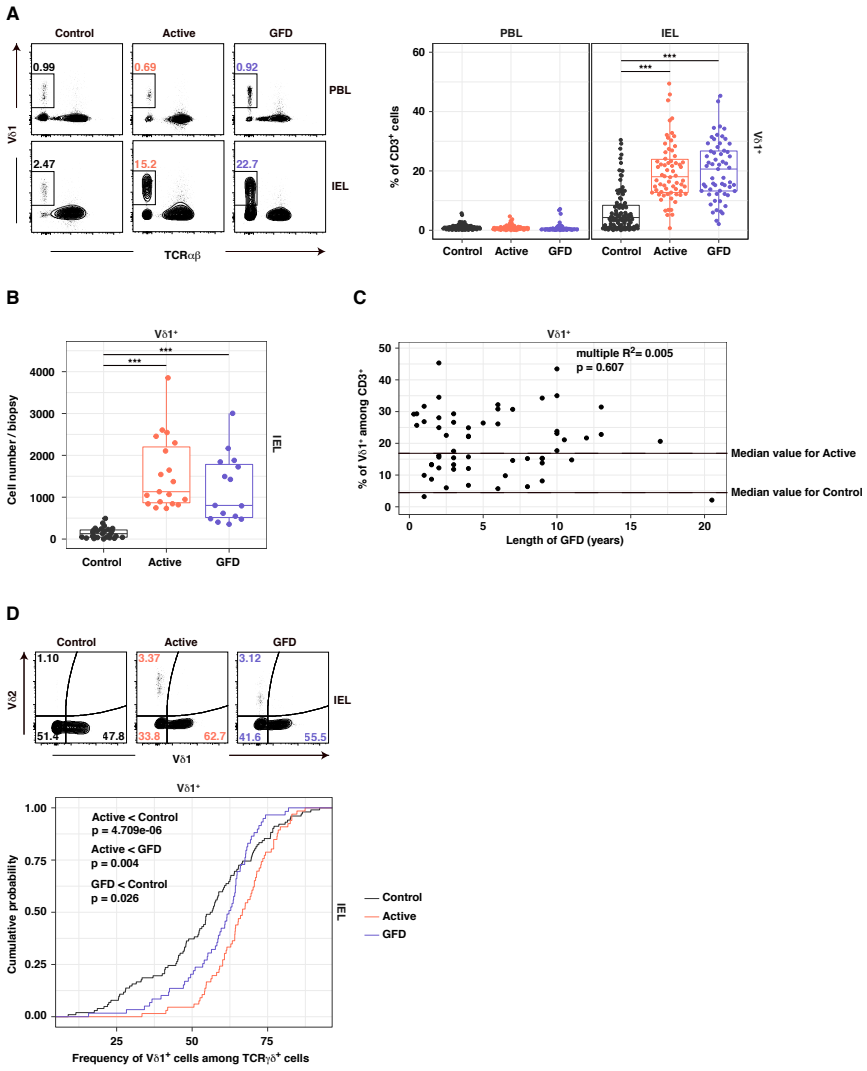

Figure 2.2: Persistent expansion of Vδ1$^+$ T cells in CeD.
(**A**) Surface expression of Vδ1 on PBLs and IELs isolated from healthy controls and patients with active or GFD-treated CeD. Left: representative contour plots showing cells pre-gated for expression of CD3 and CD45. Right: data summarized as the frequency of Vδ1$^+$ cells among total CD3+ lymphocytes. Box plots display the first and third quartiles. ***p<0.001; one-way ANOVA followed by Tukeys test for multiple comparisons. (**B**) Cells were isolated from 35 biopsies per patient. Absolute numbers of Vδ1$^+$ T cells were determined using flow cytometry. Box plots display the first and third quartiles. ***p<0.001; one-way ANOVA followed by Tukeys test for multiple comparisons. (**C**) Cells were pre-gated for expression of CD3 and CD45. Data represent the frequency of Vδ1$^+$ IELs among total CD3+ lymphocytes versus the duration of treatment with a GFD. Correlations were tested using linear regression. (**D**) Cells were pre-gated for expression of CD3, CD45, and TCR$\gamma\delta$. Top: representative contour plots showing the frequency of Vδ1$^+$ IELs among total TCR$\gamma\delta^+$ T cells. Bottom: cumulative distribution showing the frequency of Vδ1$^+$ IELs among total TCR$\gamma\delta^+$ T cells. Healthy controls: n = 99. Patients with active CeD: n = 62. Patients with GFD-treated CeD: n = 57. Actual p values are shown; Kolmogorov-Smirnov test.

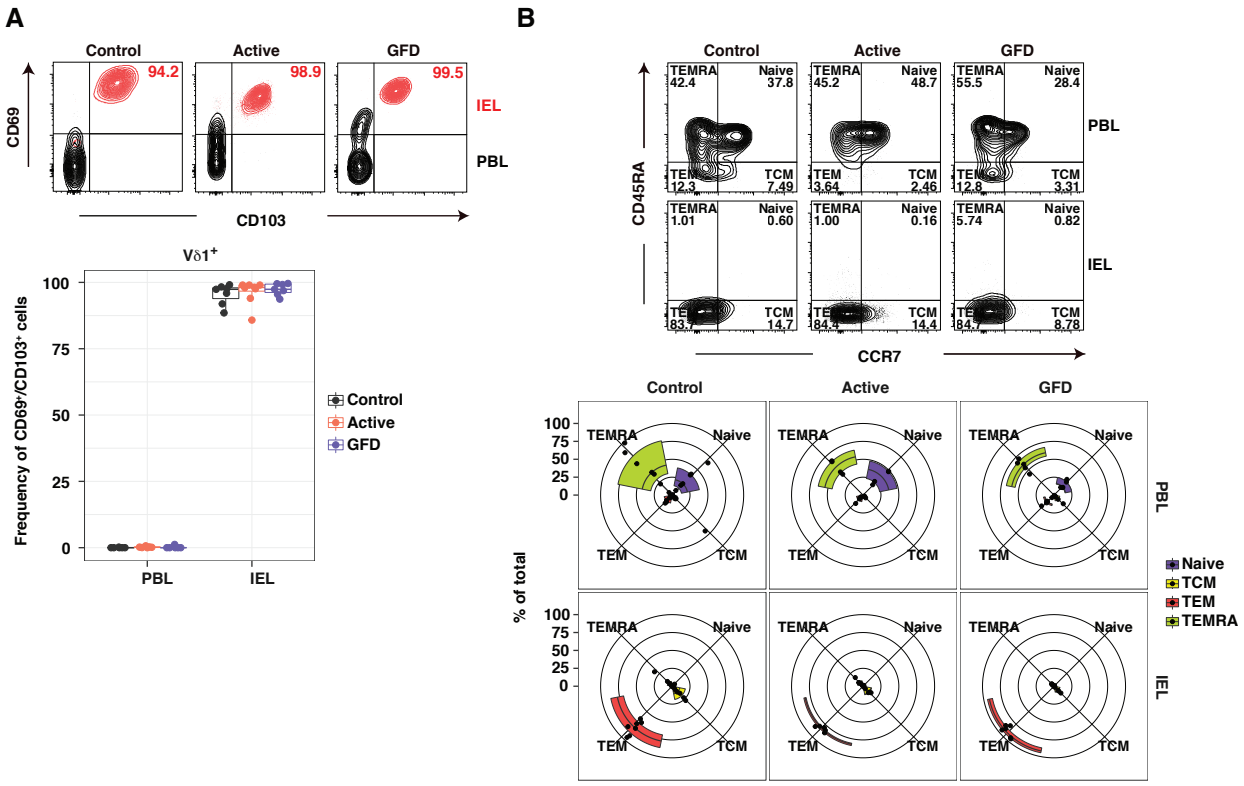

Figure 2.3: Vδ1$^+$ IELs display a tissue-resident phenotype in CeD.
(**A**) Top: representative contour plots showing expression of CD69 and CD103 on cells pre-gated for expression of CD3, CD45, and Vδ1. PBLs: black; IELs: red. Bottom: data summarized as the frequency of CD69$^+$/CD103$^+$ cells. Box plots display the first and third quartiles. (**B**) Top: representative contour plots showing expression of CD45RA and CCR7 on cells pre-gated for expression of CD3, TCR$\gamma\delta$, and Vδ1. Bottom: data summarized in radar plots, where values above 0 radiate from the center for cells identified as nave, central memory (TCM), effector memory (TEM), or terminal effector (TEMRA).

IELs expressed low levels of CD45RA and CCR7, indicative of an effector memory (TEM) phenotype[98,99], whereas the corresponding Vδ1$^+$ PBLs comprised a mixture of nave and terminally differentiated effector (TEMRA) cells (Fig. 2.3B). These results showed that disease-associated expansions of Vδ1$^+$ IELs were integrated as bone fide tissue-resident memory cells in the small intestinal microenvironment of patients with CeD.

2.4.2 Innate-like Vδ1$^+$ IELs with cytolytic potential are lost in CeD

In contrast to TCR$\alpha\beta^+$ CD8$\alpha\beta^+$ IELs[81,100], Vδ1$^+$ IELs isolated from CeD patients failed to upregulate activating NK receptors (Fig. 2.4.1A and Fig. 2.4.1B), while Vδ1$^+$ IELs

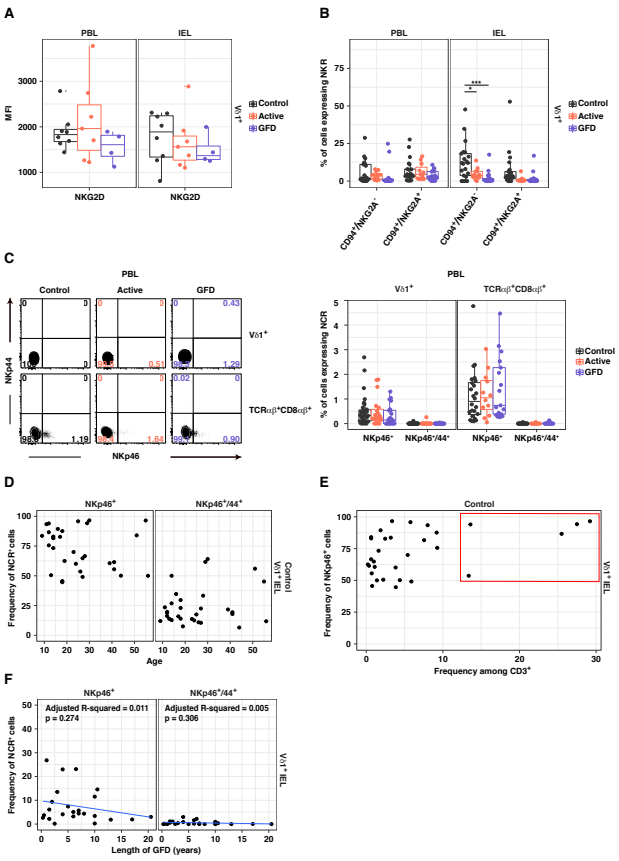

Figure 2.4: Innate-like Vδ1$^+$ IELs are lost in CeD.
(**A**) Surface expression of NKG2D on Vδ1$^+$ PBLs and IELs isolated from healthy controls and patients with active or GFD-treated CeD. Mean fluorescence intensity (MFI) data are summarized in box plots displaying the first and third quartiles. (**B**) Surface expression of CD94 and NKG2A on Vδ1$^+$ PBLs and IELs isolated from healthy controls and patients with active or GFD-treated CeD. Data are summarized in box plots displaying the first and third quartiles. CD94$^+$/NKG2A$^-$ (activating); CD94$^+$/NKG2A$^+$ (inhibitory). *p<0.05, ***p<0.001; one-way ANOVA followed by Tukeys test for multiple comparisons. (**C**) Left: representative contour plots showing expression of NKp46 and NKp44 on PBLs. Vδ1$^+$ cells were pre-gated for expression of CD3, CD45, and Vδ1. TCR$\alpha\beta^+$ CD8$\alpha\beta^+$ cells were pre-gated for expression of CD3, CD45, TCRβ, and CD8α. Right: data summarized in box plots displaying the first and third quartiles. (**D**) Surface expression of NKp46 and NKp44 on Vδ1$^+$ IELs isolated from healthy controls. Data are summarized as the frequency of NKp46$^+$ or NKp46$^+$/NKp44$^+$ Vδ1$^+$ IELs versus age. (E) Surface expression of NKp46 and NKp44 on Vδ1$^+$ IELs isolated from healthy controls. Data are summarized as the frequency of NKp46$^+$ or NKp46$^+$/NKp44$^+$ Vδ1$^+$ IELs among total CD3$^+$ lymphocytes. The red box depicts individuals with expansions of Vδ1$^+$ IELs similar in magnitude to those found in patients with CeD. (F) Surface expression of NKp46 and NKp44 on Vδ1$^+$ IELs isolated from patients with active CeD. Data are summarized as the frequency of NKp46+ or NKp46$^+$/NKp44$^+$ Vδ1$^+$ IELs versus age. The red box depicts patients ¡16 years of age with higher frequencies of NKp46+ Vδ1$^+$ IELs. (G) Surface expression of NKp46 and NKp44 on Vδ1$^+$ IELs isolated from patients with GFD-treated CeD. Data are summarized as the frequency of NKp46$^+$ or NKp46$^+$/NKp44$^+$ Vδ1$^+$ IELs versus the duration of treatment with a GFD.

isolated from healthy controls expressed higher levels of the activating NK receptor complex CD94+/NKG2A relative to CeD Vδ1$^+$ IELs (Fig. 2.4.1B). In particular, a vast majority of

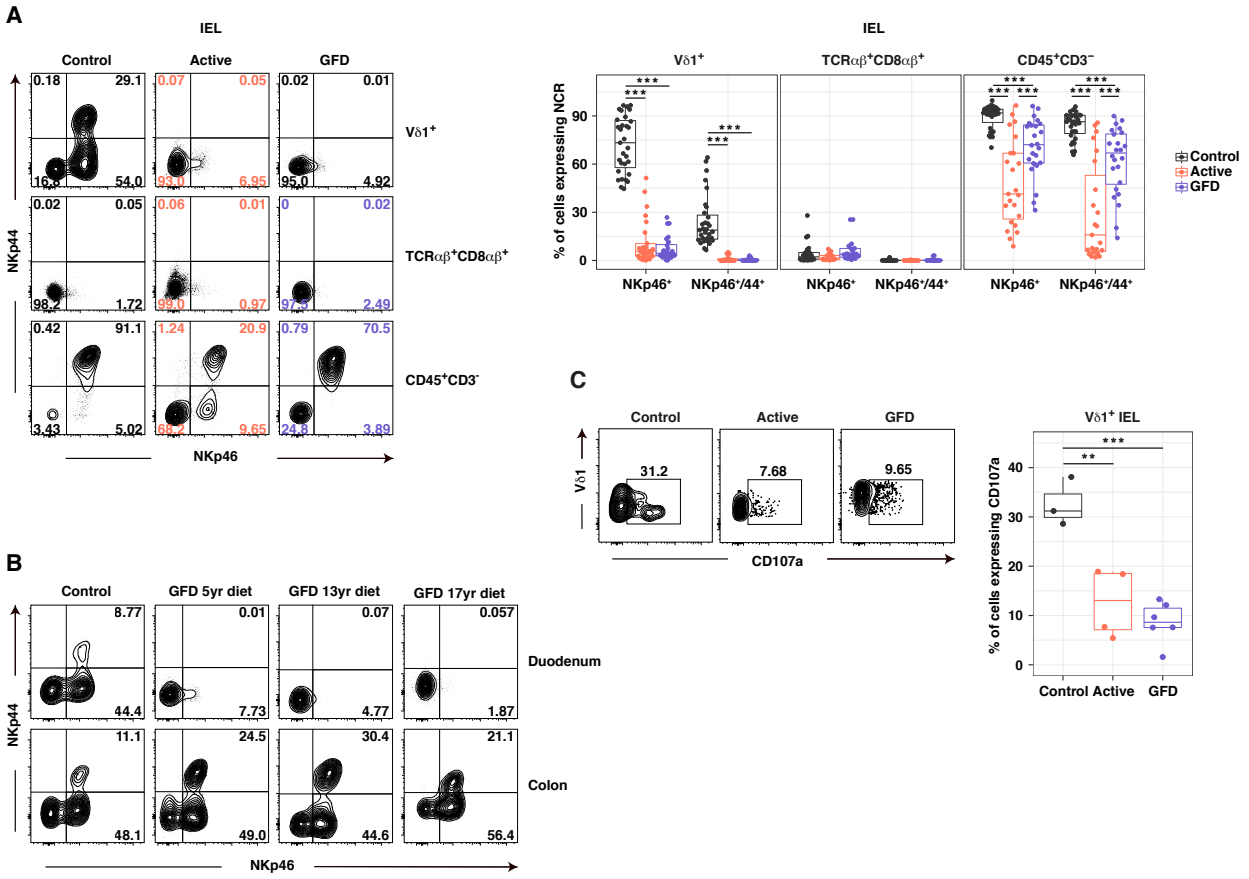

Figure 2.5: Innate-like Vδ1$^+$ IELs with cytolytic potential are lost in CeD.
(**A**) Left: representative contour plots showing expression of NKp46 and NKp44 on IELs. Vδ1$^+$ cells were pre-gated for expression of CD3, CD45, and Vδ1. TCR$\alpha\beta^+$ CD8$\alpha\beta^+$ cells were pre-gated for expression of CD3, CD45, TCRβ, and CD8α. CD45$^+$ CD3$^-$ cells were pre-gated for expression of CD45 in the absence of CD3. Right: data summarized in box plots displaying the first and third quartiles. ***p<0.001; one-way ANOVA followed by Tukeys test for multiple comparisons. (**B**) Representative contour plots showing expression of NKp46 and NKp44 on Vδ1$^+$ IELs isolated from donor-matched duodenal and right colonic biopsies. (**C**) Left: representative contour plots showing expression of CD107a on Vδ1$^+$ IELs after stimulation with phorbol myristate acetate and ionomycin. Right: data summarized in box plots displaying the first and third quartiles. **p<0.01, ***p<0.001; one-way ANOVA followed by Tukeys test for multiple comparisons.

Vδ1$^+$ IELs, but not Vδ1$^+$ PBLs in healthy controls expressed NKp46 alone or in association with NKp44 (Fig. 2.5A and Fig. 2.4.1C). These natural cytotoxicity receptors (NCRs) associate with ITAM-bearing adapter molecules and are classically found on innate lymphocytes[25], but not on TCR$\alpha\beta^+$ CD8$\alpha\beta^+$ IELs[101]. Of note, NKp46 and NKp44 were stably expressed on Vδ1$^+$ IELs isolated from healthy controls, irrespective of age (Fig. 2.4.1D) and in situ expansion (Fig. 2.4.1E). Strikingly, the vast majority of Vδ1$^+$ IELs isolated from

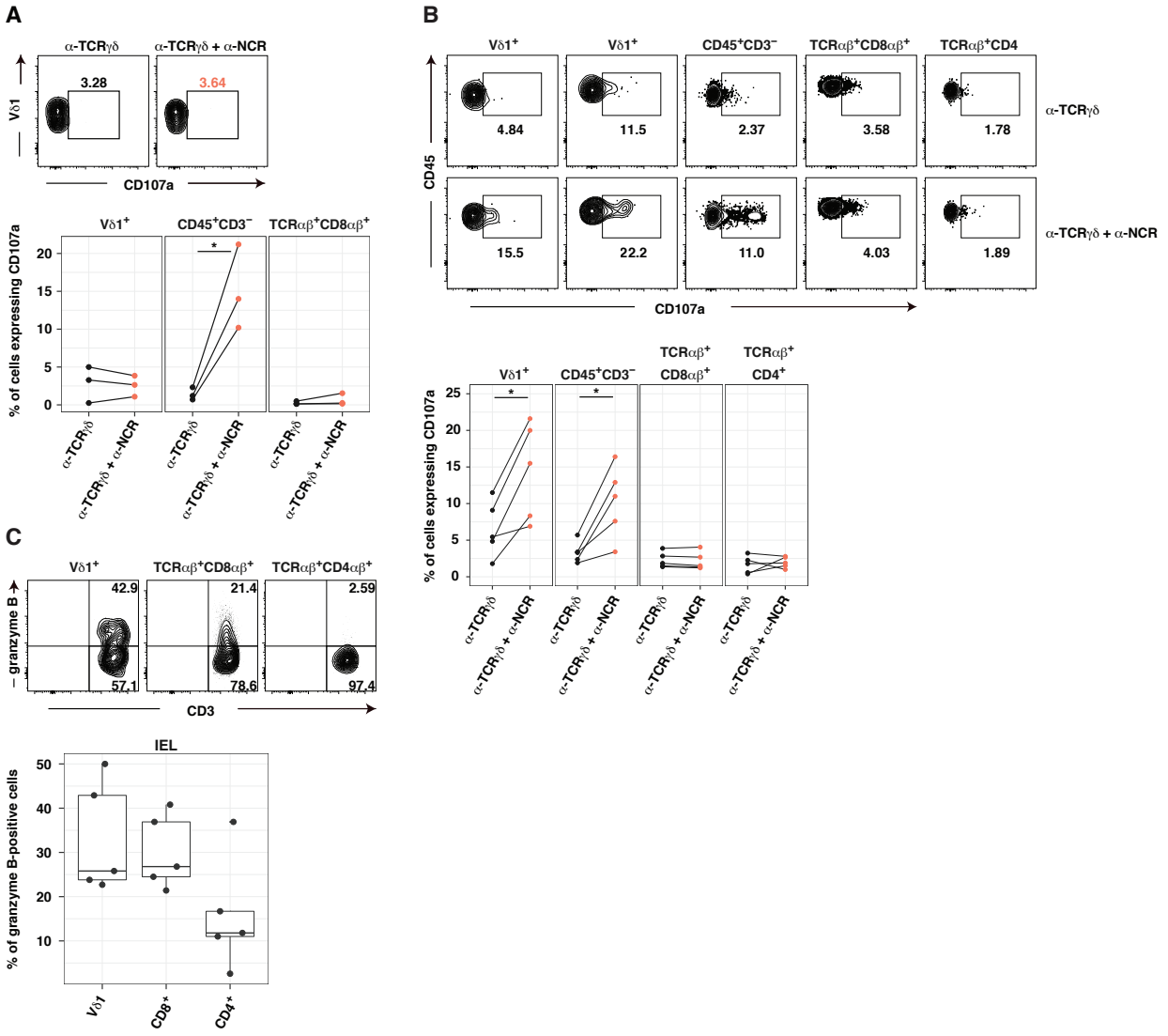

Figure 2.6: Innate-like Vδ1$^+$ IELs exhibit cytolytic properties.
(**A**) IELs were stimulated with plate-bound αTCR$\gamma\delta$ $\pm\alpha$NKp46 and αNKp44. Top: representative contour plots showing expression of CD107a on Vδ1$^+$ IELs. Bottom: data summary (n = 3). *p<0.05; paired T-test. (**B**) IELs were stimulated as in (B) after overnight incubation with IL-15 (n = 5). *p<0.05; paired T-test. (**C**) Top: representative contour plots showing expression of intracellular granzyme B among various subsets of IELs. Bottom: data summary (n = 5).

patients with active or GFD-treated CeD lacked expression of NKp46 and were almost always NKp44 negative (Fig. 2.5A). Unlike NCR$^+$ CD3$^-$ IELs, the loss of NCR+ Vδ1$^+$ IELs was refractory to long-term treatment with a GFD illustrating the long-lasting alterations to the Vδ1$^+$ IEL compartment in CeD are not simply the result of the microenvironment but rather cell specific (Fig. 2.5A and Fig. 2.4.1F). While the loss of NKp46 and NKp44 Vδ1$^+$ IELs

was permanent, this loss was site specific because Vδ1$^+$ IELs expressing NKp46 and NKp44 were exclusively absent from the duodenum, the site of tissue destruction in CeD, and not the colon in three CeD patients on a GFD for 5-17 years (Fig. 2.5B). These results suggested that dietary gluten-induced inflammation precipitated an irretrievable and active site-specific loss of NK-like Vδ1$^+$ IELs in patients with CeD.

To assess the functional capacity of the innate-like Vδ1$^+$ IELs found in healthy controls, we first determined the role of NCRs expressed on healthy Vδ1$^+$ IELs by assessing their capacity to induce ex vivo degranulation. Vδ1$^+$ IELs were poor at degranulating, as measured by surface mobilization of CD107a, when stimulated with either the TCR or TCR in conjunction with NCRs (Fig. 2.6A). Degranulation by healthy state Vδ1$^+$ IELs was observed when cells were pre-treated with Interleukin (IL)-15, which is upregulated under inflammatory conditions and is known to promote cytolytic activity in T cells[55,102] (Fig. 2.6B). Importantly, a significantly greater proportion of IL-15 treated Vδ1$^+$ IELs mobilized CD107a when the TCR was co-engaged with NKp46 and NKp44 relative to TCR alone, indicating that these NCRs are functional while highlighting the importance of innate signals in the regulation of innate-like Vδ1$^+$ IELs (Fig. 2.6B). Finally, healthy control Vδ1$^+$ IELs expressed high levels of the cytolytic effector molecule granzyme B (Fig. 2.6C) and degranulated at higher frequencies compared with Vδ1$^+$ IELs isolated from patients with active or GFD-treated CeD (Fig. 2.5C), suggesting that healthy control Vδ1$^+$ IELs may display higher cytolytic capacities *in vivo*. Taken together, these findings, in conjunction with the phenotypic data, revealed that under physiological conditions the small intestine harbored a unique set of innate-like and potentially cytolytic Vδ1$^+$ IELs that were displaced in the setting of CeD.

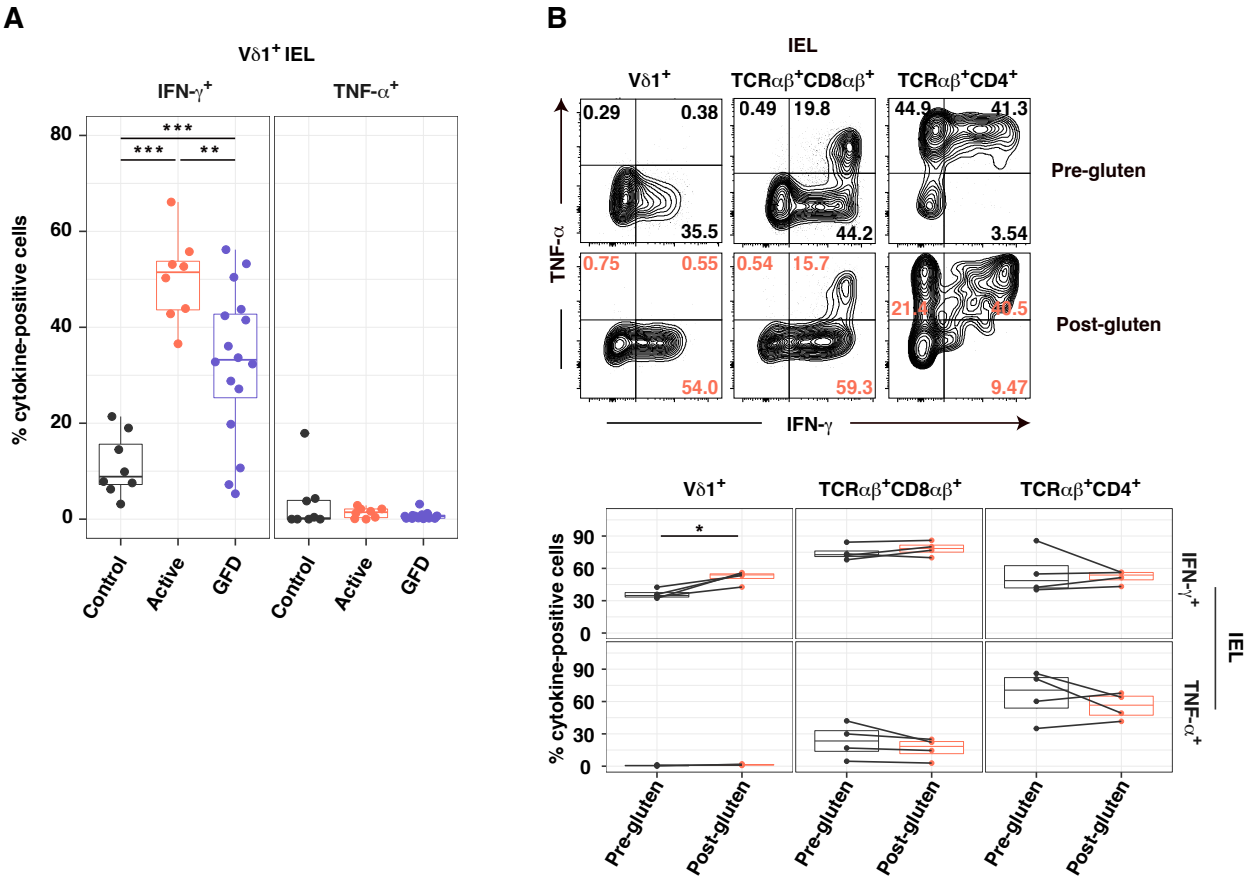

Figure 2.7: Gluten-dependent IFN-γ-producing Vδ1$^+$ IELs emerge in CeD.
(**A**) Cells were stimulated with phorbol myristate acetate and ionomycin and stained intracellularly for IFN-γ and TNF-α. Data are summarized in box plots displaying the first and third quartiles. **p<0.01, ***p<0.001; one-way ANOVA followed by Tukeys test for multiple comparisons. (**B**) Patients with GFD-treated CeD (length of diet: 1.5 years, 4years, 7 years, and 20.5 years) were challenged daily with gluten for six weeks. Cells isolated from biopsies taken before and after gluten challenge were treated as in (A). Top: representative contour plots from the same individual showing expression of IFN-γ and TNF-α. Bottom: data summarized in box plots displaying the first and third quartiles. *p<0.05; paired T-test.

2.4.3 Gluten-dependent IFN-γ-producing Vδ1$^+$ IELs emerge in CeD

To refine these functional observations, we extended our analysis to cytokine production. Unexpectedly, analysis of IFN-γ and TNF-α production showed that healthy Vδ1$^+$ IELs are poor producers of cytokines (Fig. 2.7A and Fig. 2.4.2A). In contrast, more than 50% of Vδ1$^+$ IELs isolated from active CeD patients produced IFN-γ (Fig. 2.7A and Fig. 2.4.2A). Importantly, CeD patients on a GFD showed a significant decrease in IFN-γ production by Vδ1$^+$ IELs as compared to patients with active disease (Fig. 2.7A). No differences were

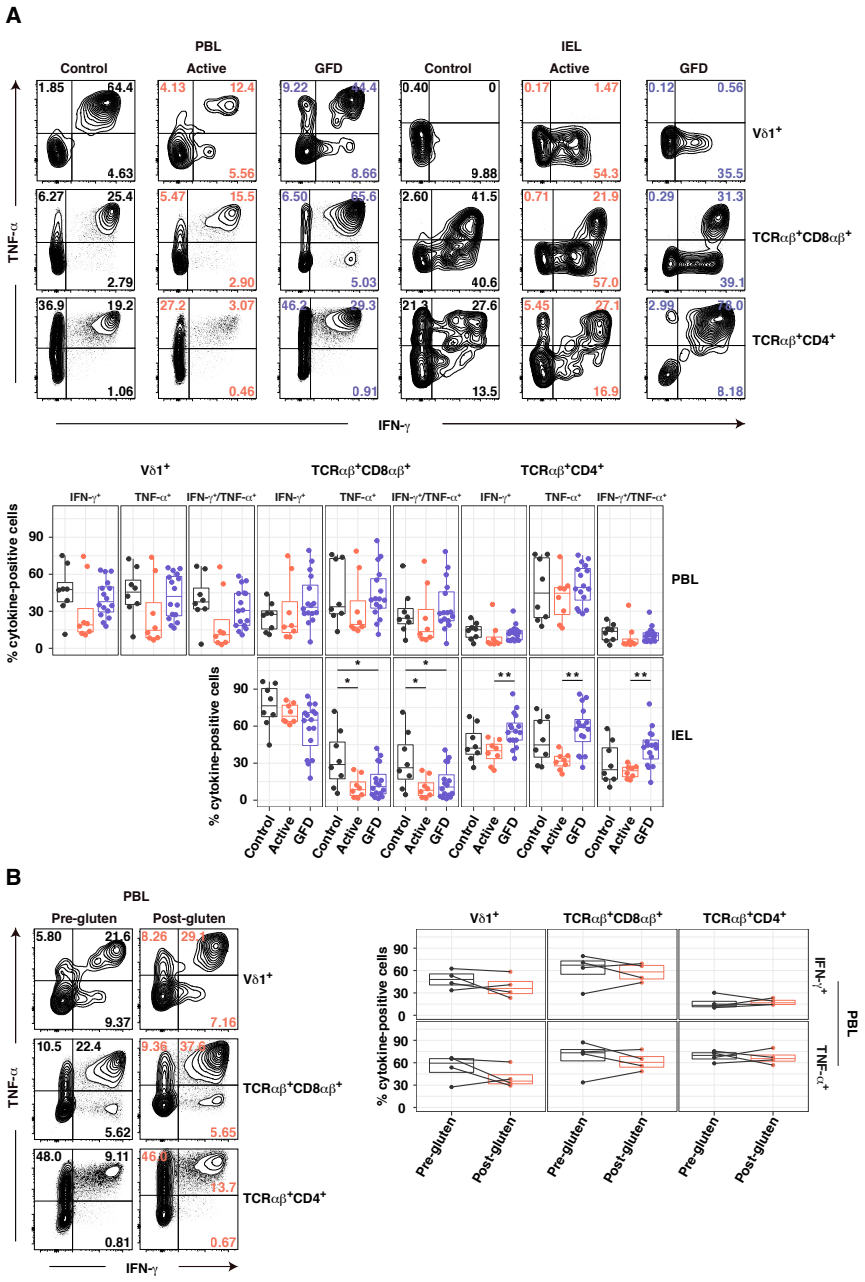

Figure 2.8: Cytokine profiles of IELs and PBLs.
(**A**) IELs and PBLs were stimulated with phorbol myristate acetate and ionomycin and stained intracellularly for IFN-γ and TNF-α. Top: representative contour plots showing expression of IFN-γ and TNF-α. Bottom: data summarized in box plots displaying the first and third quartiles. *p<0.05, *p<0.01; one-way ANOVA followed by Tukeys test for multiple comparisons. (**B**) Patients with GFD-treated CeD were challenged daily with gluten for six weeks. PBLs isolated before and after gluten challenge were stimulated with phorbol myristate acetate and ionomycin and stained intracellularly for IFN-γ and TNF-α. Left: representative contour plots showing production of IFN-γ and TNF-α among Vδ1$^+$ and TCR$\alpha\beta^+$ (CD8$\alpha\beta^+$ or CD4$^+$) PBLs before and after gluten challenge. Right: data summarized in box plots displaying the first and third quartiles.

observed for TNF-α production by Vδ1$^+$ IELs (Fig. 2.7A and Fig. 2.4.2A), and no significant inter-group differences were observed with respect to the production of IFN-γ and TNF-α among PBLs (Fig. 2.4.2A). Moreover, neither TCR$\alpha\beta^+$ CD8$\alpha\beta^+$ nor TCR$\alpha\beta^+$ CD4$^+$ IELs displayed enhanced production of IFN-γ in patients with active CeD (Fig. 2.4.2A). These data suggested a gluten-dependent and cell type-restricted gain-of-function among Vδ1$^+$ IELs in patients with active CeD.

To examine the antigen dependency of IFN-γ production among Vδ1$^+$ IELs, we formally challenged four patients with GFD-treated CeD. Small intestinal biopsies were taken before and after the administration of dietary gluten over a period of six weeks. A significant increase in IFN-γ production was observed among Vδ1$^+$ IELs isolated after gluten challenge relative to donor-matched Vδ1$^+$ IELs isolated prior to gluten challenge (Fig. 2B). Moreover, no such chronological differences were observed among donor-matched TCR$\alpha\beta^+$ IELs or among TCR$\alpha\beta^+$ or Vδ1$^+$ PBLs (Fig. 2.7B and Fig. 2.4.2B).

These observations demonstrated that in patients with CeD, dietary gluten drives the accumulation of cytokine-producing Vδ1$^+$ IELs producing IFN-γ in a gluten-dependent manner, providing a basis for why they would not cause tissue damage in patients on a GFD while potentially playing a role in the pathogenesis of active CeD.

Table 2.1: Gene modules

NK Module	Cytokine Module	Transcription Factors	TCR Activation Module
NCR1	*EGF*	*TBX21*	*BCL10*
NCR2	*FGF2*	*GATA3*	*CARD11*
NCR3	*FLT3L*	*FOXP3*	*CD247*
KLRC1	*GCSF*	*RORC*	*CD3D*
KLRC2	*GMCSF*	*EOMES*	*CD3E*

KLRC3	*IFNG*	*STAT1*	*CD3G*
TYROBP	*IL17A*	*STAT2*	*CHUK*
KIR2DL4	*IL4*	*STAT3*	*CSK*
KIR2DL1	*IL5*	*STAT4*	*ENAH*
KIR2DL3	*IL3*	*STAT5*	*EVL*
KIR3DL3	*IL6*	*RUNX1*	*FYB*
KIR3DL2	*IL7*	*RUNX2*	*GRAP2*
KIR3DL1	*CXCL8*	*RUNX3*	*HLA-DPA1*
KIR3DL3	*IL9*	*PLZF*	*HLA-DPB1*
FCGR3A	*MCP3*	*THPOK*	*HLA-DQA1*
GNLY	*CCL4*	*TCF7*	*HLA-DQA2*
CTSW	*CCL3*	*FOXP1*	*HLA-DRB1*
PRF1	*TGFA*	*FOXO1*	*HLA-DRB5*
CD70	*TNFA*	*ELF1*	*IKBKB*
SIT1	*LTA*	*IKAROS*	*IKBKG*
ICAM2	*VEGF*	*ETS1*	*ITK*
SLAMF1	*SPP1*	*SATB1*	*LAT*
GZMA	*IL10*	*IRF4*	*LCK*
GZMB	*AREG*	*IRF8*	*LCP2*
GZMK	*IL33*	*IRF2*	*LOC646626*
CD56	*IL22*	*IRF1*	*MALT1*
PRF1	*IL21*	*IRF3*	*MAP3K7*
FASL	*IL27*	*IRF5*	*NCK1*
	TGFB	*IRF7*	*NFKBIA*
	IL2	*BLIMP1*	*PAG1*
	RANTES	*HOBIT*	*PAK1*

LEF1	*PAK2*
KLF3	*PDPK1*
ZEB2	*PIK3CA*
	PIK3CB
	PIK3R1
	PIK3R2
	PLCG1
	PRKCQ
	PTEN
	PTPRC
	RELA
	RIPK2
	TAB2
	TMEM189-UBE2V1
	TRAF6
	TRAT1
	UBE2N
	VASP
	WAS
	ZAP70
	NR4A1
	CD25
	CD69
	IL7R
	CCR7
	ZAP70

NFKB1

CTLA4

MKI67

PD1/PDCD1

CD137

CD38

CD57

CD5

CD6

CD28

2.4.4 The transcriptional program of Vδ1$^+$ IELs is permanently altered in CeD

To further assess that healthy and CeD Vδ1$^+$ IELs represent different $\gamma\delta$+ T cell subsets, we performed ex vivo RNA sequencing (RNA-seq) on NKp46$^+$ (NCR$^+$) Vδ1$^+$ IELs isolated from healthy controls and NKp46$^-$ (NCR$^-$) Vδ1$^+$ IELs isolated from patients with active or GFD-treated CeD (Fig. 2.5A). A total of 645 genes exhibited differential expression between NCR+ Vδ1$^+$ IELs isolated from healthy controls and NCR$^-$ Vδ1$^+$ IELs isolated from patients with active CeD (Fig. 2.9A). Similar differences in terms of magnitude were observed in comparisons between NCR+ Vδ1$^+$ IELs isolated from healthy controls and NCR$^-$ Vδ1$^+$ IELs isolated from patients with GFD-treated CeD (Fig. 2.9B). Unbiased multidimensional scaling (MDS) analysis (Fig. 2.9C), as well as minimum spanning tree (MST) analysis[103] (Fig. 2.10A), further confirmed that NCR$^+$ Vδ1$^+$ IELs isolated from healthy controls formed distinct clusters relative to NCR$^-$ Vδ1$^+$ IELs isolated from patients with active or GFD-treated CeD (Fig. 2.10A and Fig. 2.9C). Of note, this distribution was

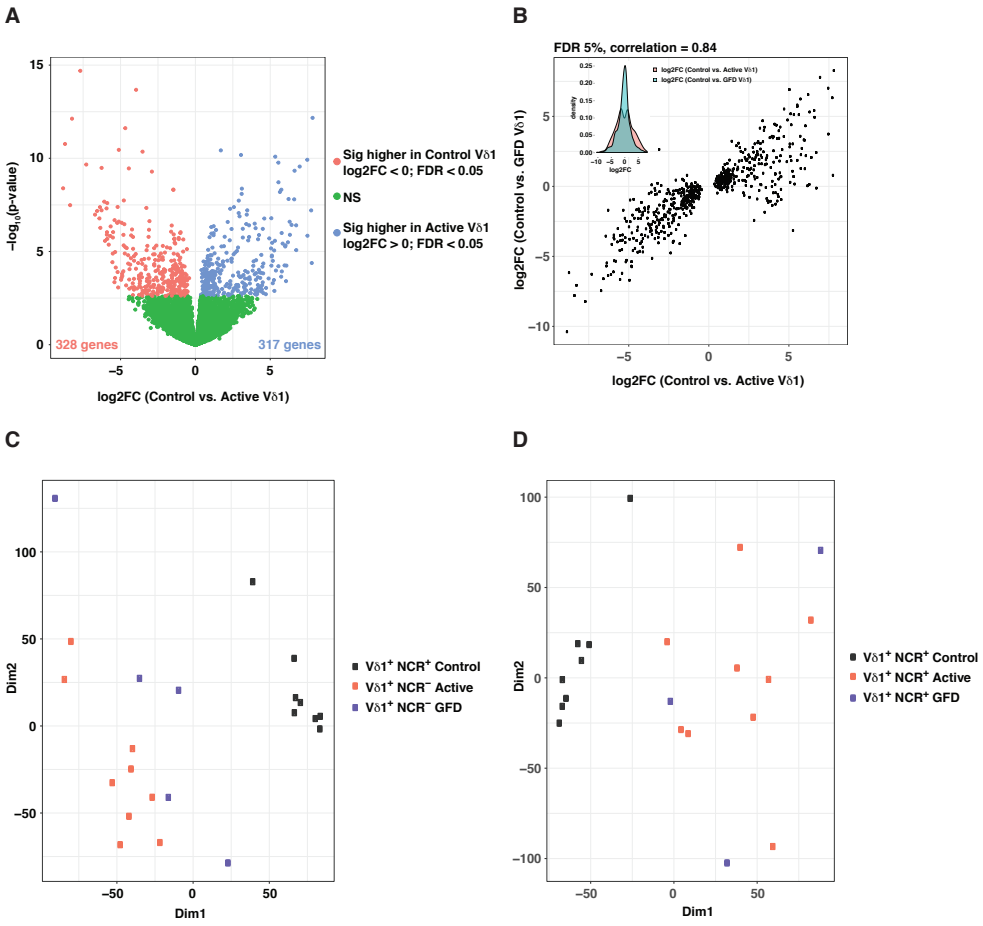

Figure 2.9: The transcriptional program of Vδ1$^+$ IELs is permanently altered in CeD. (**A**) Volcano plot showing differentially expressed genes (DEGs) between NCR$^+$ Vδ1$^+$ IELs isolated from healthy controls (n = 8) and NCR$^-$ Vδ1$^+$ IELs isolated from patients with active CeD (n = 9). DEGs highlighted in blue were more highly expressed in NCR$^-$ Vδ1$^+$ IELs isolated from patients with active CeD (FDR <5%), and DEGs highlighted in red were more highly expressed in NCR$^+$ Vδ1$^+$ IELs isolated from healthy controls (FDR <5%). (**B**) DEGs shown in (A) were used to correlate (Pearson) the magnitude of gene expression differences between NCR$^+$ Vδ1$^+$ IELs isolated from healthy controls and NCR$^-$ Vδ1$^+$ IELs isolated from patients with active CeD (x-axis) versus the magnitude of gene expression differences between NCR$^+$ Vδ1$^+$ IELs isolated from healthy controls and NCR$^-$ Vδ1$^+$ IELs isolated from patients with GFD-treated CeD (y-axis). Genes with log2FC values >0 were more highly expressed in patients with active or GFD-treated CeD relative to healthy controls, and genes with log2FC values <0 were more highly expressed in healthy controls relative to patients with active or GFD-treated CeD. Top left: log2FC distribution for all genes in the dot plot summarized as a histogram for each comparison. (**C**) Multidimensional scaling plot showing gene expression profile similarity among NCR$^+$ Vδ1$^+$ IELs isolated from healthy controls (n = 8), NCR$^-$ Vδ1$^+$ IELs isolated from patients with active CeD (n = 9), and NCR$^-$ Vδ1$^+$ IELs isolated from patients with GFD-treated CeD (n = 5). (**D**) Multidimensional scaling plot showing gene expression profile similarity among NCR$^+$ Vδ1$^+$ IELs isolated from healthy controls (n = 8), NCR$^+$ Vδ1$^+$ IELs isolated from patients with active CeD (n = 9), and NCR$^+$ Vδ1$^+$ IELs isolated from patients with GFD-treated CeD (n = 3).

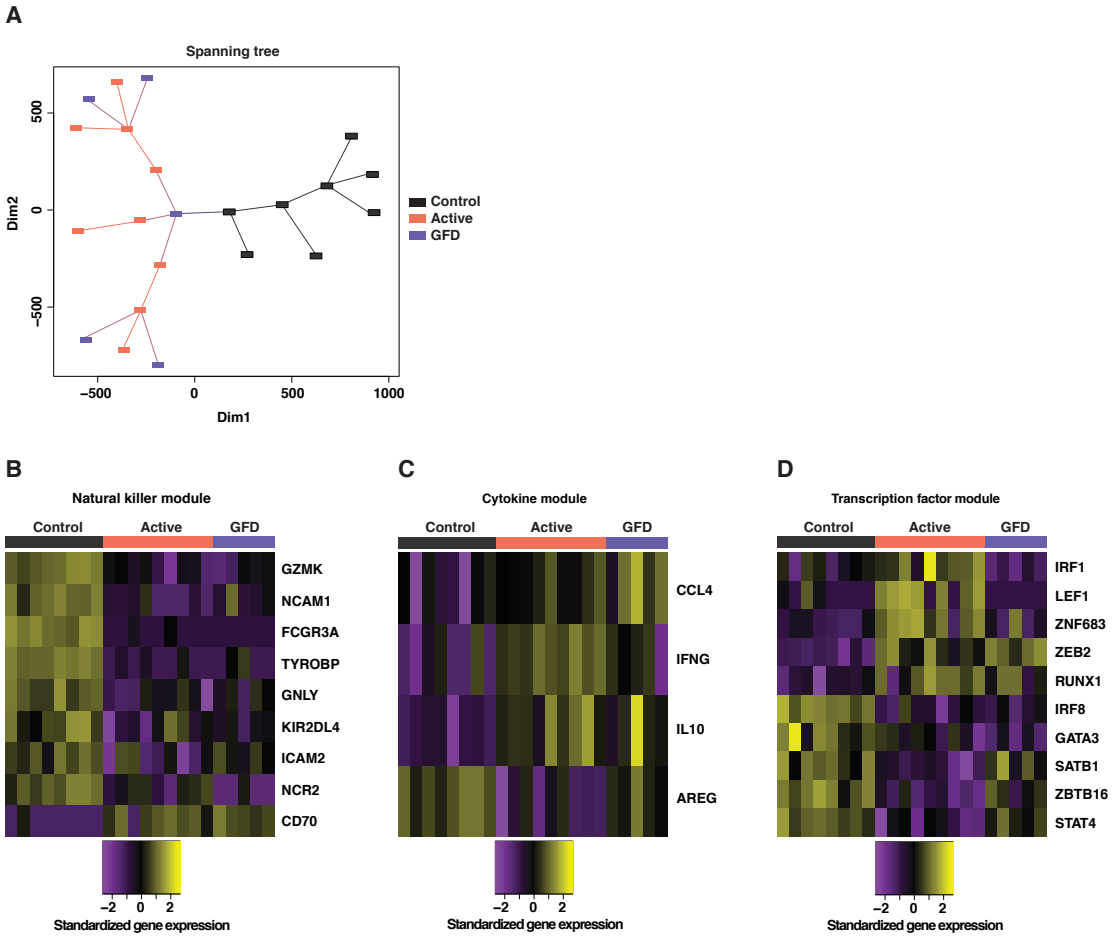

Figure 2.10: The transcriptional program of Vδ1$^+$ IELs is permanently altered in CeD. (**A**) The transcriptional profiles of NCR$^+$ Vδ1$^+$ IELs isolated from healthy controls (n = 8), NCR$^-$ Vδ1$^+$ IELs isolated from patients with active CeD (n = 9), and NCR$^-$ Vδ1$^+$ IELs isolated from patients with GFD-treated (n = 5) were compared in two-dimensional space using minimum spanning tree (MST) analysis. The length of connecting paths displays the dissimilarity between samples. (**B**) A list of differentially expressed genes (DEGs) passing an FDR <10% was generated from any two-way contrast between NCR$^+$ Vδ1$^+$ IELs isolated from healthy controls (n = 8), NCR$^-$ Vδ1$^+$ IELs isolated from patients with active CeD (n = 9), and NCR$^-$ Vδ1$^+$ IELs isolated from patients with GFD-treated CeD (n = 5). This list was then filtered for genes found in our NK module (Table 2.1) and summarized in a heat map. To facilitate visualization across groups, expression values were standardized (mean centered) on a per gene basis. (**C**) Heat map displaying genes from the cytokine module (Table 2.1) that pass the criteria described in (B). (**D**) Heat map displaying genes from the transcription factor module (Table 2.1) that pass the criteria as described in (B).

also conserved in comparisons between NCR$^+$ Vδ1$^+$ IELs isolated from healthy controls and residual NCR$^+$ Vδ1$^+$ IELs isolated from patients with active or GFD-treated CeD (Fig. 2.9D).

Targeted analysis of a subset of genes encoding archetypical NK receptors and cytolytic effector molecules (Table 2.1, NK module) (28), confirmed the innate-like nature and cytolytic

potential of V$\delta1^+$ IELs isolated from healthy controls (Fig. 2.10B). In particular, *GZMK*, *FCGR3A*, and *TYROBP* were significantly overexpressed among NCR$^+$ V$\delta1^+$ IELs isolated from healthy controls relative to NCR$^-$ V$\delta1^+$ IELs isolated from patients with active or GFD-treated CeD (Fig. 2.10B). A similar analysis of genes encoding various cytokines, chemokines, and growth factors (Table 2.1, cytokine module) revealed that *IFNG*, *CCL4*, and *IL10* were significantly overexpressed among NCR$^-$ V$\delta1^+$ IELs isolated from patients with active or GFD-treated CeD relative to NCR$^+$ V$\delta1^+$ IELs isolated from healthy controls (Fig. 2.10C). In contrast, AREG, which encodes amphiregulin, a growth factor implicated in tissue repair[104], was significantly overexpressed in NCR$^+$ V$\delta1^+$ IELs isolated from healthy controls relative to NCR$^-$ V$\delta1^+$ IELs isolated from patients with active or GFD-treated CeD (Fig. 2.10C). Of note, transcripts encoding for IL-17, IL-4, IL-13 and IL-9 were not detected in any of the V$\delta1^+$ IEL subsets studied. Finally, analysis of immunologically relevant transcription factors (Table 2.1, transcription factor module) showed that *IRF8* and *GATA3* transcripts were enriched in healthy control NCR+ V$\delta1^+$ IELs whereas *ZEB2* and *RUNX1* transcripts were enriched in CeD NCR$^-$ V$\delta1^+$IELs (Fig. 2.10D). Interestingly, V$\delta1^+$ IELs isolated from patients with active CeD exhibited a unique profile characterized by higher levels of *IRF1*, *LEF1*, and *ZNF683* expression relative to V$\delta1^+$ IELs isolated from either healthy controls or patients with GFD-treated CeD (Fig. 2.10D).

Collectively, these results demonstrated that disease-associated changes in the corresponding functional profiles were permanently imprinted at the transcriptional level and refractory to gluten exclusion.

Table 2.2: TCR sequencing cohort

Group	Patient ID	Tissue	Age	Sex	HLA	Time on a GFD (years)	Cell number sorted for sequencing
Control	7	IEL	14	F	DQ2.5/DQ2.2		768
Control	7	PBL	14	F	DQ2.5/DQ2.2		4368
Control	13	IEL	18	F	DQ2/DQ8neg		446
Control	13	PBL	18	F	DQ2/DQ8neg		2188
Control	40	IEL	17	F	DQ2/DQ8neg		273
Control	40	PBL	17	F	DQ2/DQ8neg		4542
Control	53	IEL	10	F	DQ8/DQX		1456
Control	53	PBL	10	F	DQ8/DQX		10000
Control	110	IEL	32	M	DQ8/DQ2.5		257
Control	110	PBL	32	M	DQ8/DQ2.5		4361
Control	111	IEL	38	F	DQ8/DQX		257
Control	111	PBL	38	F	DQ8/DQX		1183
Control	144	IEL	10	M	DQ8/DQX		751
Control	144	PBL	10	M	DQ8/DQX		1266
Control	106	IEL	54	F	DQ2/DQ8neg		946
Control	106	PBL	54	F	DQ2/DQ8neg		NA
Active	22	IEL	44	M	DQ2.5/DQX		431
Active	22	PBL	44	M	DQ2.5/DQX		5000
Active	35	IEL	11	M	DQ8/DQ2.5		2238
Active	35	PBL	11	M	DQ8/DQ2.5		6591
Active	46	IEL	19	F	DQ2.5/DQX		5000
Active	46	PBL	19	F	DQ2.5/DQX		5000

Active	47	IEL	13	F	DQ2.5/DQX		10000
Active	47	PBL	13	F	DQ2.5/DQX		10000
Active	51	IEL	51	F	DQ8/DQX		10000
Active	51	PBL	51	F	DQ8/DQX		1394
Active	81	IEL	30	F	DQ2.5/DQ2.2		5000
Active	81	PBL	30	F	DQ2.5/DQ2.2		4012
Active	112	IEL	37	F	DQ2.5/DQX		3625
Active	112	PBL	37	F	DQ2.5/DQX		3625
Active	143	IEL	16	M	DQ2.5/DQX		2843
Active	143	PBL	16	M	DQ2.5/DQX		504
GFD	3	IEL	53	F	DQ2.5/DQX	4	5000
GFD	3	PBL	53	F	DQ2.5/DQX	4	5000
GFD	28	IEL	37	M	DQ2.5/DQX	3	1688
GFD	28	PBL	37	M	DQ2.5/DQX	3	1244
GFD	33	IEL	55	F	DQ2.5/DQX	6	1164
GFD	33	PBL	55	F	DQ2.5/DQX	6	3182
GFD	41	IEL	37	F	DQ2.5/DQ2.5	2	1945
GFD	41	PBL	37	F	DQ2.5/DQ2.5	2	2811
GFD	113	IEL	29	F	DQ8/DQ2.5	4	1356
GFD	113	PBL	29	F	DQ8/DQ2.5	4	1356
GFD	9	IEL	17	M	DQ8/DQ2.5	3	5640
GFD	9	PBL	17	M	DQ8/DQ2.5	3	NA
GFD	43	IEL	31	F	DQ2.5/DQ2.2	4	3001
GFD	43	PBL	31	F	DQ2.5/DQ2.2	4	NA

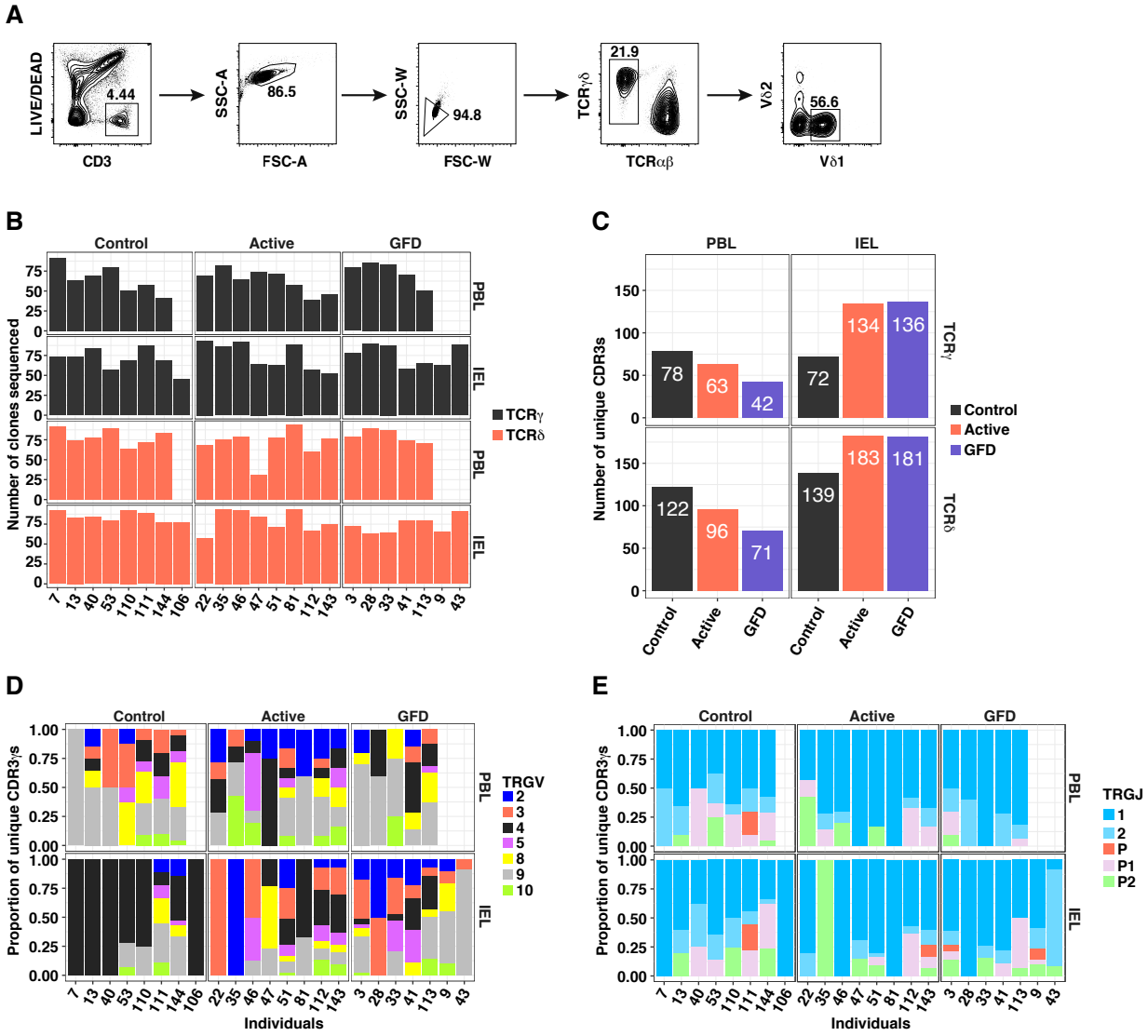

Figure 2.11: The TRGV4 gene-associated gut signature is lost among Vδ1$^+$ IELs in CeD. (**A**) Gating strategy: live CD3$^+$/TCR$\gamma\delta^+$/Vδ1$^+$ lymphocytes were flow-sorted for molecular analysis of expressed TCRs. (**B**) Number of clones per individual/tissue yielding productive sequences for TCRγ and TCRδ. (**C**) Number of unique CDR3 sequences per group/tissue for TCRγ and TCRδ. (**D**) The proportion of unique CDR3γ sequences expressing different γ-chain variable segments (TRGV gene-encoded) summarized in a stacked bar plot by individual (n = 58). (**E**) The proportion of unique CDR3γ sequences expressing different γ-chain TCR joining segments (TRGJ gene-encoded) summarized in a stacked bar plot by individual (n = 58).

2.4.5 The Vδ1$^+$ IEL TCR repertoire is permanently reshaped in CeD

To establish if the switch from NCR$^+$ innate-like Vδ1$^+$ IELs in the healthy state to gluten sensitive IFN-γ producing Vδ1$^+$ IELs in CeD was the reflection of a cellular turnover or an alteration to pre-existing cells, we used an unbiased molecular approach to characterize all expressed TRG and TRD gene rearrangements in flow-sorted Vδ1$^+$ T cell populations isolated directly ex vivo from donor-matched PBLs and IELs (healthy controls, n = 8; patients with active CeD, n = 8; patients with GFD-treated CeD, n = 7; Fig. 2.11A-C and Table 2.2). In healthy controls, we found an extreme preference for TRGV4 gene use among Vδ1$^+$ IELs relative to Vδ1$^+$ PBLs (Fig. 2.4.5A, Fig. 2.11D, and Table 2.5). Irrespective of treatment status, however, no such enrichment was observed in patients with CeD (Fig. 2.4.5A, Fig. 2.11D, and Table 2.5). Accordingly, TRGV4 gene transcripts were significantly reduced among Vδ1$^+$ IELs isolated from patients with active or GFD-treated CeD relative to healthy controls (Fig. 2.4.5A, Fig. 2.11D, and Table 2.5). This disease-associated loss of TRGV4 gene transcripts (Fig. 2.4.5A) was not linked with HLA alleles that predispose to CeD (Table 2.2). In contrast, TRGV3 gene transcripts were significantly less frequent among Vδ1$^+$ IELs isolated from healthy controls relative to Vδ1$^+$ IELs isolated from patients with active CeD (Fig. 2.4.5A, Fig. 2.11D, and Table 2.5). Of note, no TRGJ gene bias was observed among groups or tissues, reflecting widespread use of the TRGJ1 gene segment (Fig. 2.11E and Table 2.6).

Collectively, these data suggested a fundamental and permanent reshaping of the Vδ1$^+$ IEL TCR repertoire in patients with CeD.

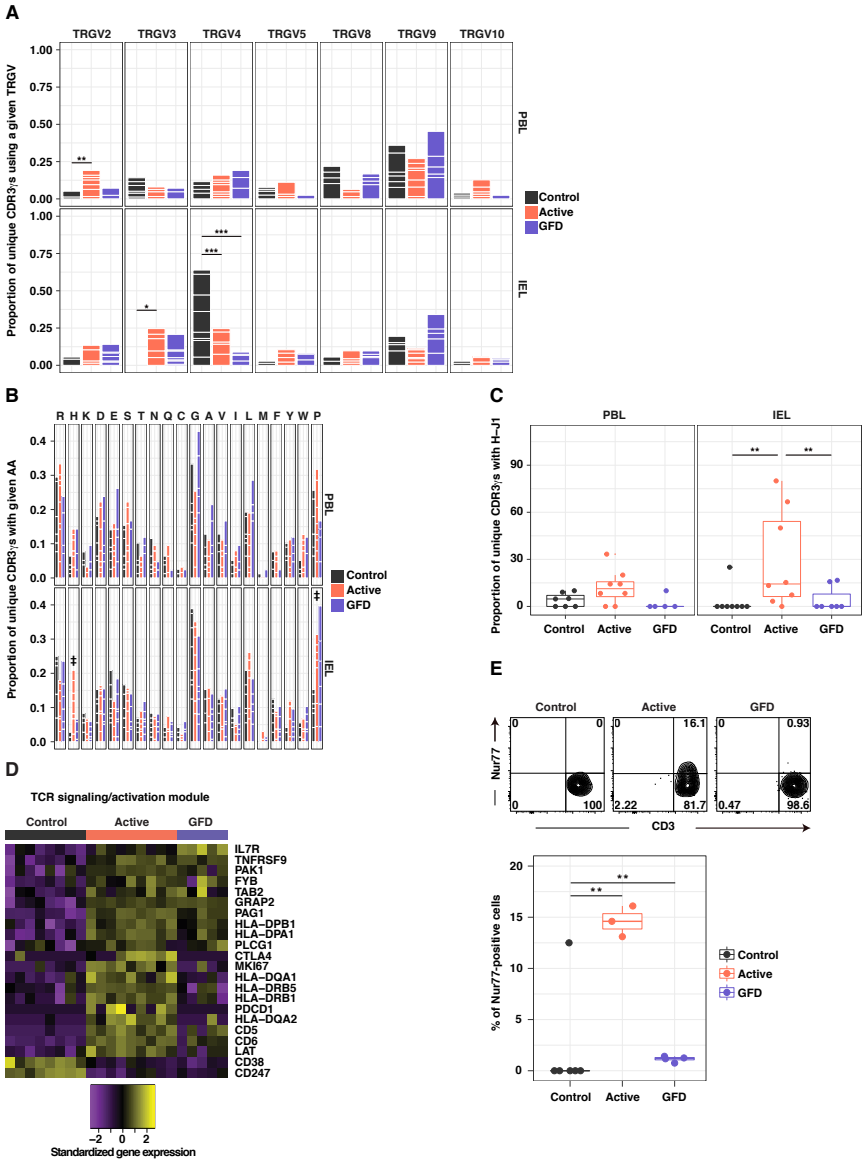

Figure 2.12: The V$\delta1^+$ IEL TCR repertoire is permanently reshaped in CeD.
(**A**) The proportion of unique clones expressing the indicated TRGV genes. White lines demarcate individual contributions to each group. Healthy controls: PBLs, n = 7; IELs, n = 8. Patients with active CeD: PBLs, n = 8; IELs, n = 8. Patients with GFD-treated CeD: PBLs, n = 5; IELs, n = 7. *p<0.05, **p<0.01, ***p<0.001; Firth penalized logistic regression and beta regression. See Table 2.5 for details. (**B**) The proportion of unique CDR3γ sequences using a particular amino acid summarized by group in stacked bar plots. White lines demarcate individual contributions to each group. Healthy controls: PBLs, n = 7; IELs, n = 8. Patients with active CeD: PBLs, n = 8; IELs, n = 8. Patients with GFD-treated CeD: PBLs, n = 5; IELs, n = 7. denotes amino acids that were significantly different between at least two groups, tested using Firth penalized logistic regression and beta regression. See Table 2.9 for details. (**C**) The frequency of unique CDR3γ sequences containing the H-J1 motif summarized in box plots. **p<0.01; Kruskal-Wallis rank sum test followed by Dunns test for multiple comparisons. (**D**) Heat map displaying genes from the TCR activation module (Table 2.1) that pass the criteria described in Fig. 3B. (**E**) Top: representative contour plots showing expression of CD3 and Nur77 in V$\delta1^+$ IELs. Bottom: data summarized in box plots displaying the first and third quartiles. **p<0.01; one-way ANOVA followed by Tukeys test for multiple comparisons.

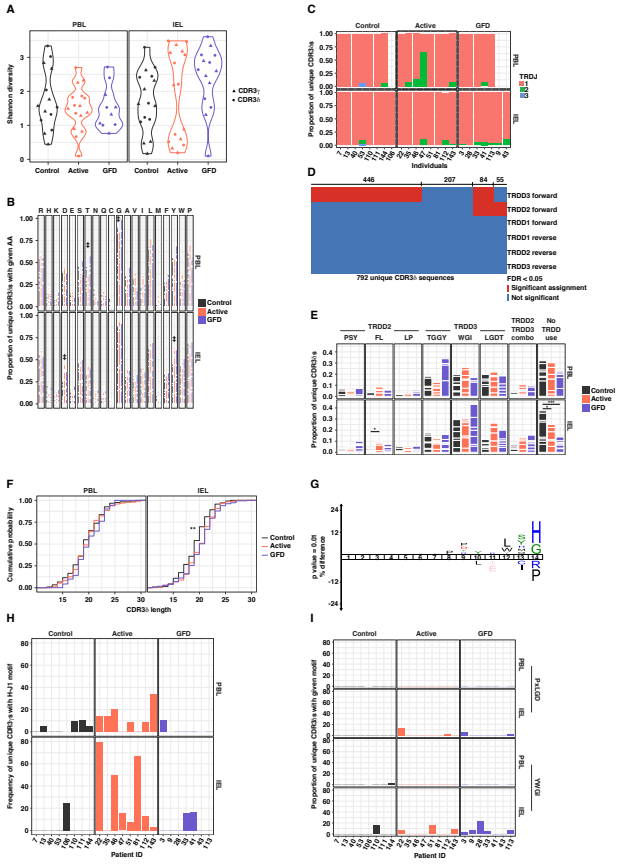

Figure 2.13: Vδ1$^+$ IELs express TCRs with longer CDR3δ loops in CeD.
(**A**) Shannon diversity indices summarized in violin plots for both CDR3γ and CDR3δ sequences. (**B**) The proportion of unique CDR3δ sequences using a particular amino acid summarized by group in a stacked bar plot. White lines demarcate individual contributions to each group. Healthy controls: PBLs, n = 7; IELs, n = 8. Patients with active CeD: PBLs, n = 8; IELs, n = 8. Patients with GFD-treated CeD: PBLs, n = 5; IELs, n = 7. denotes amino acids that were significantly different between at least two groups, tested using Firths penalized logistic regression and beta regression. See Table 2.7 for details. (**C**) The proportion of unique CDR3δ sequences expressing different joining segments (TRDJ gene-encoded) summarized in a stacked bar plot by individual (n = 58). (**D**) Statistical assignment of TRDD gene use for each unique CDR3δ sequence. Each candidate forward and reverse TRDD gene sequence (rows) was tested for a significant substring match to each unique CDR3δ sequence (columns). Significant TRDD gene assignments (FDR <0.05) are shown in red; non-significant TRDD gene assignments (FDR >0.05) are shown in blue. (**E**) The proportion of unique CDR3δ sequences using a given feature summarized by group in a stacked bar plot. White lines demarcate contributions of individuals to each group. Healthy controls: PBLs, n = 7; IELs, n = 8. Patients with active CeD: PBLs, n = 8; IELs, n = 8. Patients with GFD-treated CeD: PBLs, n = 5; IELs, n = 7. **p<0.05, ***p<0.001; Firths penalized logistic regression and beta regression. See Table 2.8 for details. (**F**) Cumulative distribution for CDR3δ length across groups. **p<0.01; Kolmogorov-Smirnov test. (**G**) Unique CDR3γ sequences among Vδ1$^+$ IELs isolated from patients with CeD visualized using iceLogo for enrichment of non-germline-encoded amino acids relative to unique CDR3γ sequences among Vδ1$^+$ IELs isolated from healthy controls and patients with GFD-treated CeD. Position 14 is closest to the TRGJ gene-encoded segment. (**H**) The frequency of unique CDR3Vγ sequences with an H-J1 motif summarized by individual, tissue, and group in bar plots. (**I**) The frequency of unique CDR3Vδ1$^+$ sequences with either a CxxxxxPxLGD (PxLGD) or a CxxxxxxxxYWGI (YWGI) motif summarized by individual, tissue, and group in bar plots.

2.4.6 A molecular signature defines Vδ1$^+$ IEL TCRs in active CeD

We next sought evidence of antigen-driven clonal expansions within the remodeled Vδ1$^+$ IEL TCR repertoires in patients with CeD. The median Shannon diversity index was substantially lower among Vδ1$^+$ IELs isolated from a subset of patients with active CeD and substantially higher among Vδ1$^+$ IELs isolated from most patients with GFD-treated CeD (Fig. 2.4.5A). These results suggested that gluten consumption stimulated the expansion of particular clonotypes in the Vδ1$^+$ IEL pool, at least in some patients with active CeD, while gluten withdrawal allowed diversification of the intra-epithelial repertoire, potentially via a loss of antigenic drive and/or de novo recruitment of non-expanded Vδ1$^+$ IELs.

In further analyses, we tested for amino acid (AA) preferences among unique CDR3δ sequences to identify Vδ1$^+$ TCR motifs associated with active CeD. No group-specific AA enrichments were detected to indicate a gluten-specific molecular signature (Fig. 2.4.5B and Table 2.7). Of note, TRDJ1 was dominant in our data set across study groups (Fig. 2.4.5B). At the genetic level, preferential use of TRDD3 in the forward frame and, to a lesser extent, TRDD2 in the forward frame was observed across the CDR3δ dataset as a whole (Fig. 2.4.5D). However, there was no evidence for preferential use of a specific TRDD gene among Vδ1$^+$ IELs isolated from patients with active CeD relative to healthy control and GFD-treated Vδ1$^+$ IELs (Fig. 2.4.5E). Overall, these data suggested that gluten-induced reshaping of the Vδ1$^+$ T cell repertoire was not associated with a clear CDR3δ motif. However, healthy control Vδ1$^+$ IELs displayed shorter CDR3δ sequences relative to CeD Vδ1$^+$ IELs (Fig. 2.4.5F). Accordingly, the fraction of Vδ1$^+$ IEL-derived CDR3δ sequences that incorporated no TRDD gene-encoded AAs was significantly higher in healthy controls relative to patients with CeD (Fig. 2.4.5E and Table 2.8).

In contrast, a similar analysis of CDR3γ sequences revealed an enrichment of histidine (H)

Table 2.3: Dominant H-J1$^+$ CDR3γ clones among patients with active CeD

Group	Patient ID	Tissue	TRGV	CDR3	TRGJ	Frequency of clone
Active	22	IEL	3	CATWDRLPHYKKLF	1	80.85 (76/94)
Active	46	IEL	3	CATWDGWRHKKLF	1	65.22 (60/92)
Active	47	IEL	4	CATWSHYYKKLF	1	28.12 (18/64)
Active	81	IEL	4	CATWDHYKKLF	1	92.13 (82/89)
Active	35	PBL	4	CATWDGPHYKKLF	1	44.44 (36/81)
Active	46	PBL	5	CATWDRHYKKLF	1	44.60 (29/65)
Active	143	PBL	9	CALWEAPWLRGPGWHYYKKLF	1	41.30 (19/46)

Table 2.4: Overlapping CD3γ sequences carrying the H-J1 motif

Group	Patient ID	Tissue	TRGV	CDR3	TRJV	Frequency of clone
Active	22	PBL	9	C A L W E V H Y Y K K L F tgt gcc ttg tgg gag gtg cat tat tat aag aaa ctc ttt	1	7.2% (5/69)
GFD	3	PBL	9	C A L W E V H Y Y K K L F tgt gcc ttg tgg gag gtg cat tat tat aag aaa ctc ttt	1	1.25% (1/80)
Active	47	IEL	4	C A T W S H Y Y K K L F tgt gcc acc tgg tcc cac tat tat aag aaa ctc ttt	1	28.1% (18/64)
Active	51	IEL	3	C A T W S H Y Y K K L F tgt gcc acc tgg tcg cat tat tat aag aaa ctc ttt	1	3.17% (2/63)
Active	46	PBL	5	C A T W D R H Y K K L F tgt gcc acc tgg gac agg cat tat aag aaa ctc ttt	1	44.61% (29/65)
Active	51	IEL	2	C A T W D R H Y K K L F tgt gcc acc tgg gac cgc cac tat aag aaa ctc ttt	1	1.59% (1/63)
Active	35	PBL	4	C A T W D G P H Y K K L F tgt gcc acc tgg gat ggg ccg cat tat aag aaa ctc ttt	1	44.44% (36/81)
Active	143	IEL	2	C A T W D G P H Y K K L F tgt gcc acc tgg gac ggg ccg cat tat aag aaa ctc ttt	1	1.89% (1/53)

in the V$\delta1^+$ IEL-derived repertoires obtained from patients with active CeD relative to repertoires obtained from healthy controls and patients with GFD-treated CeD (Fig. 2.4.5B and Table 2.9). This observation was supported by iceLogo motif analysis[105], which revealed a significant enrichment for H adjacent to the Jγ segment among CDR3γ sequences obtained from patients with active CeD (Fig. 2.4.5F). Analysis of the 27 public CDR3γ sequences in our data set (Table 2.10) revealed that 4 public TCRs shared between 6 active CeD patients carried the H. Notably, the H was found adjacent to the Jγ segment 1 (TRGJ1) (H-J1 motif) (Table 2.4), and the H-J1 carrying CDR3γ sequences associated with various TRGV gene segments (Table 2.4). We next wanted to determine whether V$\delta1^+$ IEL TCRs harboring the H-J1 motif were specific to CeD and expanded in patients with active CeD. First, a significantly higher fraction of unique CDR3γ sequences carried the H-J1 motif in the V$\delta1^+$ IEL-derived repertoires obtained from patients with active CeD relative to both the V$\delta1^+$ IEL-derived repertoires obtained from healthy controls and GFD-treated CeD (Fig. 2.4.5C). More specifically, H-J1$^+$ CDR3γ sequences were present in seven patients with active CeD (87.5%) and two patients with GFD-treated CeD (25%) (Fig. 2.4.5C and Fig. 2.4.5H). Interestingly, the H-J1 motif was found in both HLA-DQ2 and HLA-DQ8 CeD patients (Fig. 2.4.5H and Table 2.2), suggesting that a specific HLA-DQ molecule does not select for TCRs harboring the H-J1 motif. To identify evidence of motif-driven clonal expansions in patients with CeD, we conducted a frequency-based analysis. The most common V$\delta1^+$ IEL-derived CDR3γ sequence detected in four patients with active CeD (50%) incorporated the H-J1 motif (Table 2.3). Similarly, the most common V$\delta1^+$ PBL-derived CDR3γ sequence detected in three patients with active CeD (37.5%) incorporated the H-J1 motif (Table 2.3). In contrast, two previously described CDR3γ motifs associated with gluten challenge, CxxxxxPxLGD (PxLGD) and CxxxxxxxxYWGI (YWGI)[106], were distributed at low frequencies in the corresponding V$\delta1^+$ repertoires obtained from patients with active or GFD-treated CeD (Fig. 2.4.5I).

In summary, these observations indicated that gluten-induced reshaping of the intraepithelial V$\delta1^+$ compartment was associated with preferential recruitment and/or expansion of clonotypes bearing the H-J1+ CDR3γ motif that receded upon gluten withdrawal. The pattern of mosaicism (same CDR3 but different TRGV) observed for H-J1$^+$ bearing TCRs (Table 2.4) hinted at a unique selection pressure focused on the somatically rearranged CDR3γ loop in patients with CeD, in contrast to the observed selection pressure on the germline encoded portion of the γ-chain for healthy V$\delta1^+$ IELs in the form of an enrichment for TRGV4 usage (Fig. 2.4.5A). Importantly, these data put forward evidence that the expansion of V$\delta1^+$ IELs in CeD is not merely a secondary response to cytokines in the inflammatory milieu but rather a specific response to a CeD specific antigen, and suggest a role for TCR$\gamma\delta^+$ specificity in the pathogenesis of CeD.

2.4.7 V$\delta1^+$ IELs display hallmarks of TCR-mediated activation in patients with CeD

The combined observations that V$\delta1^+$ IELs acquired the ability to produce IFN-γ in response to gluten challenge (Fig. 2.7B) and preferentially incorporated clonotypes bearing a shared H-J1$^+$ CDR3γ motif in patients with CeD (Table 2.3) suggested the possibility of *in vivo* activation via the TCR. Analysis of a set of genes associated with T cell activation and TCR signaling[107] showed that NCR$^-$ V$\delta1^+$ IELs isolated from patients with active CeD significantly overexpressed transcripts associated with antigenic stimulation relative to NCR$^+$ V$\delta1^+$ IELs isolated from healthy controls (Fig. 2.4.5D). Genes such as *MKI67*, *CTLA4*, and *PDCD1* were not only expressed at lower levels in NCR$^+$ V$\delta1^+$ IELs isolated from healthy controls but also in NCR$^-$ V$\delta1^+$ IELs isolated from patients with GFD-treated CeD relative to active CeD (Fig. 2.4.5D), suggesting a decreased activation status that fits with the lack of selection pressure observed for GFD CeD TCRs (Fig. 2.4.5A and Fig. 2.4.5C). Analysis of the transcription factor Nur77 expression, which is commonly used as a proxy for

TCR-mediated activation[108], further supported a direct link between gluten exposure and the activation status of NCR$^-$ Vδ1$^+$ IELs (Fig. 2.4.5E). Collectively, these data provided additional evidence that specific TCR engagement contributed to the activation of Vδ1$^+$ IELs observed in the setting of CeD.

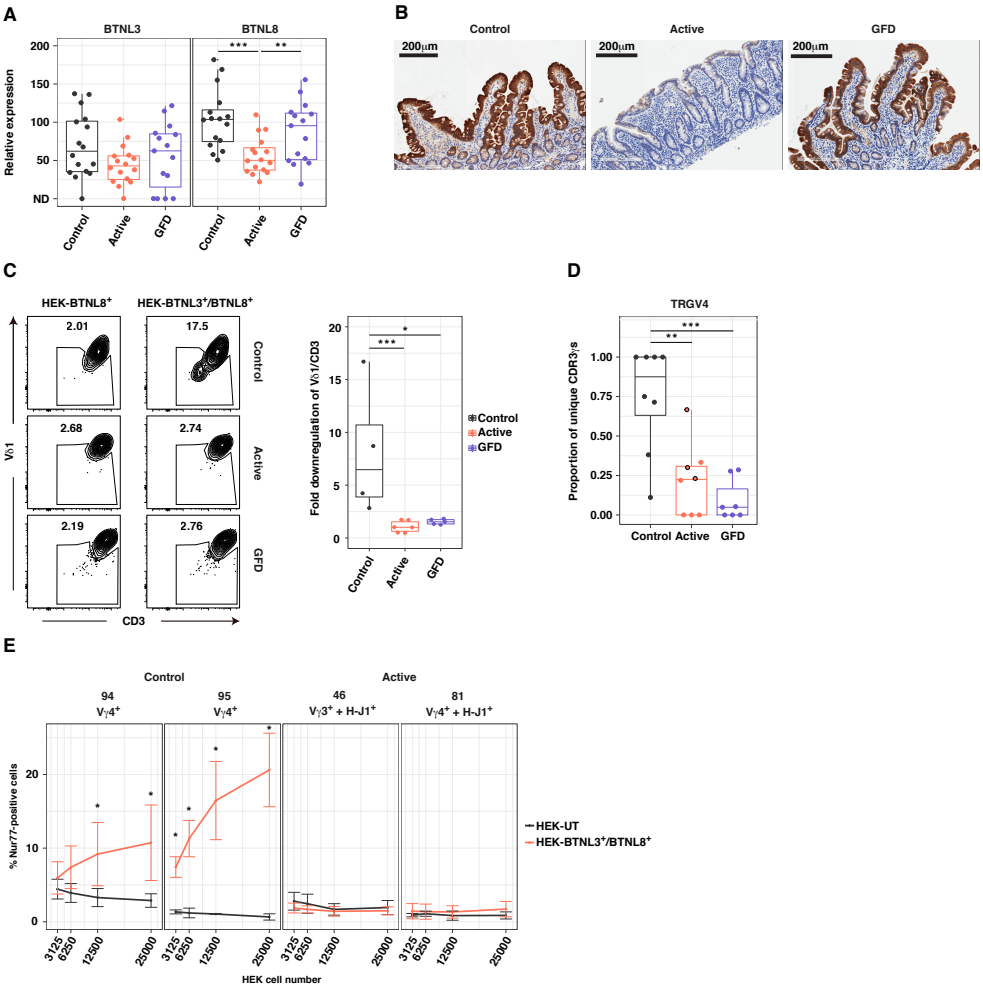

Figure 2.14: BTNL3/8-reactive Vδ1$^+$ IELs are lost in CeD.
(**A**) Quantitative PCR for BTNL3 and BTNL8 was performed on RNA extracted from small intestinal biopsies. Data are shown relative to expression of the housekeeping gene GAPDH. Box plots display the first and third quartiles. **p<0.01, ***p<0.001; Kruskal-Wallis rank sum test followed by Dunns test for multiple comparisons. (**B**) Immunohistochemical analysis of BTNL8 expression on duodenal sections obtained healthy controls and patients with active or GFD-treated CeD. (**C**) The proportion of unique CDR3γ sequences expressing TRGV4 gene transcripts summarized by group in box plots displaying the first and third quartiles. Circles highlighted in black for patients with active CeD denote instances where the dominant TRGV4 transcript contained the H-J1 motif. (**D**) *ex vivo* isolated IELs were co-cultured with HEK293T-BTNL8$^+$ or HEK293T-BTNL3/8$^+$ for 24hrs. Left: representative contour plots showing expression of CD3 and Vδ1 on Vδ1$^+$ IELs. Gating strategy was patient specific and set based on the HEK293T-BTNL8$^+$ condition. Right: data is summarized in box plots displaying the first and third quartiles. *p<0.05, ***p<0.001; Kruskal-Wallis rank sum test followed by Dunns test for multiple comparisons. (**E**) SKW3 cell lines stably expressing clonal TCRs were cultured with varying numbers of untransduced HEK293T cells (HEK293T-UT) or HEK293T cells transduced with both BTNL3 and BTNL8 (HEK293T-BTNL3/8$^+$). Data are summarized for expression of Nur77 from 35 independent experiments per TCR. *p<0.05; paired T-test comparing responses to HEK293T-UT versus HEK293T-BTNL3/8$^+$.

2.4.8 BTNL3/8-reactive Vδ1$^+$ IELs are permanently lost in CeD

Recent studies have shown that butyrophilin (BTN) and butyrophilin-like (BTNL) molecules play a key role in $\gamma\delta$ T cell biology[20,109]. In line with the notion that human colonic Vγ4$^+$ IELs may be selected by BTNL molecules expressed on intestinal epithelial cells (IECs)[20], we found that the loss of TRGV4 gene transcripts in the Vδ1$^+$ IELs isolated from patients with active CeD (Fig. 2.4.5A) was associated with a decrease in BTNL8 gene transcripts (Fig. 2.4.7A) and protein expression levels in the small intestine (Fig. 2.4.7B). Moreover, gluten withdrawal failed to restore *TRGV4* gene use among Vδ1$^+$ IELs, despite normalization of BTNL8 expression (Fig. 2.4.7A-B and Fig. 2.4.8A), suggesting that the recovery of BTNL molecules after exclusion of dietary gluten was insufficient to reconstitute the niche that selects naturally-occurring Vγ4$^+$/Vδ1$^+$ IELs. In line with the notion that once the niche for Vγ4$^+$/Vδ1$^+$ IELs is lost it cannot be reestablished, the Vγ7$^+$ IEL subset (the mouse homolog of human Vγ4$^+$ IELs) failed to be rescued when expression of BTNL molecules was delayed until after the neonatal period where Vγ7$^+$ IEL expansion normally occurs in mice[20].

To further confirm that BTNL3/8-reactive Vδ1$^+$ IELs are permanently lost in CeD, we cultured HEK-293T cells stably expressing either BTNL8 alone or BTNL3 and BTNL8 with freshly isolated Vδ1$^+$ IELs from healthy controls and patients with active CeD (Fig. 2.4.7C and Fig. 2.4.8B), and assessed TCR activation using CD3 downregulation as a proxy[20]. In contrast to Vδ1$^+$ IELs isolated from healthy controls, Vδ1$^+$ IELs isolated from patients with active or GFD-treated CeD were not activated in the presence of BTNL3/8 (Fig. 2.4.7C), despite efficient stimulation via generic cross-linking of the TCR (Fig. 2.4.8C). Moreover, akin to the site-specific depletion of NCR$^+$ Vδ1$^+$ IELs (Fig. 2.5B), BTNL3/8-reactive Vδ1$^+$ IELs were lost from the duodenum, but not the colon, in patients with GFD-treated CeD (Fig. 2.4.8D). These data suggested that the duodenum, like the colon[20], harbored

BTNL3/8-reactive Vγ4$^+$/Vδ1$^+$ IELs under homeostatic conditions, and that expression of BTNL3/8 molecules was required to maintain the *TRGV4* gene-associated gut signature among Vδ1$^+$ IELs.

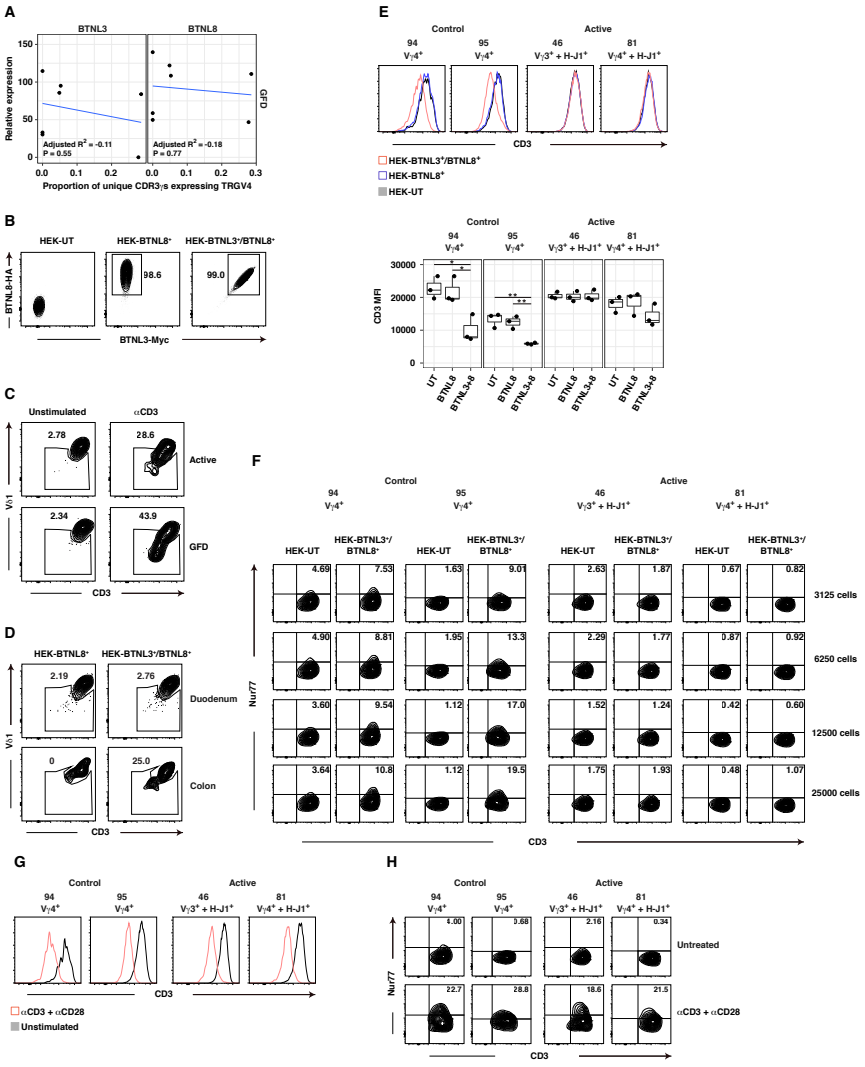

Figure 2.15: BTNL3/8-reactive Vδ1$^+$ IELs are lost in CeD.
(**A**) The proportion of unique CDR3γ sequences expressing TRGV4 transcripts plotted versus relative expression of BTNL3 and BTNL8 for patients with GFD-treated CeD (n = 7). Correlations were tested using linear regression. (**B**) Representative contour plots showing surface expression of BTNL3 (myc$^+$) and BTNL8 (HA$^+$) on untransduced (UT) HEK293T cells (left), HEK293T cells transduced with BTNL8-HA (middle), or HEK293T cells transduced with BTNL3-myc and BTNL8-HA (right). (**C**) Freshly isolated IELs were simulated for 2 hr with 1.5 g/mL of plate-bound purified αCD3. Contour plots display expression of CD3 and Vδ1 on Vδ1$^+$ IELs. (**D**) Freshly isolated IELs were co-cultured for 24 hr with HEK293T-BTNL8$^+$ or HEK293T-BTNL3/8$^+$ cells. Contour plots display expression of CD3 and Vδ1 on Vδ1$^+$ IELs. (**E**) SKW3 cell lines stably expressing clonal TCRs were co-cultured for 24 hr with HEK293T-UT (black), HEK293T-BTNL8$^+$ (purple), or HEK293T-BTNL3/8$^+$ cells (red). Top: representative histogram overlays displaying surface expression of CD3 on SKW3 cells. Bottom: data summarized from three independent experiments. *p<0.05, **p<0.01; one-way ANOVA followed by Tukeys test for multiple comparisons. (**F**) SKW3 cell lines stably expressing clonal TCRs were co-cultured for 2 hr with varying numbers of HEK293T-UT or HEK293T-BTNL3/8$^+$ cells. Representative contour plots from a single experiment display expression of CD3 and Nur77. (**G**) Histogram overlays showing surface expression of CD3 on unstimulated (black) or αCD3/αCD28-stimulated SKW3 T cells (red) transduced with the indicated TCRs. (**H**) Representative contour plots showing surface expression of CD3 and intracellular expression of Nur77 for the indicated SKW transductants co-cultured with HEK293T-UT cells (untreated) or stimulated with αCD3/αCD28 beads.

Interestingly, in the instances where Vγ4$^+$/Vδ1$^+$ IELs were present in active CeD patients they expressed TCRs that were enriched for the H-J1 motif (Fig. 5D). As it was shown that Vγ4$^+$ T cells isolated from healthy human colon react to BTNL3/8 molecules[20], we formally test whether active CeD derived Vγ4$^+$/Vδ1$^+$ TCRs harboring the H-J1 motif were capable of recognizing BTNL3/8 molecules. Accordingly, we generated a set of SKW3 T cell clones stably expressing representative TCRs. More specifically, we tested two Vγ4$^+$/Vδ1$^+$ TCRs isolated from healthy controls, a Vγ3$^+$/Vδ1$^+$ TCR isolated from an active CeD patient, and most importantly a Vγ4$^+$/Vδ1$^+$ H-J1 carrying TCR that accounted for greater than 65% of unique sequences in an active CeD patient (Fig. 2.4.7E and Fig. 2.11D). SKW3 T cells were incubated with HEK-293T cells stably expressing both BTNL3 and BTNL8, and functional interactions were quantified using flow cytometry to measure the downregulation of CD3 (Fig. 2.4.8E) and the induction of Nur77 (Fig. 2.4.7E). As expected, the two Vγ4$^+$/Vδ1$^+$ IEL-derived TCRs reconstructed from healthy controls triggered dose-dependent responses to BTNL3/8 (Fig. 2.4.7E, Fig. 2.4.8E, and Fig. 2.4.8F), whereas the Vγ3$^+$/Vδ1$^+$ IEL-derived TCR reconstructed from a patient with active CeD failed to recognize BTNL3/8 (Fig. 2.4.7E, Fig. 2.4.8E, and Fig. 2.4.8F). Most strikingly, the Vγ4$^+$/Vδ1$^+$ IEL-derived TCR incorporating the CeD-associated H-J1$^+$ CDR3γ motif failed to recognize BTNL3/8 (Fig. 2.4.7E, Fig. 2.4.8E, and Fig. 2.4.8F). Of note, all expressed TCRs transduced a functional signal in the presence of αCD3/αCD28 beads (Fig. 2.4.8G and Fig. 2.4.8H).

These results provided direct evidence to support the contention that gluten-induced remodeling of the Vδ1$^+$ IEL compartment in patients with CeD was linked with a loss of productive TCR-mediated interactions with BTNL3/8.

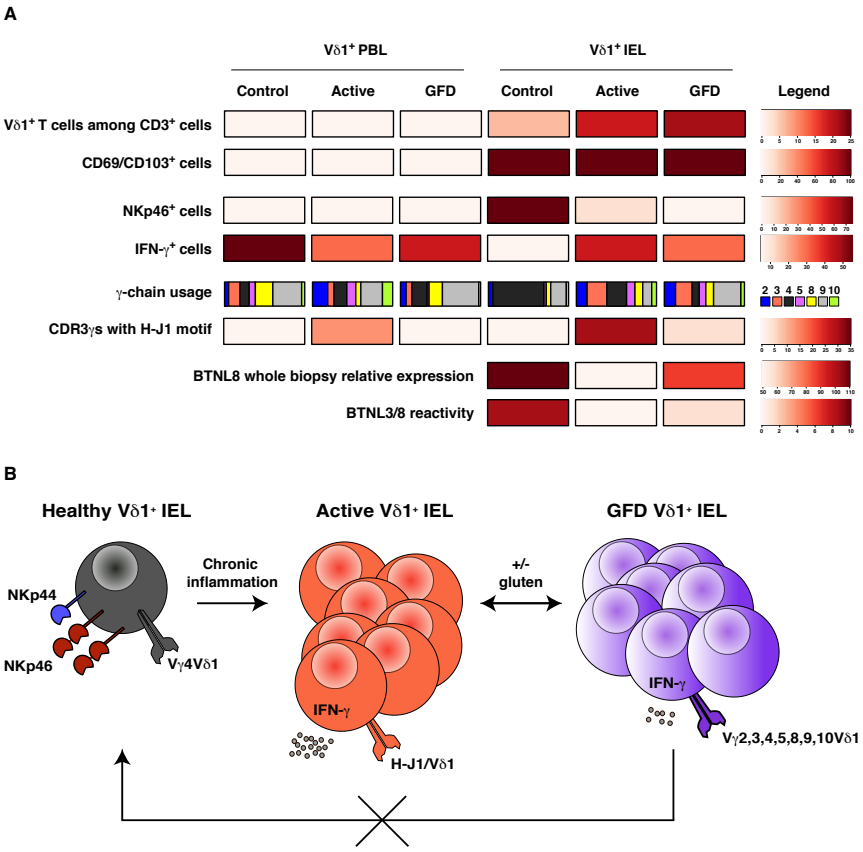

Figure 2.16: The tissue-resident Vδ1$^+$ IEL compartment is permanently reshaped in CeD. (**A**) Top: Vδ1$^+$ IELs are expanded in patients with CeD and adopt a tissue-resident phenotype characterized by expression of CD69 and CD103. Mean frequency values are summarized by group/tissue. Middle/top: Vδ1$^+$ IELs expressing NKp46 are lost in CeD and replaced by IFN-δ-producing Vδ1$^+$ IELs. Mean frequency values are summarized by group/tissue. Middle/bottom: Vδ1$^+$ IELs lose the TRGV4 gene-associated gut signature in patients with CeD (data summarized by group). This loss is associated with the emergence of CDR3γ sequences incorporating the H-J1 motif among Vδ1$^+$ IELs in patients with active CeD. These H-J1$^+$ CDR3γ sequences become less common after exclusion of dietary gluten. Bottom: BTNL8 expression is lost in patients with active CeD, and Vδ1$^+$ IELs no longer recognize BTNL3/8. Although BTNL8 expression levels recover on a strict GFD, BTNL3/8 reactivity is permanently lost among Vδ1$^+$ IELs. (**B**) Vδ1$^+$ IELs in the healthy state (black) express NKp46 and NKp44, as well as Vγ4$^+$/Vδ1$^+$ TCRs that recognize BTNL3/8. These activating NCRs allow healthy Vδ1$^+$ IELs to recognize and eliminate stressed, infected, or malignant IECs. In patients with CeD, decreased expression of BTNL3 and BTNL8 is accompanied by a loss of Vγ4$^+$/Vδ1$^+$ IELs, which are replaced by Vδ1$^+$ IELs (red) that produce IFN-γ in a gluten-dependent manner and express TCRγ chains enriched for the H-J1$^+$ CDR3γ motif that fail to recognize BTNL3/8. These H-J1$^+$ Vδ1$^+$ IELs contract after withdrawal of dietary gluten, but are not replaced by NCR+ Vγ4$^+$/Vδ1$^+$ IELs. Instead, Vδ1$^+$ IELs in patients with GFD-treated CeD are enriched for TCRs that fail to recognize BTNL3/8. Repertoire diversity also increases (purple color gradient), suggesting of a lack of selection pressure in the absence of gluten-induced inflammation. This model is consistent with a fundamental reshaping of the tissue-resident Vδ1$^+$ IEL compartment after the onset of CeD.

2.4.9 Dynamic remodeling of the Vδ1$^+$ IEL compartment precedes tissue damage in CeD

The Vδ1$^+$ IEL compartment underwent dynamic changes both during the chronic inflammatory process associated with active CeD and during the resolution phase associated with strict adherence to a GFD (Fig. 2.4.8A and Fig. 2.4.8B). However, it was still unclear whether these alterations were causally or reactively linked with tissue damage. To address this issue, we analyzed patients with potential CeD (Fig. 2.4.9), defined as a state of CD4+ T cell-mediated intolerance to dietary gluten without histological evidence of villous atrophy[83,84]. Potential CeD encompasses a heterogeneous group of patients with a wide range of Vδ1$^+$ IEL infiltration that is overall significantly increased compared to healthy controls (Fig. 2.4.9A). Furthermore, potential CeD patients display to different degrees the loss of BTNL8 gene transcripts in the duodenum (Fig. S12B), loss of Vδ1$^+$ IEL expressing NCRs (Fig. 2.4.9C), and TRGV4 gene transcripts (Fig. 2.4.9D). This heterogeneity is exemplified by two potential CeD patients, where one patient exhibited an expansion of BTNL3/8-reactive NCR+ Vδ1$^+$ IEL with conserved ex vivo reactivity to BTNL3/8, while the other patient had normal numbers of Vδ1$^+$ IEL but they lacked NCR expression and were not BTNL3/8-reactive (Fig. 2.4.9E). These observations suggest loss of the naturally occurring innate like Vδ1$^+$ IEL subset may precede the adaptive Vδ1$^+$ IEL response. This is supported by the finding occasional Vδ1$^+$ IEL clonotypes bearing the H-J1 CDR3γ motif are found in potential CeD patients (Fig. 2.4.9F). Together, these data suggested that gluten intolerance was associated with a dynamic remodeling of the Vδ1$^+$ IEL compartment prior to the development of tissue destruction in patients with potential CeD.

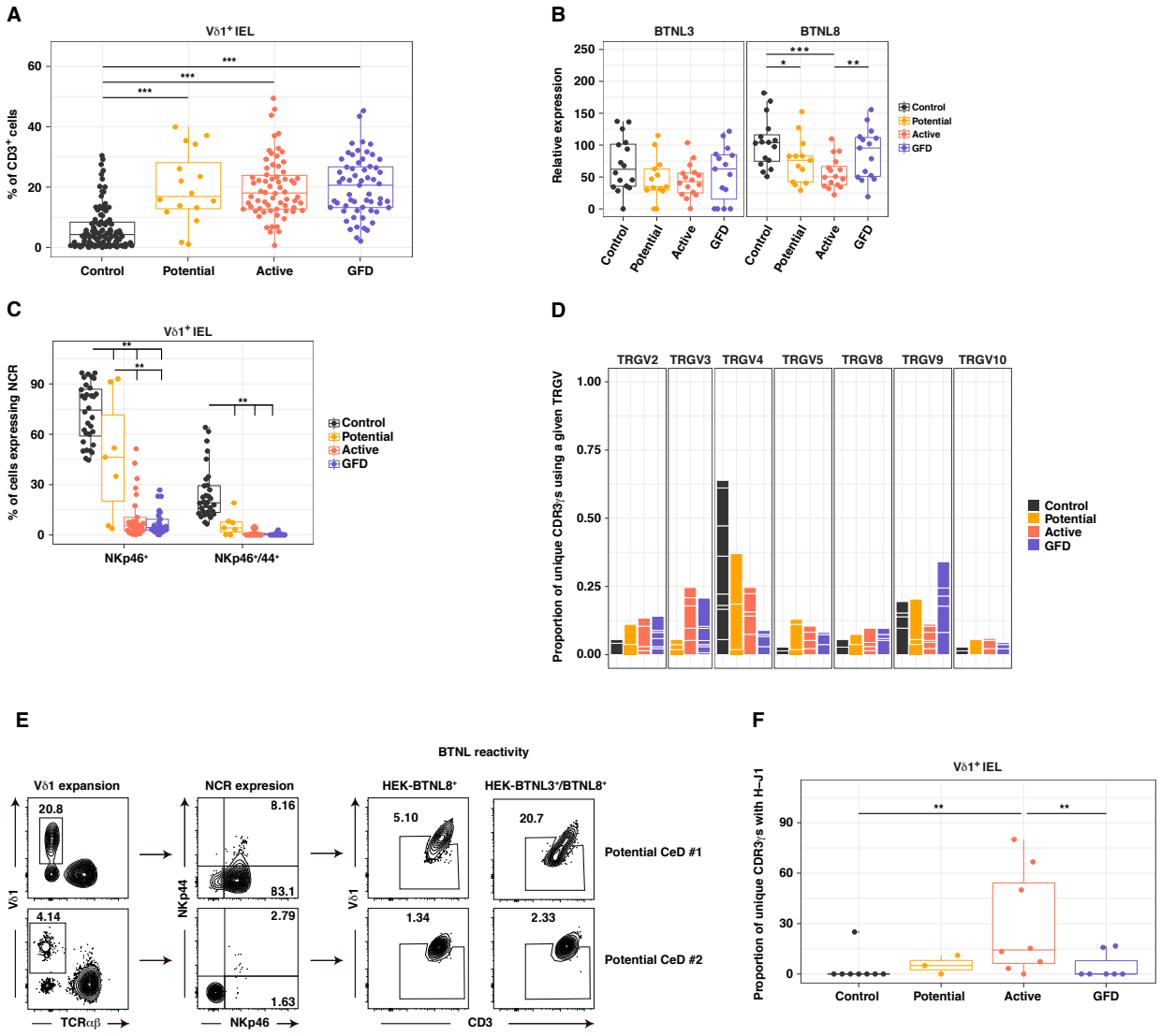

Figure 2.17: Alterations to the Vδ1$^+$ IEL compartment precede tissue damage in CeD.
(**A**) Frequency of Vδ1$^+$ cells among total CD3$^+$ lymphocytes. Data are summarized in box plots displaying the first and third quartiles. ***p<0.001; one-way ANOVA followed by Tukeys test for multiple comparisons. (**B**) Quantitative PCR for BTNL3 and BTNL8 was performed on RNA extracted from small intestinal biopsies. Data are shown relative to expression of the housekeeping gene GAPDH. Box plots display the first and third quartiles. *p<0.05, ***p<0.001; Kruskal-Wallis rank sum test followed by Dunns test for multiple comparisons. (**C**) Frequency of Vδ1$^+$ IELs expressing NKp46 and NKp44 summarized in box plots displaying the first and third quartiles. **p<0.01; one-way ANOVA followed by Tukeys test for multiple comparisons. (**D**) The proportion of unique IEL clones expressing the indicated TRGV genes. White lines demarcate individual contributions to each group. Healthy controls: n = 8. Patients with potential CeD: n = 3. Patients with active CeD: n = 8. Patients with GFD-treated CeD: n = 7. (**E**) Contour plots showing expression of NKp46 and NKp44 on Vδ1$^+$ IELs (left) and expression of CD3 and Vδ1 after *ex vivo* co-culture of IELs for 24 hr with HEK293T-BTNL8$^+$ or HEK293T-BTNL3/8$^+$ cells (right) for two patients with potential CeD. (**F**) The frequency of unique CDR3γ sequences incorporating the H-J1 motif summarized in box plots. **p<0.01; Kruskal-Wallis rank sum test followed by Dunns test for multiple comparisons.

2.5 Discussion

In addition to lacking the capacity for re-circulation, tissue-resident lymphocytes are thought to be stable, long-lived populations[1]. This model of stability would have to accommodate the persistence of tissue-resident lymphocytes in the face of constant insults at barrier surfaces such as the gut and skin, two sites capable of generating new T_{RM} T cells. Furthermore, pre-existing T_{RM} T cells would have to resist displacement during secondary responses by newly generated T_{RM} T cells. These assumptions were recently tested in two studies focusing on inducible T_{RM} T cells generated in response to virus infection[10,11]. The combined results from these two studies demonstrated that T_{RM} T cells generated against a given antigen do not displace T_{RM} T cells previously generated against a non-related antigen[11] and recall responses are dominated by pre-existing T_{RM} T cells generated during the initial insult[10,11]. As for the majority of studies investigating T_{RM} T cells, the two studies described above focused on acute infection/inflammation models, so it remained to be determined how stable T_{RM} T cells as well as naturally occurring tissue-resident lymphocytes are in the face of chronic inflammation such as can be the case in autoimmune disease in humans. CeD, a complex T cell-mediated inflammatory disorder with an autoimmune component[81], provides a unique human model to study this question as it provides the possibility to study patients at different stages of the disease and to control for the presence or absence of the disease-driving antigen, i.e. dietary gluten.

In this study, we demonstrate that under physiological conditions the tissue-resident TCR$\gamma\delta^+$ IEL compartment is characterized by a unique subset of innate NK-like V$\gamma4^+$/V$\delta1^+$ IELs capable of recognizing BTNL3/BTNL8 molecules and poised to help maintain homeostasis either by eliminating virus-infected or malignant cells via activation of their NCRs that recognize stress-induced ligands[25] or by promoting tissue healing via production of amphiregulin[104]. Remarkably, in healthy individuals this subset persists through life. However, our study

reveals that in the face of extended periods of chronic inflammation as is in the case for active CeD patients, the tissue-resident Vδ1$^+$ IEL compartment is profoundly altered, even after exclusion of the disease driving antigen gluten and resolution of inflammation. This alteration was characterized by an irretrievable loss of innate-like Vγ4$^+$/Vδ1$^+$ IELs in CeD patients and the emergence of gluten-sensitive IFN-γ producing Vδ1$^+$ IELs characterized by clonal expansions associated with a H-J1 CDR3 motif and loss of BTNL3/BTNL8 reactivity. These data challenge the stability of tissue-resident lymphocytes and provide evidence that chronic inflammation can result in long-lasting profound alterations to tissue-resident lymphocyte compartments.

More specifically, our data demonstrating fundamental alterations to TCR repertoire in combination with the dramatic switch in functional profile and capacity of Vd1+ IEL in CeD provide evidence to dispute the assumption that pre-existing tissue resident Vd1+ IEL are expanded in CeD and point more to a recruitment of new cells to the tissue microenvironment that subsequently acquire their tissue resident phenotype in response to tissue specific signals. It was recently demonstrated that BTNL molecules in the small intestine are required early in life for the expansion and establishment of the murine Vγ7$^+$ IEL niche[20]. Although delayed expression of BTNL molecules was sufficient to endow Vγ7$^+$ IEL with a unique profile characteristic of recognition and signaling in response to BTNL molecules, the delayed expression of these molecules alone was not able to expand the Vγ7$^+$ IEL compartment, suggesting there is an optimal window for niche establishment and that BTNL expression is critical for Vγ7$^+$ IEL expansion and/or survival. We propose a multi-step model whereby the naturally occurring healthy Vγ4$^+$/Vδ1$^+$ IEL subset may initially expand in response to gluten induced inflammation as observed in potential CeD patients where NCR expression and BTNL3/BTNL8 reactivity is conserved. In other potential CeD patients we observe a loss of NCR$^+$ and BTNL3/BTNL8 reactive Vδ1$^+$ IELs suggesting there is tipping point where the chronic loss of BTNL8 expression observed in a subset of potential CeD patients

and active CeD patients leads to the eventual loss of the healthy Vγ4$^+$/Vδ1$^+$ IEL subset, cells that are likely dependent on their ligand for survival, and that this loss opens up a gap which is then filled by tissue infiltrating TCR$\gamma\delta^+$ T cells recruited from blood into the inflamed celiac mucosa. This source of new IEL is supported by the observation that several active CeD patients carried clonally expanded H-J1 expressing T cells in their blood, suggestive of priming in gut-associated lymphoid tissue (GALT)[89] by a ligand induced in the CeD tissue environment. The lack of recovery of the innate-like Vγ4$^+$/Vδ1$^+$ IEL subset in GFD patients where the mucosa has healed and BTNL8 expression recovers to normal levels can be explained similarly to the inability of the mouse Vγ7$^+$ IEL compartment to reconstitute after pro-longed absence of BTNL molecules early in life[20]. This is most likely due to the loss of a niche that cannot be recovered once the window for niche establishment has passed and different Vγ IEL subsets have established residence within the epithelium. Furthermore, our data not only challenges the prevailing hypothesis that the expansion of TCR$\gamma\delta^+$ T cells in CeD is a response of preexisting local, tissue resident TCR$\gamma\delta^+$ T cells, but also the notion that their proposed function is to limit infiltration by systemic T cells[31], thereby not participating in directly in disease pathogenesis[87,90]. The notion that TCRgd+ T cells in CeD do not play a role in the pathogenesis of CeD was in particular supported by the observation that, unlike TCR$\alpha\beta^+$CD8$\alpha\beta^+$ IELs, they remain expanded once villous atrophy has receded and the intestine has recovered a normal morphology[87]. Our observations provoke a reconsideration of the role of TCR$\gamma\delta^+$ IEL in CeD pathogenesis primarily because H-J1$^+$ Vδ1$^+$ IEL in active CeD display signs of antigen-driven clonal expansion and ongoing active TCR engagement, as attested by their transcriptional program and the expression of Nur77. In contrast, in GFD-treated CeD patients the H-J1$^+$ Vδ1$^+$ IEL subset contracted and was replaced by a polyclonal and resting Vδ1$^+$ IEL population. Furthermore, a significantly lower fraction of GFD Vδ1$^+$ IELs produced IFN-γ compared to active CeD Vδ1$^+$ IELs and further gained the capacity to produce IFN-γ in response to gluten challenge. These observations indicate that CeD Vδ1$^+$ IELs can be activated

in a gluten-dependent manner and suggest that they may participate in the development of villous atrophy through the gluten-dependent production of IFN-γ. It is notable that TCR$\gamma\delta^+$ IELs are the only IEL subset producing IFN-γ in response to gluten challenge, which was shown to induce upregulation of HLA-E on intestinal epithelial cells[101] and MHC class I molecules[110], which in turn can contribute to the activation of TCR$\alpha\beta^+$CD8$\alpha\beta^+$ IELs, the primary effector T cell subset responsible for intestinal epithelial cell destruction in CeD[81].

In conclusion, in contrast to mouse models studying the impact of acute infection on adaptively induced tissue-resident lymphocytes, our study concludes that long-lasting site-specific inflammation as seen in autoimmune and chronic inflammatory disorders can lead to the reconfiguration of the tissue-resident T cell compartment and leave immunological scars[111]. Our study establishes that even upon exclusion of the disease-driving antigen and subsequent resolution of inflammation that coincides with recovery of their natural ligand, naturally occurring tissue-resident T cells, which establish residence early in life and remain stable in healthy individuals, can be permanently displaced. The loss of tissue-resident subsets with unique innate specificities and cytolytic properties may have implications for the ability of CeD patients to fight epithelial tumors[112] and potentially compromise, at least partially, the ability to fight intracellular infections[25].

2.6 STAR*Methods

2.6.1 Patients and samples

Patients were classified into four groups for the purposes of this study. Control symptoms of upper gastrointestinal tract disease, with no histological evidence of duodenal inflammation, no family history of CeD, and negative serology for TG2. Active histological evidence of villous atrophy, with positive serology for TG2. GFD established diagnosis of CeD, with

no histological evidence of villous atrophy, and negative serology for TG2. Potential no histological evidence of villous atrophy, with positive serology for TG2. Exclusion criteria included immunosuppressive medication and coincident diagnoses of Barretts esophagus, eosinophilic esophagitis, cancer, cirrhosis, or inflammatory bowel disease (IBD). In challenge experiments, patients with GFD-treated CeD consumed 6 g of gluten daily for six weeks. Duodenal biopsies were taken from 35 distinct sites, together with 28 mL of venous blood, under protocol 12623B approved by the Chicago Biomedicine Institutional Review Board.

2.6.2 Lymphocyte isolation

PBLs were isolated from whole blood via standard density gradient centrifugation. IELs were isolated from duodenal biopsies via mechanical disruption. Briefly, duodenal tissues were shaken at 250 rpm for 30 min at 37C in 7 mL of RPMI 1640 medium supplemented with 1% dialyzed fetal bovine serum (Biowest), 2 mM EDTA (Corning), and 1.5 mM MgCl2 (Thermo Fisher Scientific). The procedure was repeated once with fresh medium to enhance cell recovery. Cells were harvested from the biopsy-free media via centrifugation and pooled for subsequent analyses.

2.6.3 Flow cytometry

The following directly conjugated antibodies were used to identify cell surface markers: αVδ1 FITC (TS8.2), αVδ1 APC (REA173), αVδ2 PerCP (B6), αVδ2 PE (B6), αTCR$\alpha\beta$ BV421 (IP26), αTCR$\gamma\delta$ PE (5A6.E9), αTCR$\gamma\delta$ PE-Cy5 (5A6.E9), αCD3 APC (UCHT1), αCD3 APC-Cy7 (UCHT1), αCD3 PE-Cy7 (UCHT1), αCD3 V450 (UCHT1), αCD4 APC (RPA-T4), αCD4 BV786 (SK3), αCD8a BUV496 (RPA-T8), αCD8α BV510 (RPA-T8), αCD8α BV650 (RPA-T8), αCD45 BV711 (HI30), αCD45RA BV510 (HI100), αCD69 PE (FN50), αCD69 PE-CF594 (FN50), αCD103 BUV395 (Ber-ACT8), αCD107a BUV395 (H4A3), αCCR7 PE-Cy7 (G043H7), αNKp44 APC (p44-8), αNKp44 PE (p44-8), αNKp46 BV605 (9E2),

αNKp46 PE (9E2), αNur77 PE (12.14), αMyc-Tag PE (9B11), and αHA-Tag Alexa Fluor 647 (6E2). For intracellular cytokine detection, cells were fixed/permeabilized using a BD Cytofix/Cytoperm Plus Fixation/Permeabilization Solution Kit (BD Biosciences) and stained with the following directly conjugated antibodies: αIFN-γ APC (4S.B3) and αTNF-α PE-Cy7 (MAb11). Antibodies were purchased from BD Biosciences, BioLegend, eBioscience, or Thermo Fisher Scientific. Dead cells were excluded from the analysis using LIVE/DEAD Fixable Aqua or LIVE/DEAD Fixable Near-IR (Thermo Fisher Scientific). All flow cytometry data were analyzed using FlowJo software version 10.2 (Tree Star).

2.6.4 Transcriptome sequencing

Full-length cDNA and sequencing libraries were generated using a modified version of the single-cell Smart-seq2 protocol[113]. Briefly, 50100 NCR^+ ($NKp46^+$) or NCR^- ($NKp46^-$) $V\delta1^+$ IELs were sorted into a lysis buffer containing oligo-dT and dNTPs. Reverse transcription was performed after hybridization of oligo-dT to poly-A RNA. The resulting cDNA was amplified over 18 thermocycles, purified using an AMPure XP Kit (Beckman Coulter), and quality controlled using a Bioanalyzer High Sensitivity DNA Kit (Agilent). A total of 0.25 ng of cDNA from each sample was tagmented, ligated with adapters (Nextera XT), amplified over 12 thermocycles, and quality controlled using a Bioanalyzer High Sensitivity DNA Kit (Agilent). Libraries were then pooled in equimolar amounts and sequenced on two lanes in duplicate using a HiSeq4000 System (Illumina).

2.6.5 HLA genotyping

DNA samples were genotyped using an ImmunoArray BeadChip (Illumina) with single nucleotide polymorphism (SNP) probes as described previously[114]. Data analysis was performed using PLINK v1.9[115]. Five of the six HLA-tagging SNPs reported by Monsuur et al.[116] were covered on the ImmunoArray BeadChip. Genotype call rates were higher than

95%. HLA-DQ was inferred from a combination of genotypes at these five SNPs[117].

2.6.6 TCR sequencing

Lymphocytes were stained for viability and surface expression of CD3, TCR$\alpha\beta$, TCR$\gamma\delta^+$, Vδ1, and Vδ2. Live V$\delta1^+$ T cells were then sorted directly into 100 L of RNAlater (Thermo Fisher Scientific) using a FACSAria III flow cytometer (BD Biosciences) according to the gating strategy presented in Figure 2.4.2A. Cell numbers and patient details are summarized in 2.2. All expressed *TRG* and *TRD* gene transcripts were amplified using an unbiased template-switch anchored RT-PCR[64]. Amplicons were subcloned, sampled, and sequenced as described previously[118]. Gene use was assigned using the ImMunoGeneTics (IMGT) nomenclature[119].

2.6.7 TCR/NKR stimulation assay

Polystyrene flat-bottom 96-well plates (Corning) were coated overnight at 4C with one of the following antibody cocktails: mix A 0.5 μg/mL αTCR$\gamma\delta$ (B1, BioLegend), 1 μg/mL mouse IgG2a κ (MOPC-173, BioLegend), and 1 μg/mL mouse IgG2b κ (MPC-11, BioLegend); or mix B 0.5 μg/mL αTCR$\gamma\delta$ (B1, BioLegend), 1 μg/mL αNKp44 (195314, RD Systems), and 1 μg/mL αNKp46 (253415, RD Systems). Lymphocytes were isolated from whole biopsies either pre-treated or not pre-treated with 10 ng/mL recombinant human IL-15 (BioLegend) for 18 hr at 4C and plated at a density of 2 x 105 cells per well (1 x 106 cells/mL) in RPMI 1640 medium supplemented with 10% human AB serum (Corning), 0.1% GolgiPlug (BD Biosciences), 0.1% GolgiStop (BD Biosciences), and 10 ng/mL recombinant human IL-15 (if pre-treated with recombinant human IL-15). Surface upregulation of CD107a was quantified via flow cytometry after incubation for 3 hr at 37C.

2.6.8 Phorbol myristate acetate/ionomycin stimulation assay

Lymphocytes were suspended in RPMI 1640 medium supplemented with 10% human AB serum (Corning), 10 ng/mL phorbol myristate acetate (Sigma-Aldrich), 150 ng/mL ionomycin calcium salt (Sigma-Aldrich), 100 U/mL recombinant human IL-2 (NIH AIDS Reagent Program), 0.1% GolgiPlug (BD Biosciences), and 0.1% GolgiStop (BD Biosciences) and distributed at 2 x 105 cells per well (1 x 106 cells/mL) in polystyrene flat-bottom 96-well plates (Corning). Surface expression of CD107a and intracellular cytokine production were quantified via flow cytometry after incubation for 3 hr at 37C.

2.6.9 Quantitative RT-PCR

Duodenal biopsies were collected in RNAlater RNA Stabilization Reagent (Qiagen). After incubation for 48 hr at 4C, excess solution was removed, and the biopsies were stored at 80C. On the day of processing, biopsy material was thawed, suspended in 500 L of Buffer RLT (Qiagen) supplemented with 1% β-mercaptoethanol (Sigma-Aldrich), and homogenized in a Bullet Blender 24 (Next Advance) using a 1:1 mix of 0.5 mm and 1.0 mm zirconium oxide beads (Next Advance). RNA was then isolated using an AllPrep DNA/RNA/Protein Mini Kit (Qiagen). cDNA was generated from 200 ng of total RNA using a GoScript Reverse Transcriptase Kit (Promega). Expression of the genes of interest was measured via quantitative RT-PCR using SYBR Advantage qPCR Premix (Clontech) on a Light Cycler 480 Instrument II (Roche). The following parameters were used for amplification: denaturation for 10 sec at 95C, annealing for 10 sec at 60C, and extension for 10 sec at 72C. Human primer sequences were as follows:

GAPDH forward: 5-ATGGGGAAGGTGAAGGTCG-3;

GAPDH reverse: 5-GGGGTCATTGATGGCAACAATA-3;

BTNL3 forward: 5- TCAGTTTCTACGAGCTGGTGTC-3;

BTNL3 reverse: 5-CCAAGGCCTGGACAAACTT-3;

BTNL8 forward: 5-GCTCTCATGCTCAGTTTGGTT-3;

and BTNL8 reverse: 5-GTCTGGCCCAAACACCTG-3.

The BTNL3 and BTNL8 primers were described previously[120].

2.6.10 Generation of HEK293T cell lines expressing BTNL3 and BTNL8

Synthetic DNA (Genscript) encoding full-length human BTNL8 alone or full-length human BTNL3 and BTNL8 separated by a P2A (Teschovirus A) ribosomal skip sequence was subcloned into pMIG (53) and used to make retroviral particles[121,122]. Retrovirally transduced (GFP+) HEK293T cells were flow-sorted based on expression of the N-terminal myc (EQKLISEEDL(GGS)) tag to identify BTNL3 and the N-terminal HA (YPYDVPDYA(GSG)) tag to identify BTNL8.

2.6.11 Generation of SKW3 cell lines expressing Vδ1$^+$ TCRs

Flow-sorted Vδ1$^+$ IELs isolated from healthy controls and patients with GFD-treated CeD were stimulated in vitro for two weeks at a starting density of 3 cells per well with irradiated B-lymphoblastoid cell lines and heterologous PBLs in RPMI 1640 medium supplemented with 300 U/mL IL-2 (NIH AIDS Reagent Program), 1 μg/mL phytohemagglutinin (Calbiochem), and 10% human AB serum (Atlanta Biologicals). Paired TCRγ and TCRδ sequences were obtained from clonally expanded Vδ1$^+$ IELs. Clonal expansions containing the H-J1 motif were sufficiently large in two patients with active CeD to allow frequency-based pairing of TCRγ and TCRδ sequences obtained directly *ex vivo* from bulk populations of Vδ1$^+$ IELs. Representative Vδ1$^+$ TCRs were stably expressed via retroviral transduction of the TCR-deficient T cell leukemia cell line SKW3 (German Collection of Microorganisms and Cell Cultures)[121,122].

2.6.12 BTNL3/8 reactivity assay ex vivo

Round-bottom 96-well plates were seeded overnight with 2 x 105 HEK293T-BTNL81$^+$ or HEK293T-BTNL3/81$^+$ cells per well to create a monolayer. IELs were isolated from whole biopsies pre-treated with 10 ng/mL recombinant human IL-15 (BioLegend) for 16 hrs at 4C and overlaid at 1 x 105 cells per well on top of the pre-plated HEK cell monolayer. Cells were co-cultured for 24 hr and analyzed via flow cytometry for surface downregulation of CD3 (UCHT1) and Vδ1 (REA173). As a positive control, IELs were simulated for 2 hr with 1.5 μg/mL of plate-bound purified αCD3 (UCHT1).

2.6.13 BTNL3/8 reactivity assay in vitro

For CD3 downregulation, round-bottom 96-well plates were seeded overnight with 2 x 105 HEK293T-UT or HEK293T-BTNL3/81$^+$ cells per well to create a monolayer, and 1 x 105 TCR$\gamma\delta^+$-SKW3 cells were then added to each well and incubated for 24 hr at 37C. For Nur77 induction, round-bottom 96-well plates were seeded overnight with 3.125 x 103, 6.25 x 103, 1.25 x 104, or 2.5 x 105 HEK293T-UT or HEK293T-BTNL3/81$^+$ cells per well to create a monolayer, and 1 x 105 TCR$\gamma\delta^+$-SKW3 cells were then added to each well and incubated for 2 hr at 37C. Flow cytometry was used to measure surface downregulation of CD3 (UCHT1) or intracellular induction of Nur77 (12.14). As a positive control, 1 x 105 TCR$\gamma\delta^+$-SKW3 cells were stimulated for 2 hr with 2.5 μL of Dynabeads Human T-Activator CD3/CD28 for T Cell Expansion and Activation (Thermo Fisher Scientific).

2.6.14 Immunohistochemistry

Duodenal biopsies were preserved in formalin and embedded in paraffin. Sections were cut to a thickness of 5 m and stained with Bond RX Automatic Stainer (Leica Biosystems). Slides were then dewaxed three times with xylene, ethanol, and water, treated for 20 min with Epitope Retrieval Solution II (Leica Biosystems), incubated for 5 min with 0.5% casein to

prevent non-specific binding, and stained for 1 hr with a 1:200 dilution of αBTNL8 (2187B, RD Systems). Antigen-antibody binding was revealed using Bond Polymer Refine Detection (Leica Biosystems). Tissue sections were then blocked with peroxidase, stained with DAB, and counter-stained with hematoxylin. Images were acquired using a ScanScope XT microscope (Leica Biosystems).

2.6.15 Transcriptome analysis

A total of 34 RNA-seq libraries were generated from flow-sorted Vδ1$^+$ IELs, including 8 from healthy controls (8 NCR$^+$), 18 from patients with active CeD (9 NCR$^+$ and 9 NCR$^-$), and 8 from patients with GFD-treated CeD (3 NCR$^+$ and 5 NCR$^-$). Adaptor sequences and low-quality score bases (Phred score ¡ 20) were trimmed using Trim Galore (version 0.4.4). The resulting reads were merged per sample and mapped to the human genome reference sequence (Ensembl GRCh38 release 87) using kallisto (version 0.43.0)[123]. To account for differences in read counts at the tails of the distribution, samples were normalized using the weighted trimmed mean of M-values algorithm (TMM), as implemented in the R package edgeR[124]. Data were then log-transformed using the voom function in the limma package[125]. Non-coding and lowly-expressed genes with an average (across all samples) log2(CPM) lower than 0 were excluded from downstream analyses, leaving a total of 16,066 genes. Linear models that accounted for differences in age and sex were used to identify genes with expression levels that varied between NCR$^+$ samples from healthy controls, NCR$^-$ samples from patients with active CeD, and NCR$^-$ samples from patients with GFD-treated CeD, as well as genes with expression levels that varied between NCR$^+$ samples from healthy controls , NCR$^+$ samples from patients with active CeD, and NCR$^+$ samples from patients with GFD-treated CeD, implemented using the lmFit function in the limma package[125].

2.6.16 General procedure for analysis of TCR characteristics

Sequences were first annotated for *TRGV/J* or *TRDV/J* using the IMGT database and V-QUEST tool[126]. TCR-sequencing data was generated from mRNA and therefore we report data from all transcribed *TRGV* genes. As it has not been formally demonstrated that *TRGV10* is non-functional we include all detected sequences in our analysis. Annotated CDR3 sequences were then imported into R for further analysis. Clonal distribution in each sample was assessed using the Shannon diversity index. Sequence characteristics (*TRV*, *TRD*, and *TRJ* gene usage, AA composition) were tested for association with patient groups and tissues. For each potentially distinguishing sequence characteristic (*TRV*, *TRD*, and *TRJ* gene usage, AA composition), enrichment was scored by overall occurrence per group and by trends in occurrence per individual. Results that weighted each unique sequence equally were found to be more robust to potentially non-representative sampling than results that weighted each unique sequence by clonal size. Therefore, unique sequences were equally weighted throughout the analysis, and the most strongly enriched features were identified as those passing both group and individual tests. For overall group enrichment testing, each unique TCR clone labeled with or without the characteristic under question was used as the response variable in Firths penalized logistic regression performed with the group label as the predictor (logistf R package). This method allowed nearly complete separation of each characteristic by the group label predictor. Linear hypothesis testing on the resulting group coefficients was then used to estimate the significance of each group comparison (multcomp R package). To test if the occurrence of a characteristic per individual shifted consistently between groups, characteristic proportions were explicitly modeled using beta regression[127]. The proportion of unique TCR clones with the characteristic under question was first calculated for each individual. These proportion values were then used as the response variable in beta regression performed with the group label as the predictor (betareg R package). Due to the common presence of 0.0 and 1.0 proportion values (completely absent or present characteristics, respectively), raw

proportion values (p) were transformed using (p(n-1)+0.5)/n, where n is the sample size, to ensure modeled values fell within the open interval (0,1) required for beta regression modeling[128]. Linear hypothesis testing on beta distribution mean coefficients per group was then used to estimate the significance of each group comparison (car R package).

2.6.17 Shannon diversity index

For each sample, the Shannon diversity index was calculated as $H = -\sum_n p_i ln p_i$, which provides a measure of repertoire diversity. To account for variations in the numbers of recovered CDR3 sequences, individual datasets were subsampled 100 times to 50 CDR3 sequences. The median index was then used to represent the score for each sample (vegan R package).

2.6.18 Analysis of TRGV and TRGJ gene usage

As described above, logistic regression was used to test for enrichment of *TRGV* and *TRGJ* gene segments in each group and each tissue. Significantly enriched gene segments were then tested for enrichment at the individual level using beta regression.

2.6.19 Analysis of CDR3 AAs

For each full-length CDR3 sequence, the longest substring of AAs from the V and J ends that matched the corresponding *TRV* and *TRJ* germline sequences was identified using reference data provided by the IMGT database[119]. The remaining AAs were considered non-germline, irrespective of potential contributions from the TRDD segment. The absence or presence of each AA was first determined in each unique CDR3. As described above, logistic regression was then used to test for the enrichment of each AA in each group, and significantly enriched AAs were tested for enrichment at the individual level using beta regression.

2.6.20 Analysis of TRDD gene usage

To determine the likely contribution of *TRDD* genes to each δ-chain sequence, an empirical statistic was generated to distinguish true germline matches from potentially spurious matches arising from random nucleotide additions. For each possible *TRDD* gene-derived nucleotide sequence, the longest substring match was first identified in each candidate CDR3 sequence, and 100,000 random nucleotide strings weighted by the observed nucleotide composition among all non-germline sequences were generated for each possible CDR3 length. By collecting match length statistics between a *TRDD* sequence and these random sequence sets, empirical null distributions of match length were obtained for each *TRDD* gene in both the forward and reverse frames. In each of these distributions, each match length bin contained at least 10 positive occurrences, assuring sufficient sampling coverage. These calculations allowed us to estimate an empirical p-value for an observed *TRDD* gene sequence match, representing the probability of obtaining a match of the observed length or longer by chance. To account for testing a *TRDD* gene sequence against every unique CDR3 sequence, the set of empirical p-values was corrected according to the Benjamini-Hochberg multiple testing procedure[129], which quantifies the false discovery rate (FDR). This procedure was applied independently to each of three possible *TRDD* genes across both the forward and reverse nucleotide sequences. Significant *TRDD* gene use was assigned at FDR values below 0.05. Sequences were further annotated for each *TRDD* gene to identify the active reading frame. As described above, logistic regression spanning all annotated unique CDR3s was used to test for enrichment of *TRDD* gene use in each group. Significantly enriched *TRDD* gene use was then tested for enrichment at the individual level using beta regression. Analysis of *TRDD* gene use, statistical testing, and sequence annotation were performed using custom code written in R.

2.6.21 iceLogo motifs

Non-germline-encoded CDR3 amino acid sequences were right-justified at the junction with the J segment and analyzed using the iceLogo java application[130]. Unique CDR3 sequences were pooled from V$\delta1^+$ IELs isolated from healthy controls and patients with GFD-treated CeD to serve as a fixed position background/reference set of sequences for visualization of AA enrichment among CDR3 sequences obtained from V$\delta1^+$ IELs isolated from patients with active CeD.

2.7 Acknowledgements

We thank the patients and their families for making this study possible, Robert Kavitt, Edwin McDonald, Atsushi Sakuraba, Joel Pekow, Neil Sengupta, and Sushila Dalal for patient care, Kathryn Lesko, Diane McKiernan, Sarbani Adhikari, and Fengshi Dong for patient recruitment, Mathieu Platteel for assistance with HLA genotyping, Steven Erickson for editing the manuscript, and staff at the University of Chicago Flow Cytometry Core Facility. This work was supported by the National Institutes of Health via T32 AI07090 to T.M., T32 GM007281 to D.G.S, R01 DK067180 to B.J., and the Digestive Diseases Research Core Center P30 DK42086 at the University of Chicago to B.J. J.R. is an Australian Research Council Laureate Fellow. D.A.P. is a Welcome Trust Senior Investigator (100326Z/12/Z).

Table 2.5: TRGV enrichment statistics: highlighting significant differences (bold) that pass both the group and individual level tests

Level Tested	Tissue	Group	Feature Tested	Active vs. Control	GFD vs. Control	Active vs. GFD	IEL vs. PBL
Group	IEL		TRGV10	0.6586	0.895	0.8408	
Group	IEL		TRGV9	0.2366	0.0878	6.37E-05	
Group	IEL		TRGV8	0.6206	0.6388	0.9991	

Group	IEL		TRGV5	0.1861	0.3732	0.7844	
Group	IEL		TRGV4	**3.33E-07**	**1.98E-13**	0.0025	
Group	IEL		TRGV3	**0.0163**	0.0258	0.6894	
Group	IEL		TRGV2	0.2381	0.2028	0.9911	
Individual	IEL		TRGV10	0.8562	0.4251	0.5324	
Individual	IEL		TRGV9	0.7448	0.1894	0.1051	
Individual	IEL		TRGV8	0.7598	0.8909	0.6659	
Individual	IEL		TRGV5	0.4378	0.8303	0.3374	
Individual	IEL		TRGV4	**0.0001**	**2.67E-06**	0.2217	
Individual	IEL		TRGV3	**0.0227**	0.1024	0.548	
Individual	IEL		TRGV2	0.5222	0.4769	0.9264	
Group	PBL		TRGV10	0.1647	0.966	0.2523	
Group	PBL		TRGV9	0.5127	0.5824	0.1425	
Group	PBL		TRGV8	0.0478	0.8136	0.239	
Group	PBL		TRGV5	0.7639	0.5881	0.3314	
Group	PBL		TRGV4	0.7376	0.4946	0.8983	
Group	PBL		TRGV3	0.5254	0.5691	0.9962	
Group	PBL		TRGV2	**0.0441**	0.8633	0.2618	
Individual	PBL		TRGV10	0.0869	0.9769	0.1177	
Individual	PBL		TRGV9	0.3522	0.5815	0.1591	
Individual	PBL		TRGV8	0.0773	0.974	0.0974	
Individual	PBL		TRGV5	0.8372	0.4867	0.3712	
Individual	PBL		TRGV4	0.3124	0.3929	0.9619	
Individual	PBL		TRGV3	0.147	0.1513	0.8559	
Individual	PBL		TRGV2	**0.0023**	0.4572	0.0402	
Group		Control	TRGV10				0.7526

Group	Control	TRGV9	0.0295
Group	Control	TRGV8	0.0089
Group	Control	TRGV5	0.2271
Group	Control	TRGV4	**2.00E-09**
Group	Control	TRGV3	**0.0285**
Group	Control	TRGV2	0.9034
Individual	Control	TRGV10	0.7983
Individual	Control	TRGV9	0.0792
Individual	Control	TRGV8	0.1212
Individual	Control	TRGV5	0.5045
Individual	Control	TRGV4	**1.58E-05**
Individual	Control	TRGV3	**0.0226**
Individual	Control	TRGV2	0.5418
Group	Active	TRGV10	0.109
Group	Active	TRGV9	**0.0065**
Group	Active	TRGV8	0.5003
Group	Active	TRGV5	0.8383
Group	Active	TRGV4	0.1878
Group	Active	TRGV3	0.0107
Group	Active	TRGV2	0.2949
Individual	Active	TRGV10	0.0613
Individual	Active	TRGV9	**0.0282**
Individual	Active	TRGV8	0.7801
Individual	Active	TRGV5	0.9327
Individual	Active	TRGV4	0.9035
Individual	Active	TRGV3	0.1424

Individual	Active	TRGV2	0.4762
Group	GFD	TRGV10	0.731
Group	GFD	TRGV9	0.1818
Group	GFD	TRGV8	0.1859
Group	GFD	TRGV5	0.2991
Group	GFD	TRGV4	0.0662
Group	GFD	TRGV3	0.0713
Group	GFD	TRGV2	0.3078
Individual	GFD	TRGV10	0.7054
Individual	GFD	TRGV9	0.3995
Individual	GFD	TRGV8	0.0711
Individual	GFD	TRGV5	0.9984
Individual	GFD	TRGV4	0.2085
Individual	GFD	TRGV3	0.1378
Individual	GFD	TRGV2	0.4699

Table 2.6: TRGJ enrichment statistics

Level Tested	Tissue	Group	Feature Tested	Active vs. Control	GFD vs. Control	Active vs. GFD	IEL vs. PBL
Group	IEL		TRJ1	0.9306	0.9978	0.9319	
Group	IEL		TRJP1	0.3945	0.0791	0.5751	
Group	IEL		TRJP2	0.8508	0.9705	0.9294	
Group	IEL		TRJ2	0.2984	0.721	0.0284	
Group	IEL		TRJP	0.9382	0.9756	0.7924	
Individual	IEL		TRJ1	0.8324	0.5546	0.6988	

Individual	IEL		TRJP1	0.1894	0.1416	0.8319	
Individual	IEL		TRJP2	0.9603	0.8388	0.8015	
Individual	IEL		TRJ2	0.3565	0.8795	0.2968	
Individual	IEL		TRJP	0.3688	0.3776	0.9866	
Group	PBL		TRJ1	0.0933	0.6495	0.6174	
Group	PBL		TRJP1	0.763	0.4682	0.8241	
Group	PBL		TRJP2	0.5907	0.719	0.3321	
Group	PBL		TRJ2	0.1366	0.9915	0.2397	
Group	PBL		TRJP	0.6304	0.7898	0.9782	
Individual	PBL		TRJ1	0.0711	0.4854	0.3491	
Individual	PBL		TRJP1	0.4882	0.3514	0.736	
Individual	PBL		TRJP2	0.444	0.7084	0.287	
Individual	PBL		TRJ2	0.0439	0.9693	0.0696	
Individual	PBL		TRJP	0.985	0.9735	0.9864	
Group	IEL	Control	TRJ1				0.1677
Group	IEL	Control	TRJP1				0.5185
Group	IEL	Control	TRJP2				0.3267
Group	IEL	Control	TRJ2				0.5131
Group	IEL	Control	TRJP				0.9289
Individual	IEL	Control	TRJ1				0.0295
Individual	IEL	Control	TRJP1				0.8857
Individual	IEL	Control	TRJP2				0.4541
Individual	IEL	Control	TRJ2				0.6069
Individual	IEL	Control	TRJP				0.6033
Group	IEL	Active	TRJ1				0.6166
Group	IEL	Active	TRJP1				0.806

Group	IEL	Active	TRJP2	0.593
Group	IEL	Active	TRJ2	0.8532
Group	IEL	Active	TRJP	0.4262
Individual	IEL	Active	TRJ1	0.696
Individual	IEL	Active	TRJP1	0.6068
Individual	IEL	Active	TRJP2	0.9481
Individual	IEL	Active	TRJ2	0.9872
Individual	IEL	Active	TRJP	0.6448
Group	IEL	GFD	TRJ1	0.7052
Group	IEL	GFD	TRJP1	0.8447
Group	IEL	GFD	TRJP2	0.8447
Group	IEL	GFD	TRJ2	0.8639
Group	IEL	GFD	TRJP	0.3991
Individual	IEL	GFD	TRJ1	0.9049
Individual	IEL	GFD	TRJP1	0.8017
Individual	IEL	GFD	TRJP2	0.3294
Individual	IEL	GFD	TRJ2	0.8732
Individual	IEL	GFD	TRJP	0.7284

Table 2.7: CDR3δ amino acid enrichment statistics: highlighting significant differences (bold) that pass both the group and individual level tests

Level Tested	Tissue	Amino Acid	Active vs. Control	GFD vs. Control	Active vs. GFD
Group	IEL	A	0.3177	0.3834	0.9905
Group	IEL	R	0.6925	0.9355	0.4243

Group	IEL	N	0.0365	0.2052	0.6386
Group	IEL	D	**0.0015**	0.085	0.2872
Group	IEL	C	0.9967	0.7203	0.7402
Group	IEL	Q	0.2356	0.7822	0.5409
Group	IEL	E	0.3595	0.9264	0.1559
Group	IEL	G	0.2735	0.7071	0.7028
Group	IEL	H	0.4007	0.8226	0.7389
Group	IEL	I	0.9184	0.4469	0.6531
Group	IEL	L	0.5511	0.4632	0.9867
Group	IEL	K	0.5682	0.3231	0.8834
Group	IEL	M	0.74	0.7575	0.9995
Group	IEL	F	0.9759	0.9573	0.9967
Group	IEL	P	0.9367	0.9438	0.7529
Group	IEL	S	0.9998	0.8886	0.8614
Group	IEL	T	0.1634	0.4437	0.7906
Group	IEL	W	0.9063	0.4003	0.6166
Group	IEL	Y	**0.0139**	**0.0133**	0.9997
Group	IEL	V	0.9082	0.9241	0.6686
Individual	IEL	A	0.0932	0.1027	0.9945
Individual	IEL	R	0.0158	0.6375	0.0603
Individual	IEL	N	0.0818	0.186	0.7108
Individual	IEL	D	**0.0015**	0.0925	0.1553
Individual	IEL	C	0.5381	0.2901	0.1018
Individual	IEL	Q	0.0662	0.5103	0.2583
Individual	IEL	E	0.5062	0.7009	0.3048
Individual	IEL	G	0.9475	0.5067	0.5482

Individual	IEL	H	0.9377	0.829	0.8884
Individual	IEL	I	0.4324	0.7931	0.3082
Individual	IEL	L	0.7453	0.7233	0.5047
Individual	IEL	K	0.8695	0.723	0.6082
Individual	IEL	M	0.9352	0.999	0.9384
Individual	IEL	F	0.188	0.7888	0.3138
Individual	IEL	P	0.9074	0.669	0.5895
Individual	IEL	S	0.6494	0.6733	0.3897
Individual	IEL	T	0.3728	0.8506	0.5006
Individual	IEL	W	0.2338	0.3849	0.7764
Individual	IEL	Y	**0.0001**	**0.0003**	0.9331
Individual	IEL	V	0.5665	0.5631	0.98
Group	PBL	A	0.9995	0.3726	0.4243
Group	PBL	R	0.9895	0.9989	0.9966
Group	PBL	N	0.3177	0.212	0.9146
Group	PBL	D	0.7552	0.9188	0.5814
Group	PBL	C	0.2183	0.1079	0.6574
Group	PBL	Q	0.8226	0.9335	0.6756
Group	PBL	E	0.9713	0.7195	0.6182
Group	PBL	G	0.5122	0.1045	**0.0303**
Group	PBL	H	0.462	0.9597	0.7245
Group	PBL	I	0.082	0.8581	0.3641
Group	PBL	L	0.3154	0.9431	0.5959
Group	PBL	K	0.6587	0.2943	0.7911
Group	PBL	M	0.4192	0.7229	0.2065
Group	PBL	F	0.9348	0.2551	0.4566

Group	PBL	P	0.3296	0.763	0.1358
Group	PBL	S	0.4341	0.6876	0.1517
Group	PBL	T	0.434	0.2607	**0.029**
Group	PBL	W	0.6076	0.9933	0.7516
Group	PBL	Y	0.9709	0.1748	0.1376
Group	PBL	V	0.7315	0.3547	0.1258
Individual	PBL	A	0.3827	0.0818	0.314
Individual	PBL	R	0.8973	0.5984	0.6716
Individual	PBL	N	0.1048	0.0942	0.7808
Individual	PBL	D	0.1369	0.5739	0.4364
Individual	PBL	C	0.4368	0.1346	0.3911
Individual	PBL	Q	0.8832	0.4715	0.5437
Individual	PBL	E	0.7272	0.4057	0.246
Individual	PBL	G	0.183	0.0324	**0.0012**
Individual	PBL	H	0.4375	0.563	0.9086
Individual	PBL	I	0.0674	0.7625	0.0522
Individual	PBL	L	0.6285	0.9956	0.6559
Individual	PBL	K	0.5018	0.2559	0.5796
Individual	PBL	M	0.2397	0.505	0.0874
Individual	PBL	F	0.8937	0.7749	0.6777
Individual	PBL	P	0.1103	0.3921	0.0205
Individual	PBL	S	0.102	0.7261	0.0653
Individual	PBL	T	0.5466	0.1458	**0.0425**
Individual	PBL	W	0.623	0.185	0.074
Individual	PBL	Y	0.4271	0.3274	0.7737
Individual	PBL	V	0.7418	0.3591	0.2175

Table 2.8: TRDD enrichment statistics: highlighting significant differences (bold) that pass both the group and individual level tests

Level tested	Tissue	Feature Tested	Active vs. Control	GFD vs. Control	Active vs. GFD
Group	IEL	TRDD2 - PSY	0.5464	0.0586	0.261
Group	IEL	TRDD2 - FL	**0.0344**	0.1455	0.6414
Group	IEL	TRDD2 - LP	0.9508	0.9861	0.8743
Group	IEL	TRDD3 - TGGY	0.5543	0.9495	0.7169
Group	IEL	TRDD3 - WGI	0.9992	0.0517	0.0282
Group	IEL	TRDD3 - LGDT	0.0044	0.1215	0.3275
Group	IEL	TRDD2/TRDD3 combinations	0.0866	0.0454	0.9391
Group	IEL	No TRDD usage	**0.0493**	**6.84E-06**	0.0207
Individual	IEL	TRDD2 - PSY	0.3223	0.0855	0.4398
Individual	IEL	TRDD2 - FL	**0.0232**	0.2631	0.2689
Individual	IEL	TRDD2 - LP	0.9727	0.7238	0.6993
Individual	IEL	TRDD3 - TGGY	0.8039	0.9785	0.7898
Individual	IEL	TRDD3 - WGI	0.8816	0.1075	0.1422
Individual	IEL	TRDD3 - LGDT	0.0563	0.3906	0.3174
Individual	IEL	TRDD2/TRDD3 combinations	0.1029	0.0783	0.856
Individual	IEL	No TRDD usage	**0.0235**	**0.0001**	0.057
Group	PBL	TRDD2 - PSY	0.9708	0.9805	0.9997
Group	PBL	TRDD2 - FL	0.2708	0.6906	0.8196
Group	PBL	TRDD2 - LP	0.9303	0.6916	0.8914
Group	PBL	TRDD3 - TGGY	0.5265	0.0394	0.0043
Group	PBL	TRDD3 - WGI	0.5054	0.8997	0.3616
Group	PBL	TRDD3 - LGDT	0.9643	0.9409	0.8521

Group	PBL	TRDD2/TRDD3 combinations	0.1133	0.166	0.996
Group	PBL	No TRDD usage	0.9607	0.3625	0.5292
Individual	PBL	TRDD2 - PSY	0.3803	0.976	0.4462
Individual	PBL	TRDD2 - FL	0.1012	0.4448	0.469
Individual	PBL	TRDD2 - LP	0.5653	0.4596	0.8156
Individual	PBL	TRDD3 - TGGY	0.8203	0.3082	0.3999
Individual	PBL	TRDD3 - WGI	0.7029	0.1147	0.0525
Individual	PBL	TRDD3 - LGDT	0.7338	0.4407	0.6296
Individual	PBL	TRDD2/TRDD3 combinations	0.0043	0.1087	0.3011
Individual	PBL	No TRDD usage	0.3553	0.2193	0.6653

Table 2.9: CDR3γ amino acid enrichment statistics: highlighting (bold) significant differences that pass both the group and individual level tests

Level Tested	Tissue	Amino Acid	Active vs. Control	GFD vs. Control	Active vs. GFD
Group	IEL	A	0.9994	0.9533	0.9198
Group	IEL	R	0.4453	0.9635	0.499
Group	IEL	N	0.9571	0.9913	0.9811
Group	IEL	D	0.9843	0.9999	0.9742
Group	IEL	C	0.6864	0.9085	0.3375
Group	IEL	Q	0.6956	0.908	0.8668
Group	IEL	E	0.2079	0.8927	0.3175
Group	IEL	G	0.847	0.4753	0.7468
Group	IEL	H	**0.0079**	0.5555	**0.0035**
Group	IEL	I	0.4335	0.9973	0.2938

Group	IEL	L	0.699	0.8923	0.2856
Group	IEL	K	0.8812	0.7538	0.9591
Group	IEL	M	0.5219	0.7947	0.7114
Group	IEL	F	0.6826	0.8597	0.9295
Group	IEL	P	**0.041**	**0.0017**	0.3246
Group	IEL	S	0.9732	0.8454	0.9199
Group	IEL	T	0.9067	0.5725	0.7375
Group	IEL	W	0.9688	0.545	0.5599
Group	IEL	Y	0.2132	0.4285	0.805
Group	IEL	V	0.9894	0.8628	0.8886
Individual	IEL	A	0.985	0.8555	0.9629
Individual	IEL	R	0.9715	0.7933	0.5802
Individual	IEL	N	0.2683	0.3112	0.9743
Individual	IEL	D	0.7852	0.4174	0.4079
Individual	IEL	C	0.2224	0.2046	0.8401
Individual	IEL	Q	0.6946	0.6814	0.981
Individual	IEL	E	0.0106	0.459	0.049
Individual	IEL	G	0.6683	0.712	0.4673
Individual	IEL	H	**0.0103**	0.7789	**0.0103**
Individual	IEL	I	0.052	0.86	0.1305
Individual	IEL	L	0.6415	0.6361	0.2565
Individual	IEL	K	0.3023	0.4028	0.9079
Individual	IEL	M	0.9335	0.4262	0.5453
Individual	IEL	F	0.1314	0.1238	0.9326
Individual	IEL	P	**0.0476**	**0.0139**	0.6589
Individual	IEL	S	0.6496	0.2954	0.4594

Individual	IEL	T	0.7227	0.565	0.8432
Individual	IEL	W	0.8419	0.8461	0.6463
Individual	IEL	Y	0.5383	0.5807	0.8745
Individual	IEL	V	0.2531	0.6799	0.159
Group	PBL	A	0.9578	0.4342	0.3378
Group	PBL	R	0.8759	0.8081	0.5736
Group	PBL	N	0.9338	0.5301	0.7144
Group	PBL	D	0.8029	0.7131	0.9761
Group	PBL	C	0.9692	0.995	0.9933
Group	PBL	Q	0.7728	0.7195	0.4372
Group	PBL	E	0.9508	0.242	0.4097
Group	PBL	G	0.5779	0.5607	0.1593
Group	PBL	H	0.2966	0.3401	0.9992
Group	PBL	I	0.7829	0.6145	0.9443
Group	PBL	L	0.9999	0.4719	0.4977
Group	PBL	K	0.5571	0.9119	0.4019
Group	PBL	M	0.8476	0.8552	0.6246
Group	PBL	F	0.9966	0.5893	0.5686
Group	PBL	P	0.705	0.542	0.2247
Group	PBL	S	0.5588	0.9715	0.7938
Group	PBL	T	0.7266	0.9406	0.5882
Group	PBL	W	0.2823	0.3834	0.9971
Group	PBL	Y	0.9823	0.9407	0.9851
Group	PBL	V	0.9577	0.8144	0.6883
Individual	PBL	A	0.909	0.3924	0.3251
Individual	PBL	R	0.8041	0.7429	0.575

Individual	PBL	N	0.9587	0.4226	0.4379
Individual	PBL	D	0.6591	0.3818	0.6191
Individual	PBL	C	0.5325	0.7098	0.8517
Individual	PBL	Q	0.7369	0.5894	0.3944
Individual	PBL	E	0.986	0.3223	0.3007
Individual	PBL	G	0.4912	0.2075	0.0554
Individual	PBL	H	0.0381	0.1031	0.8062
Individual	PBL	I	0.6128	0.4903	0.8053
Individual	PBL	L	0.9603	0.5877	0.6086
Individual	PBL	K	0.592	0.3497	0.1458
Individual	PBL	M	0.7644	0.306	0.436
Individual	PBL	F	0.7965	0.593	0.4369
Individual	PBL	P	0.7344	0.3311	0.1949
Individual	PBL	S	0.705	0.4522	0.269
Individual	PBL	T	0.7365	0.523	0.3342
Individual	PBL	W	0.1548	0.469	0.5736
Individual	PBL	Y	0.7474	0.3907	0.5563
Individual	PBL	V	0.9522	0.7103	0.6624

Table 2.10: Overlapping CDR3 sequences

Group	Patient ID	Tissue	Chain	TRV	CDR3	TRJ	Freq
Active	35	IEL	TRD	1	CALGDQRVPIPW..TGGYRHTDKLIF	1	86.17
Active	46	PBL	TRD	1	CALGDQRVPIPW..TGGYRHTDKLIF	1	1.27

Active	51	IEL	TRD	1	CALGEGFQR..LGDCKLIF	1	2.78
Active	51	PBL	TRD	1	CALGEGFQR..LGDCKLIF	1	23.08
Active	143	IEL	TRD	1	CALGGAPLG..DTRKDKLIF	1	1.33
Active	143	PBL	TRD	1	CALGGAPLG..DTRKDKLIF	1	53.25
GFD	3	IEL	TRG	9	CALWEVDYKKLF	1	5.13
GFD	3	PBL	TRG	9	CALWEVDYKKLF	1	61.25
GFD	3	PBL	TRG	9	CALWEVHYYKKLF	2	1.25
Active	22	PBL	TRG	9	CALWEVHYYKKLF	1	7.25
GFD	33	IEL	TRG	9	CALWEVLYKKLF	1	3.41
Active	46	IEL	TRG	9	CALWEVLYKKLF	1	1.09
Active	51	IEL	TRG	9	CALWEVLYKKLF	1	1.59
GFD	3	IEL	TRG	9	CALWEVRYKKLF	1	2.56
GFD	4	PBL	TRG	9	CALWEVRYKKLF	1	97.78
Active	51	IEL	TRG	9	CALWEVRYKKLF	1	1.59
Active	81	IEL	TRG	9	CALWEVRYKKLF	1	6.74
GFD	9	IEL	TRG	9	CALWEVRYYKKLF	1	7.94
Active	22	PBL	TRG	9	CALWEVRYYKKLF	1	1.45
GFD	28	IEL	TRG	3	CATWDGGEKLF	1	98.89
GFD	41	PBL	TRG	2	CATWDGGEKLF	1	25.71
Control	106	IEL	TRG	4	CATWDGGEKLF	1	86.96
GFD	3	IEL	TRG	2	CATWDGLYYKKLF	1	2.56
Active	112	IEL	TRG	4	CATWDGLYYKKLF	1	1.75

Active	35	PBL	TRG	4	CATWDGPHYKKLF	1	43.90
Active	143	IEL	TRG	2	CATWDGPHYKKLF	1	1.89
Active	22	PBL	TRG	2	CATWDGPNYKKLF	1	4.35
Active	51	IEL	TRG	2	CATWDGPNYKKLF	1	3.17
GFD	3	IEL	TRG	2	CATWDGPNYYKKLF	2	5.13
Active	46	PBL	TRG	2	CATWDGPNYYKKLF	2	1.54
Active	47	PBL	TRG	2	CATWDGPRYYKKLF	1	56.76
Active	143	PBL	TRG	4	CATWDGPRYYKKLF	1	6.52
Control	13	PBL	TRG	4	CATWDGQGYKKLF	2	11.11
Active	51	IEL	TRG	2	CATWDGQGYKKLF	1	1.59
Active	143	IEL	TRG	4	CATWDGRGSDWIKTF	P2	1.89
Control	144	IEL	TRG	4	CATWDGRGSDWIKTF	P2	2.90
Control	53	IEL	TRG	4	CATWDGRTTGWFKIF	P1	5.26
Control	144	PBL	TRG	8	CATWDGRTTGWFKIF	P1	2.44
Active	51	PBL	TRG	2	CATWDGTNYYKKLF	1	12.50
Control	144	IEL	TRG	4	CATWDGTNYYKKLF	2	2.90
Control	13	PBL	TRG	2	CATWDGYKKLF	1	4.76
GFD	41	IEL	TRG	2	CATWDGYKKLF	1	8.62
Active	81	PBL	TRG	2	CATWDGYKKLF	1	32.76
GFD	3	IEL	TRG	2	CATWDGYYKKLF	1	1.28
Control	13	PBL	TRG	2	CATWDGYYKKLF	1	7.94
GFD	41	IEL	TRG	2	CATWDGYYKKLF	1	5.17
Active	143	PBL	TRG	2	CATWDGYYKKLF	1	28.26
Active	143	IEL	TRG	4	CATWDGYYKKLF	1	3.77
Active	47	IEL	TRG	8	CATWDNYKKLF	1	14.06
Active	112	PBL	TRG	8	CATWDNYKKLF	1	5.13

GFD	33	IEL	TRG	4	CATWDPYYKKLF	1	1.14
GFD	41	PBL	TRG	3	CATWDPYYKKLF	1	18.57
Active	46	PBL	TRG	5	CATWDRHYKKLF	1	44.62
Active	51	IEL	TRG	2	CATWDRHYKKLF	1	1.59
GFD	3	IEL	TRG	3	CATWDRPEKLF	1	2.56
GFD	33	IEL	TRG	3	CATWDRPEKLF	1	3.41
Active	143	IEL	TRG	3	CATWDRPEKLF	1	1.89
GFD	3	IEL	TRG	5	CATWDRPGYKKLF	1	1.28
Control	111	PBL	TRG	5	CATWDRPGYKKLF	1	1.72
Control	53	PBL	TRG	3	CATWDSPNYYKKLF	2	18.75
Active	112	IEL	TRG	3	CATWDSPNYYKKLF	2	1.75
GFD	113	IEL	TRG	4	CATWDTTGWFKIF	P1	10.77
Active	143	PBL	TRG	8	CATWDTTGWFKIF	P1	4.35
GFD	4	PBL	TRG	8	CATWDYYKKLF	1	1.11
GFD	28	PBL	TRG	4	CATWDYYKKLF	1	43.53
Active	51	PBL	TRG	8	CATWDYYKKLF	1	6.94
Control	110	PBL	TRG	5	CATWDYYKKLF	1	13.73
GFD	113	PBL	TRG	3	CATWGRLYYKKLF	1	1.96
Control	144	PBL	TRG	8	CATWGRLYYKKLF	1	4.88
Active	47	IEL	TRG	4	CATWSHYYKKLF	1	28.13
Active	51	IEL	TRG	3	CATWSHYYKKLF	1	3.17
GFD	3	IEL	TRG	8	CATWVYYKKLF	1	1.28
GFD	4	IEL	TRG	5	CATWVYYKKLF	1	11.76
GFD	41	IEL	TRG	4	CATWVYYKKLF	1	3.45

CHAPTER 3

THE ENTIRE TCR$\gamma\delta^+$ IEL COMPARTMENT IS ALTERED IN CELIAC DISEASE

3.1 Rationale

In humans, the Vδ1 chain is the most abundant δ-chain used in the IEL compartment[131], accounting for 50-75% of all TCR$\gamma\delta^+$ IELs (Fig. 2.3D). Having observed profound alterations to the V$\delta1^+$ IEL compartment in patients with CeD, we set out to investigate whether V$\delta1^-$ IELs also took on innate-like properties in the healthy state and whether these cells were also lost in patients with CeD. An integration of data on the entire TCR$\gamma\delta^+$ IEL compartment would aid in building a model that explains the observed turnover of cells in CeD patients while also shedding light on the role of these cells in disease by providing information on what is unique to V$\delta1^+$ IELs as well as what alterations are shared for the compartment as a whole.

3.2 Results

3.2.1 Innate like V$\delta1^-$ IELs are lost in favor of IFN-γ producing IELs in CeD

V$\delta1^-$ IELs constituted a significantly higher fraction of CD3$^+$ T cells in CeD patients relative to healthy controls (Fig. 3.1A). The expansion of TCR$\gamma\delta^+$ IELs was already shown to be biased towards V$\delta1^+$ IELs in active CeD patients relative to both controls and GFD-treated CeD patients (Fig. 2.3D). This could then potentially explain the modest increase in the representation of V$\delta1^-$ IELs amongst CD3$^+$ T cells in active CeD patients relative to controls (Fig. 3.1A). It is known that TCR$\alpha\beta^+$CD8TCR$\alpha\beta^+$ IELs expand in active CeD patients and recede on a GFD, while TCR$\gamma\delta^+$ IELs remain expanded[87]. This observation can help

explain why Vδ1$^-$ IELs are overrepresented amongst CD3$^+$ T cells in GFD-treated CeD patients relative to active CeD patients, especially when taken together with the observation that Vδ1$^+$ IELs are preferentially expanded in active CeD patients (Fig. 2.3D).

Vδ1$^-$ IELs took on a tissue-resident phenotype (Fig. 3.1B) with hallmarks of effector memory cells (Fig. 3.1C), similarly to Vδ1$^+$ IELs (Fig. 3.1).

To assess whether the expansion of Vδ1$^-$ IELs in CeD was associated with a phenotypical switch as was observed for Vδ1$^+$ IELs (Fig. 2.5 and 2.7), we investigated the expression of NCRs and cytokine producing capacity in both the healthy and celiac state. Similarly to Vδ1$^+$ IELs, the majority of Vδ1$^-$ IELs expressed NKp46 and NKp44 in the healthy state and lacked expression of these two NCRs in both active and GFD-treated CeD patients (Fig. 3.1D). This switch in phenotype was also accompanied by a significant increase in the capacity of Vδ1$^-$ IELs to produce IFN-γ in active CeD patients relative to healthy controls (Fig. 3.1E). However, it is worth noting that a sizable fraction of healthy Vδ1$^-$ IELs produced IFN-γ suggesting there may be some differences in the steady state between Vδ1$^+$ and Vδ1$^-$ IELs (Fig. 2.7A and Fig. 3.1E). Furthermore, in GFD-treated patients challenged with gluten, a higher fraction of Vδ1$^-$ IELs produced IFN-γ post challenge in three out of four patients tested, although this increase did not reach statistical significance (Fig. 3.1F).

Collectively, these data suggested Vδ1$^-$ IELs take on a similar phenotype to Vδ1$^+$ IELs in the healthy state and that these cells are replaced in CeD patients by IFN-γ producing IELs that may also be gluten sensitive.

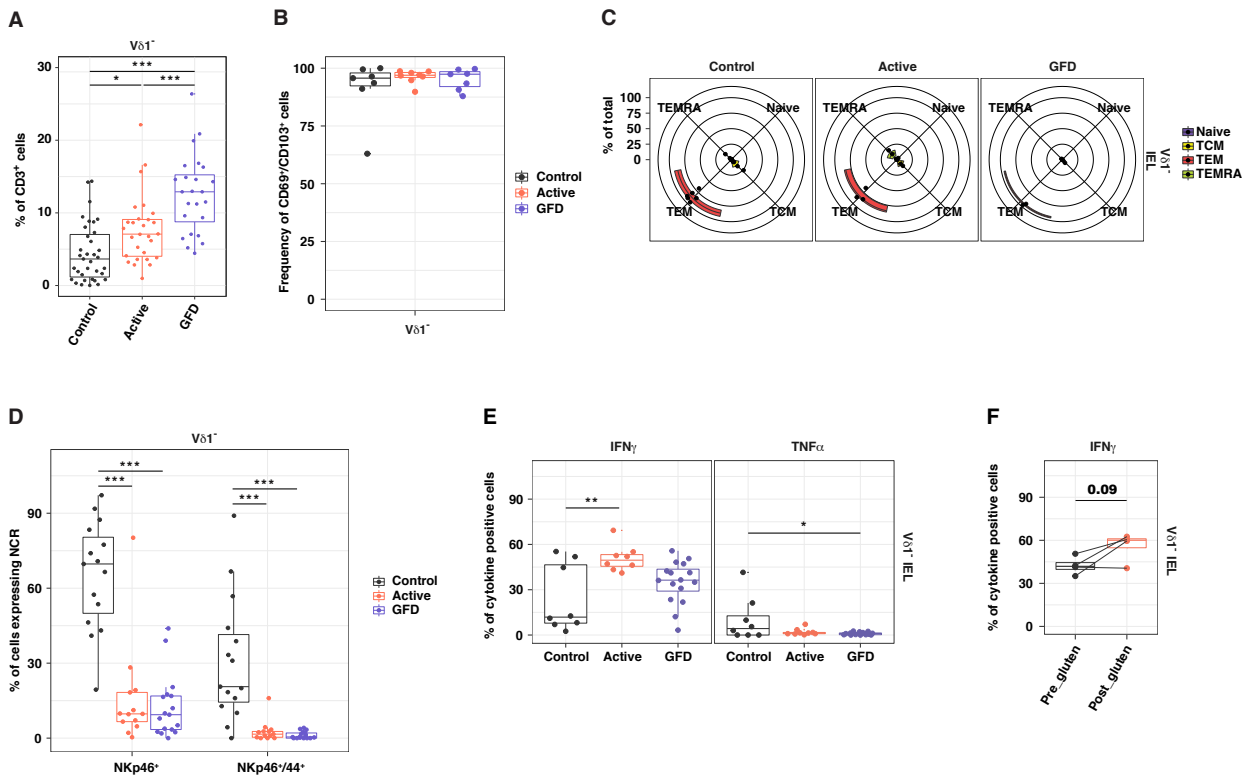

Figure 3.1: Innate like Vδ1$^-$ IELs are lost in favor of IFN-γ producing IELs in CeD
(**A**) Data summarized as the frequency of Vδ1$^-$ IELs among total CD3$^+$ lymphocytes. Box plots display the first and third quartiles. *p<0.05, ***p<0.001; one-way ANOVA followed by Tukeys test for multiple comparisons. (**B**) Cells pre-gated for expression of CD3, CD45, and absence of Vδ1 summarized as the frequency of CD69$^+$/CD103$^+$ cells. Box plots display the first and third quartiles. (**C**) Expression of CD45RA and CCR7 on Vδ1$^-$ IELs summarized in radar plots, where values above 0 radiate from the center for cells identified as nave, central memory (TCM), effector memory (TEM), or terminal effector (TEMRA). (**D**) Expression of NKp46 and NKp44 on Vδ1$^-$ IELs is summarized in box plots displaying the first and third quartiles. ***p<0.001; one-way ANOVA followed by Tukeys test for multiple comparisons. (**E**) Cells were stimulated with phorbol myristate acetate and ionomycin and stained intracellularly for IFN-γ and TNF-α. Data are summarized in box plots displaying the first and third quartiles. *p<0.05, **p<0.01; one-way ANOVA followed by Tukeys test for multiple comparisons. (**F**) Patients with GFD-treated CeD (length of diet: 1.5 years, 4years, 7 years, and 20.5 years) were challenged daily with gluten for six weeks. Cells isolated from biopsies taken before and after gluten challenge were treated as in (E). Top: representative contour plots from the same individual showing expression of IFN-γ and TNF-α. Bottom: data summarized in box plots displaying the first and third quartiles. paired T-test.

3.2.2 The Vδ1$^-$ IEL TCR repertoire is altered in CeD

Having observed restricted usage of *TRGV4* in healthy Vδ1$^+$ IELs and a subsequent loss of *TRGV4* bias coupled with enrichment for H-J1 bearing TCRs in active CeD (Fig. 2.4.5), we set out to detrmine if Vδ1$^-$ IELs exhibited similar alterations to the steady state repertoire. First, we wanted to test whether *TRGV4* usage was specific to Vδ1$^+$ IELs or whether the

steady state TCR$\gamma\delta^+$ IEL compartment was globally restricted to *TRGV4* usage. To do so, we sequenced the V$\delta1^-$ TCR repertoires from four healthy individuals that exhibited 70-100% *TRGV4* usage for their previously sequenced V$\delta1^+$ TCR repertoires. Surprisingly, healthy V$\delta1^-$ IELs also exhibited extreme bias towards *TRGV4* usage (Fig. 3.2A). To test if V$\gamma4^+$V$\delta1^-$ IELs were also lost in CeD patients, we chose to sequence the V$\delta1^-$ TCR repertoires of 4 active CeD patients that had clonal expansions of V$\delta1^+$ TCRs bearing the H-J1 CDR3γ motif and 2 GFD-treated CeD patients without an enrichment for *TRGV4* usage in their V$\delta1^+$ TCR repertoires. Again, similarly to V$\delta1^+$ IELs, V$\delta1^-$ IELs lost the enrichment for *TRGV4* usage in active CeD patients and maintained this loss in GFD-treated CeD patients (Fig. 3.2A). Of note, *TRGV3* was the predominant δ-chain used amongst V$\delta1^-$ IELs and no significant changes in δ-chain usage were observed between healthy individuals and patients with CeD (Fig. 3.2B).

These data demonstrated the healthy state is characterized by *TRGV4* restricted TCR$\gamma\delta^+$ IELs and that the entire TCR$\gamma\delta^+$ IEL compartment undergoes a lasting turnover.

3.2.3 H-J1 bearing TCRs are not enriched in V$\delta1^-$ repertoires

The alterations to the V$\delta1^+$ IEL TCR repertoire in active CeD patients was associated with clonal expansions bearing a H-J1 CDR3γ motif (Fig. 2.4.5C). Having chosen to sequence the V$\delta1^-$ TCR repertoires of 4 active CeD patients that had clonal expansions of V$\delta1^+$ TCRs bearing the H-J1 CDR3γ motif, we were able to test whether this selection was specific to V$\delta1^+$ IELs. Strikingly, V$\delta1^-$ IEL repertoires did not exhibit enrichment for H-J1$^+$ CDR3γ sequences in any of the 4 individuals tested (Fig. 3.2C). More specifically, the V$\delta1^-$ TCR repertoires were characterized by high diversity CDR3γ usage in contrast to the matched V$\delta1^+$ repertories (Fig. 3.2D).

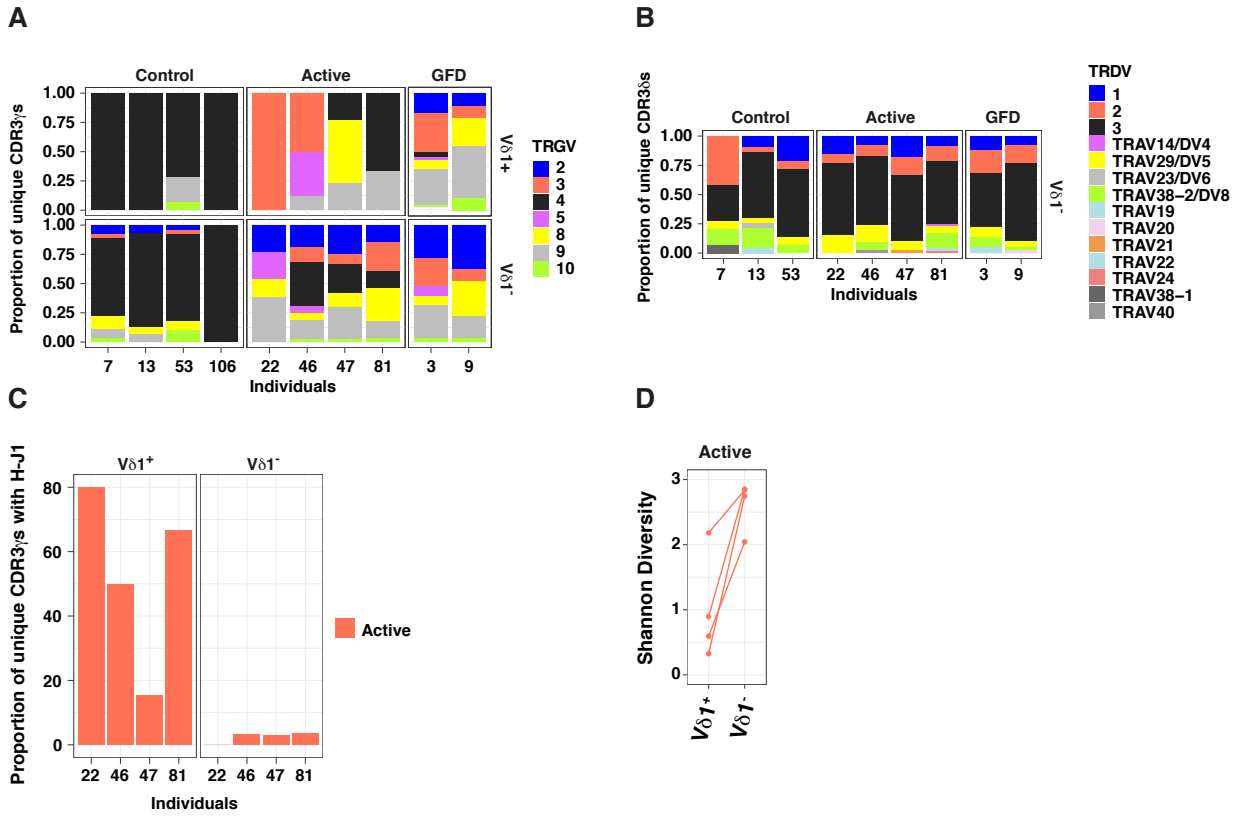

Figure 3.2: The V$\delta1^-$ IEL TCR repertoire is altered in CeD
(**A**) The proportion of unique clones expressing the indicated TRGV genes summarized by individual for V$\delta1^+$ and V$\delta1^-$ sorted IELs. Healthy controls: n = 4. Patients with active CeD: n = 4. GFD-treated CeD: IELs, n = 2. (**B**) The proportion of unique clones expressing the indicated TRDV genes summarized by individual for V$\delta1^-$ sorted IELs. Healthy controls: n = 4. Patients with active CeD: n = 4. GFD-treated CeD: IELs, n = 2. (**C**) The frequency of unique CDR3γ sequences containing the H-J1 motif summarized by individual for V$\delta1^+$ and V$\delta1^-$ sorted IELs from active CeD patients. (**D**) Shannon diversity for CDR3γ sequences of active CeD patients, paired by individual for V$\delta1^+$ and V$\delta1^-$ sorted IELs.

Together, these data demonstrated the expansion of H-J1$^+$ IELs in active CeD patients was specific to V$\delta1^+$ IELs and that V$\delta1^-$ IELs may not undergo similar selection in CeD given their high CDR3 diversity.

3.2.4 BTNL3/8 reactive V$\delta1^-$ IELs are lost in CeD

The heavy bias for V$\gamma4$ usage within the V$\delta1^-$ IEL compartment prompted us to assess reactivity of V$\delta1^-$ IELs to BTNL3/8. V$\delta1^-$ IELs isolated from healthy individuals displayed reactivity in the form of surface TCR downmodulation when incubated with HEK-293T cells

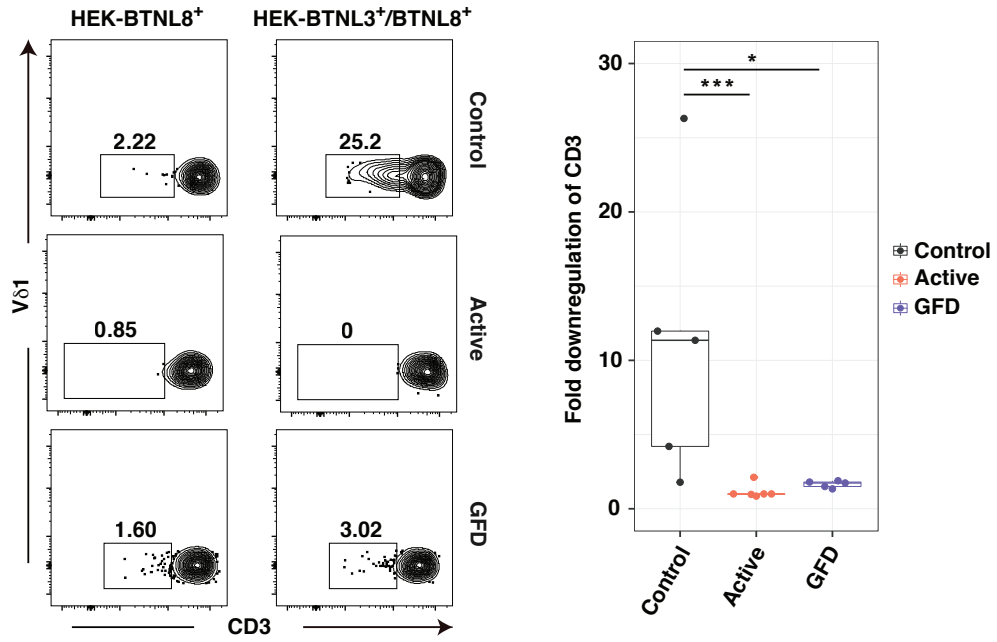

Figure 3.3: BTNL3/8 reactive Vδ1$^-$ IELs are lost in CeD
ex vivo isolated IELs were co-cultured with HEK293T-BTNL8$^+$ or HEK293T-BTNL3/8$^+$ for 24hrs. Left: representative contour plots showing expression of CD3 and Vδ1 on Vδ1$^-$ IELs. Gating strategy was patient specific and set based on the HEK293T-BTNL8$^+$ condition. Right: data is summarized in box plots displaying the first and third quartiles. *p<0.05, ***p<0.001; Kruskal-Wallis rank sum test followed by Dunns test for multiple comparisons.

expressing BTNL3 and BNTL8 molecules (Fig. 3.3. As expected, based on the alterations in TCR repertoire, Vδ1$^-$ IELs from CeD patients failed to react to BTNL3/8 (Fig. 3.3.

These observations suggested that Vγ4 most likely dominates the interaction with BTNL3/8 and that pairings other than Vδ1 can support recognition. Finally, the data demonstrate a total lack of BTNL reactivity within the TCR$\gamma\delta^+$ IEL compartment of patients with CeD.

3.2.5 Dynamic remodeling of the Vδ1$^-$ IEL compartment precedes tissue damage in CeD

The complete set of data on Vδ1$^+$ and Vδ1$^-$ IELs suggested the Vδ1$^-$ IEL compartment may exhibit signs of turnover prior to the initiation of tissue destruction as was observed for

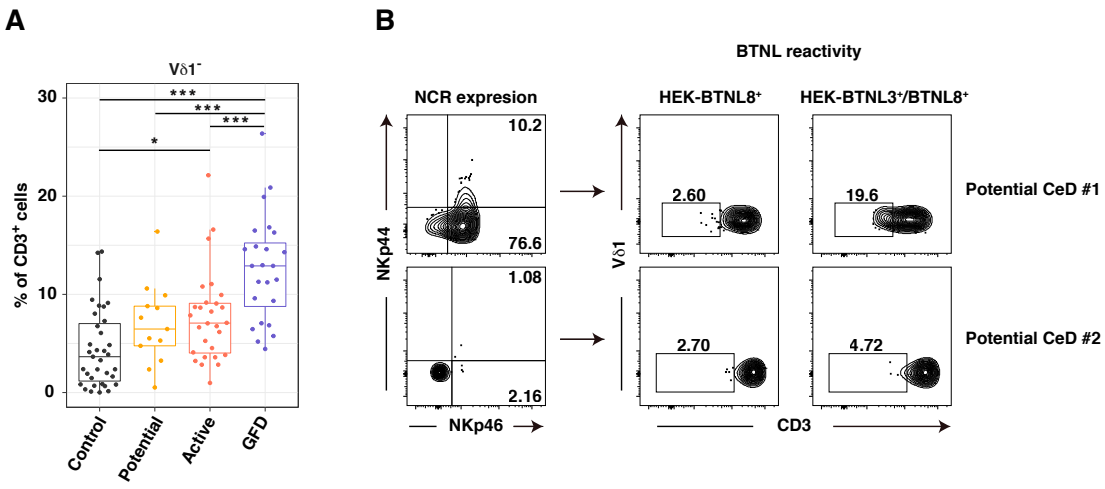

Figure 3.4: Dynamic remodeling of the Vδ1$^-$ IEL compartment precedes tissue damage in CeD

(**A** Frequency of Vδ1$^-$ cells among total CD3$^+$ lymphocytes. Data are summarized in box plots displaying the first and third quartiles. *p<0.05, ***p<0.001; one-way ANOVA followed by Tukeys test for multiple comparisons. (**B**) Contour plots showing expression of NKp46 and NKp44 on Vδ1$^-$ IELs (left) and expression of CD3 and Vδ1 after *ex vivo* co-culture of IELs for 24 hr with HEK293T-BTNL8$^+$ or HEK293T-BTNL3/8$^+$ cells (right) for two patients with potential CeD.

Vδ1$^+$ IELs in potential CeD patients (Fig. 2.4.9). Vδ1$^-$ IELs were not significantly increased in potential CeD patients when compared to healthy controls, although the data showed a trend towards that direction (Fig. 3.4A). Given the clear increase observed for Vδ1$^+$ IELs (Fig. 2.4.9A), this would suggest the events leading up to the initiation of active disease could be biased towards Vδ1$^-$ IELs.

As previously mentioned, potential CeD consists of a heterogenous group of patients and as was observed for Vδ1$^+$ IELs (Fig. 2.4.9E), Vδ1$^-$ IELs with high expression of NCRs, the presumable Vγ4$^+$ subset, displayed reactivity to BTNL3 and BTNL8, whereas Vδ1$^-$ from a potential CeD patient that no longer expressed NCRs, indicative of loss of the naturally occurring subset, did not react with BTNL3 and BTNL8 (Fig. 3.4B). Thus, the loss in tolerance to gluten is associated with a dynamic remodeling of the entire TCR$\gamma\delta^+$ IEL compartment prior to the development of tissue destruction in patients with potential CeD, with a bias towards expansion of Vδ1$^+$ IELs.

3.3 Discussion

Analysis of V$\delta1^-$ IELs revealed that the entire healthy state compartment is characterized by *TRGV4* expressing TCRs. As was shown for V$\delta1^+$ IELs, the steady state IEL compartment was characterized by NCR expressing cells that were lost in CeD patients in favor of IFN-γ producing IELs that also no longer exhibited bias towards *TRGV4* usage and consequently could no longer recognize BTNL3/8. Importantly, the V$\delta1^-$ IEL repertoire did not exhibit evidence of antigen driven selection as the repertoire was diverse and lacked H-J1$^+$ expansions. These data suggested although the turnover was a global feature of the TCR$\gamma\delta^+$ IEL compartment, likely driven by the loss of BTNL3/8 expression in CeD, the biased expansion of V$\delta1^+$ IELs in CeD is most likely driven by a disease specific ligand, the investigation of which is the source of future studies.

3.4 Methods

Data for V$\delta1^-$ IELs was generated from the same individuals as the data generated for V$\delta1^+$ IELs. Therefore, all the methods used have already been described in the STAR*Methods section above.

CHAPTER 4

DISCUSSION

4.1 TCR$\gamma\delta^+$ repertoire

4.1.1 General features of the human TCR$\gamma\delta^+$ repertoire

Our study provides the first TCR sequencing data set where both the δ-chain and γ-chain were sequenced from *ex vivo* sorted human TCR$\gamma\delta^+$ IELs. Whereas previous studies of TCR$\gamma\delta^+$ IELs in human tissues had focused on analysis of the δ-chain[60–62], our analysis of the γ-chain revealed the repertoires in both the healthy state and celiac state can be exclusively segregated based on features of the γ-chain. The overall study design of sequencing donor matched IELs and PBLs from healthy individuals and patients with active and treated CeD allows for commentary on tissue specific features of the repertoire as well as general features of the repertoire that are independent of disease status.

In line with previous studies our data support a lack of overlap in TCRs between the blood and gut within a given individual[60–62], which is in line with the tissue-resident nature of IELs. Although it is clear that overlap between the two tissues is not prevalent, one would need to sequence more material from both sites to definitively determine if there is no crosstalk. As was reported for the repertoire in peripheral blood[63], the gut repertoire was private for the δ-chain with all overlaps between individuals being accounted for by γ-chain CDR3s. The δ-chain is the more complex of the two with the CDR3 being generated by recombination of a *TRDV* segment, up to two *TRDD* segments, and a *TRDJ* segment thus reducing the probability of finding overlaps between individuals. Alternatively, overlaps within the γ-chain could be due to shared ligands such as in the case of overlapping γ-chain CDR3s with the H-J1 motif in active CeD patients. It it likely that the enrichment of overlaps within the γ-chain is a combination of less recombinatorail diversity (only *TRGV* and *TRGJ*) and

selection events.

By sorting Vδ1$^+$ IELs specifically, we were able to generate meaningful data on γ-chain usage without the need for single cell TCR sequencing. For instance, by choosing to sort Vδ1$^+$ IELs we were able to demonstrate an almost exclusive pairing of healthy state Vδ1 TCRs with Vγ4. Additionally, if we had chosen to sort all TCR$\gamma\delta^+$ IELs, we would have significantly reduced our power to observe the enrichment of clonal expansions that carried the H-J1$^+$ CDR3γ motif given Vδ1$^-$ IELs were not enriched for pairings with H-J1$^+$ CDR3γs. Our analysis of amino acid usage within the non-germ-line encoded region of the CDR3, which allowed for the identification of the H, across tissues and both the γ and γ-chains also generated useful information about the nature of amino acids that are tolerated within the CDR3 loop. For instance, glycine (G) was universally the most well represented amino acid within the CDR3 with leucine (L), arginine (R), and proline (P) also being found in the majority of CDR3s. Glycine is likely favorable within the floppy CDR3 loop due to its minimal side chain. These so called 'amino acid usage maps' could be generated for other cells with recombined antigen receptors such as TCR$\alpha\beta^+$ T cells and B cells to determine if the footprint observed for TCR$\gamma\delta^+$ CDR3 loops is unique or in favor of a structural hierarchy when it comes to CDR3 loops.

An unbiased, statistically driven analysis was applied to decipher *TRDD* gene usage within Vδ1$^+$ repertoires. The faithful assignment of *TRDD* gene segment usage is particularly challenging as it is known that two *TRDD* gene segments can be integrated into a single TCR with the added possibility that they can be read in the forward and reverse frames[71]. Interestingly, we were only able to call *TRDD2* and *TRDD3* gene segments in the forward frame at a false discovery rate (FDR) of 5% with a higher representation of *TRDD3* gene segments encoding the motifs TTGY, WGI, and LGDT. It still needs to be determined whether this is a feature of Vδ1$^+$ T cells or whether all δ-chains exhibit this bias.

4.1.2 TCR$\gamma\delta^+$ IEL repertoire in the steady state

Integrating the results generated from sequencing both the V$\delta1^+$ and V$\delta1^-$ IEL repertoires revealed the defining feature of the healthy state repertoire is the restricted usage of the V$\gamma4$ chain. In light of this restriction, it was surprising that we did not find any overlapping CDR3γs between healthy controls. This would suggest that selection of the repertoire in the steady state is not heavily dependent on CDR3 but rather dictated by germ-line encoded regions of the V$\gamma4$ chain. However, we did find clonal expansions within individual IEL repertoires similarly to what has been reported for TCR$\alpha\beta^+$ IELs in both mouse and human[132–134]. The recent identification of Btnl1 and Btnl6 as the selecting ligand for V$\gamma7^+$ IELs in mouse and the extension of those observations to showing human colonic V$\gamma4^+$ cells react to BTNL3/8[20], in conjunction with our BTNL3/8 reactivity data, suggests BTNL3 and BTNL8 may be the ligand for TCR$\gamma\delta^+$ IELs in the steady state. The clonality at the level of the individual is then most likely explained by stochastic events where particular clones establish residence at a given site in the intestine, given BTNL molecules are not capable of presenting variable antigens. An importnat result is we observed BTNL reactivity in both the V$\delta1^+$ and V$\delta1^-$ IEL compartments in healthy individuals, suggesting the interactions with BTNL3/8 may be driven by V$\gamma4$. This is in contrast to what was shown for two V$\delta1^+$ TCRs using different Vγ-chains that were crystalized with CD1d[68,69], where the majority of TCR/ligand contacts were shown to involve the V$\delta1$-chain and in the case of CD1d complexed with the lipid sulfitide the interaction was almost entirely dictated by the V$\delta1$-chain for a V$\gamma4^+\delta1^+$ TCR[69]. It is possible that V$\gamma4^+\delta1^+$ IELs may have multiple specificities in the steady state if the right lipid antigen presents itself. That being said, there is still no definitive evidence that V$\delta1^+$ IELs can recognize CD1d and in our hands we have not observed any reactivity of human IELs to CD1d unloaded tetramers (data not shown) whereas healthy

Vδ1$^+$ IELs readily displayed reactivity to BTNL3/8.

4.1.3 TCR$\gamma\delta^+$ IEL repertoire in CeD

By studying the TCR$\gamma\delta^+$ IEL repertoire of healthy individuals and patients in different stages of CeD, we were able to define features that are unique to the healthy state and uncovered lasting alterations to the repertoire in the disease state.

The heavy bias towards *TRGV4* usage amongst IELs dissipated in CeD patients for both Vδ1$^+$ and Vδ1$^-$ IELs. This was substantiated by a loss of BTNL3/8 reactive TCR$\gamma\delta^+$ IELs in CeD patients. Alterations to the repertoire were not restricted to the γ-chain as it was also observed that Vδ-chain CDR3s were significantly longer in CeD IELs with significantly more CDR3s incorporating *TRDD* gene segments. This is an intersting observation that may have less to do with disease and more to do with requirements set on the δ-chain by BTNL3/8 interactions. For instance, of the three Vγ4$^+$ TCR clones that we tested, there was an inverse correlation between the length of the CDR3δ and reactivity to BTNL3/8, with the shortest CDR3δ displaying the highest reactivity. The H-J1$^+$ Vγ4 clone that exhibited no reactivity to BTNL3/8 had a significantly longer CDR3δ and therefore it must be considered that the lack of BTNL3/8 reactivity observed in CeD patients may be in part due to longer CDR3δs.

In addition to the global alterations to the repertoire observed in CeD patients, we uncovered clonal expansions in active CeD patients with a shared H-J1$^+$ CDR3γ motif indicative of antigen driven selection in the inflamed state, which we speculate on in more details in the future directions chapter. Expanded H-J1$^+$ TCRs retracted in GFD-treated CeD patients, following the dynamics classically associated with adaptive immunity. Interestingly, retraction of H-J1$^+$ clones was associated with an overall increase in TCR diversity in GFD patients

suggesting selecting pressures may not exist in the GFD state for the newly minted TCR$\gamma\delta^+$ IEL compartment. The lack of recovery of V$\gamma4^+$ IELs in GFD-treated CeD patients, although BTNL3/8 expression recovers, poses a very intersting conundrum. Given the observed lack in selective pressures in the GFD state, why is it then that BTNL3/8 expression cannot lead to the expansion of residual V$\gamma4^+$ clones? The expansion of the V$\gamma7^+$ IEL compartment in mice was shown to depend on the expression of Btnl1[20]. More specifically, in Btnl1 deficient mice, V$\gamma7^+$ IELs were only capable of expanding when Btnl1 was expressed in the first three weeks of life[20]. When Btnl1 was expressed later in life, V$\gamma7^+$ IELs were still capable of recognizing Btnl1 based on phenotypic alterations, but the cells were not capable of expanding[20]. This suggests that BTNL expression alone is not sufficient to recover V$\gamma4^+$ IELs in GFD patients and that niche dynamics dictate the so called real-estate available for various IEL subsets to establish tissue-residence. Also, it is possible that the TCR$\gamma\delta^+$ IELs infiltrating the celiac mucosa may be better fit in the new environment and capable of consistently outcompeting the re-establishment of the innate-like V$\gamma4^+$ IEL compartment.

In contrast to a report studying the TCR repertoire of CD103$^+$ TCR$\gamma\delta^+$ T cells in the blood of CeD patients challenged with gluten, we did not find an enrichment in IELs of TCRs sharing the CDR3δ motifs reported[106]. Interestingly, this study showed CD103$^+$ CD38$^+$ cells appear in the blood of GFD CeD patients six days after gluten-challenge, but the origin of these cells is difficult to explain and is poorly discussed[106]. The authors suggest these cells originiate from priming events in mesenteric lymph nodes, but the expression of CD103 on the surface would suggest that these cells originate from the gut as there have not been any studies demonstrating the acquisition of CD103 and CD38 upon priming in lymph nodes. It is unlikely that these cells arose from pre-existing IELs as this would require active trafficking out of the epithelium through the lymph and thoracic duct and eventually into the blood. The lack of these sequences in our data set also excludes IEL origin. Whether established tissue-resident cells in the lamina propria can egress out of the gut, and if so under what

conditions, remains to be determined. However, there is evidence that cells may transiently traffic into tissues and egress via lymph in a CCR7 dependent manner[135,136] or a CCR7 independent manner under chronic inflammation[137]. Alternatively, cells may undergo priming in Payer's patches (Pp) where perhaps the conditions are more favorable for acquisition of CD103 and CD38, implicating the expression of the selecting ligand, given the observed CDR3 motif, within Pp. Given our observation that H-J1$^+$ clones retract on a GFD, this would suggest expression of the celiac ligand should be restricted to active CeD patients and it is unlikely that this antigen can be induced in time to prime sufficient numbers of TCR$\gamma\delta^+$ T cells to be found in blood after 6 days. Altogether, it is difficult to reconcile the two data sets but regardless of the origin of the cells in the study by Han et. al, it seems these cells never establish residence in the IEL compartment raising questions about the relevance of these observations.

The data generated on Vδ1$^-$ IELs is difficult to fully interpret in the context of CeD. For controls, Vδ1$^-$ IELs were shown to be heavily biased towards *TRGV4* usage, in line with Vδ1$^+$ IELs, and this bias was lost in CeD, also similarly to Vδ1$^+$ IELs. However, we did not find any evidence of selection in Vδ1$^-$ IEL repertoires in active CeD. It is possible that Vδ1$^+$ IELs are selectively expanded in active CeD, but our study design does not allow us to exclude the possibility for selection within the Vδ1$^-$ IEL repertoire. This is based on the fact that due to limitations in available antibodies, we cannot sort specific δ subsets. It is therefore possible that under-represented δ subsets may exhibit selection in active CeD but we do not have sufficient resolution to quantify this when sequencing bulk Vδ1$^-$ IELs.

Together, our data dispute the prevailing hypothesis that expansions of TCR$\gamma\delta^+$ IELs in CeD patients arise from the pre-existing healthy subset[31] in response to innate cues such as IL-15. Instead, we propose the repertoire is refreshed by infiltrating TCR$\gamma\delta^+$ IELs that are recruited to the inflammatory celiac lesion, a model which we will discuss in more detail

below.

4.2 TCR$\gamma\delta^+$ IEL function

By combining surface marker expression profiling, RNA-sequencing, and a variety of *ex vivo* functional assays we were able to provide the first data on the functional capacity of TCR$\gamma\delta^+$ IELs in the healthy small intestine as well as in CeD.

4.2.1 TCR$\gamma\delta^+$ IEL function in the healthy state

Our in depth analysis of TCR$\gamma\delta^+$ IELs revealed that under physiological conditions the small intestine is populated by a suset of innate NK-like IELs. These cells are characterized by expression of the activating NCRs NKp44 and NKp46 and displayed high levels of Granzyme B and had the capacity to degranulate upon engagement of their TCR in conjunction with NKp44 and NKp46. The TCR on its own was not capable of inducing high levels of degranulation and cells needed to be incubated with IL-15 prior to displaying maximum degranulation capacity. These observations have several implications. First, it suggests the TCR may not be sensitive in the steady state which would fit with observations made for V$\gamma7^+$ IELs in mouse[20]. Constitutive expression of BTNL ligands may induce TCR anergy in these cells. That IL-15 was required to induce maximal functional output would then be in line with the notion that IELs are in an "activated yet resting" state and require exogenous triggers to unleash their function[38]. This was similarly demonstrated for the "licensing" of TCR$\alpha\beta^+$CD8$\alpha\beta^+$ IELs by IL-15[55]. Given the ligands for these NCRs are also tightly regulated[25], this creates a two-checkpoint system to ensure controlled targeting of infected or tumorigenic epithelial cells.

Transcriptional profilling of NCR$^+$ V$\delta1^+$ IELs further supported the cytolytic profile of these cells but also revleaded amphiregulin was significantly expressed. Given its known functions in tissue healing[104], the expression of amphiregulin arms NCR$^+$ V$\delta1^+$ IELs with the capacity

to both eliminate target cells as well as initiate the subsequent events required for tissue repair. It was previously discussed that IEL compartments tend to be characterized by redundancy but the dual expression of NCRs and amphiregulin by NCR$^+$ Vδ1$^+$ IELs makes them the only T cell subset in the IEL compartment with this dual capacity as TCR$\alpha\beta^+$CD8$\alpha\beta^+$ IELs do not express either NKp44 or NKp46.

4.2.2 TCR$\gamma\delta^+$ IEL function in CeD

The switch in TCR repertoire observed in CeD was also associated with a switch in phenotype from cytolytic like cells towards cells more suited to the production of cytokines such as IFN-γ. The most informative result about the potential function of Vδ1$^+$ IELs in CeD came from the observation that GFD patients challenged with gluten for six-weeks had elevated frequencies of Vδ1$^+$ IELs producing IFN-γ post challenge, demonstrating Vδ1$^+$ IELs in CeD are sensitive to gluten. This sensitivity was also highlighted in the enriched expression of TCR activation genes in Vδ1$^+$ IELs from active CeD patients relative to both control and GFD IELs. Data from potential CeD patients demonstrated the turnover in cells can precede tissue damage so Vδ1$^+$ IELs in CeD have the potential to produce IFN-γ, although this still needs to be demonstrated, leading up to the initiation of tissue damage. Vδ1$^+$ IELs were also the only cell type that gained the capacity to produce IFN-γ in response to gluten so it is possible that once again although other cells types have the capacity to produce IFN-γ highlighting the redundancy of function within the IELs, Vδ1$^+$ IELs may play a specific role in the response to gluten. Therefore, we propose Vδ1$^+$ IELs may participate in the pathogenesis of CeD by producing IFN-γ, in response to the break in tolerance to gluten, which is known to induce up-regulation of stress ligands like HLA-E[101] that can serve as targets for TCR$\alpha\beta^+$CD8$\alpha\beta^+$ IELs[101,138], the primary effector T cell subset thought to be responsible for intestinal epithelial cell destruction in CeD[55,87,101].

The role of TCR$\gamma\delta^+$ IELs in the GFD state is less clear. The cells maintain the capacity to produce IFN-γ when stimulated *ex vivo* but no longer display a transcriptional signature of T cell activation. Considering the high diversity of TCRs in the GFD state and presumable absence of a ligand, it is possible these cells are lost without a cause, waiting for the re-introduction of gluten to be thrust back into action.

4.3 Tissue-resident lymphocyte turnover

By aiming to better characterize the nature of the TCR$\gamma\delta^+$ IEL infiltration in CeD, we unintentionally uncovered a phenomenon whereby the tissue-resident TCR$\gamma\delta^+$ compartment undergoes a profound reshaping. One of the open questions in the tissue-resident field centers around the stability and longevity of these cells and in particular how these compartments hold up in the face of chronic inflammation. Another intersting level of complexity that our study sheds light on is the interplay between the naturally occurring and induced tissue-resident subsets. Finally, our study supports a new model explaining the expansion of TCR$\gamma\delta^+$ IELs in CeD with implications for other complex immune disorders.

4.3.1 The impact of chronic inflammation on tissue-resident lymphocytes

The majority of studies investigating the dynamics of tissue-resident lymphocytes have relied on the use of acute viral infection models[30]. These models are powerful because the inducing agent can be controlled and genetically modified and the extent of the immune responses to a variety of viruses has been extensively studied. These studies are limited though because the net impact of the virus on the host is usually tightly controlled by the experimenter to ensure survival of the animal and the extent of inflammation is acute. Even for viruses that are characterized as "chronic" infections this usually involves a latent phase of infection where inflammation is not at its peak. It was shown that induced tissue-resident memory cells are stable populations that are not easily displaced by recurring infectious insults[10,11], but

the stability of these populations is yet to be tested in tissues where inflammation not only impacts immunity but also the tissue itself. Furthermore, the stability of naturally occurring tissue-resident lymphocytes is mostly assumed based on studies conducted for induced T_{RM}. Therefore, the question of how stable naturally occurring and induced tissue-resident compartments are in the face of chronic inflammation such as is the case for CeD where patients can suffer for years without being diagnosed remains unanswered.

Chronic inflammation in CeD has a net negative impact on the overall health of the tissue with the eventual destruction of epithelial cells and the disruption of villous architecture and consequently nutrient absorption. This level of impact on a tissue cannot be replicated by acute viral infection. Such an impact on the tissue is highlighted by the observation that expression of BTNL8 on epithelial cells, the selecting ligand of the naturally occurring tissue-resident TCR$\gamma\delta^+$ IEL[20], is lost in patients with active CeD, most likely for extended periods of time. These cells would then need to maintain their residence in the absence of cognate ligand signaling and in the face of recruitment of new lymphocytes into the tissue driven my chemokine gradients that are established as part of the inflammatory response[139]. Our data suggest that the naturally occurring TCR$\gamma\delta^+$ IELs are not capable of withstanding these events and eventually are superseded by infiltrating TCR$\gamma\delta^+$ T cells that establish residence in the inflamed IEL niche.

Our study implicates adaptive immune processes, based on the presence of clonal expansion of a public H-J1$^+$ CDR3γ motif in active CeD and subsequent retraction in GFD CeD, in the dynamics of the tissue-resident TCR$\gamma\delta^+$ IEL compartment in CeD. That TCR$\gamma\delta^+$ T cells may exhibit the capacity for adaptive immunity has been proposed in both mouse[140] and human[63,64,141]. A critical feature of adaptive immunity that we have not yet demonstrated is an antigen specific recall response. Although we observed a gluten dependent production of IFN-γ by Vδ1$^+$ IELs in CeD, it still needs to be determined whether or not H-J1$^+$ T

cells re-expand in patients upon gluten challenge. This would then position the TCR$\gamma\delta^+$ IELs found in CeD as induced T_{RM} cells as opposed to naturally occurring unconventional T cells, which we show occupy the niche in the steady state with unique properties and restricted TCRs. Adaptive immunity aside, Our study puts forward the first evidence for the replacement of a naturally occurring tissue-resident T cell by an induced tissue-resident T cell of the same lineage, in our case a TCR$\gamma\delta^+$ T cell. A similar phenomenon was observed for the displacement of the naturally occurring skin-resident $\gamma\delta^+$ T cell[12] after acute viral infection. However, in this study skin-resident $\gamma\delta^+$ T cells were displaced by adaptively induced TCR$\alpha\beta^+$ T_{RM} and the displacement was limited to the lesion and not absolute as $\gamma\delta^+$ T cells were still readily found in the lesion. Moreover, the longevity of this observation was not determined so it remains possible skin-resident $\gamma\delta^+$ T cells may eventually repopulate the affected area. This is in contrast to our model where the naturally occurring TCR$\gamma\delta^+$ IELs remain displaced in favor of induced TCR$\gamma\delta^+$ IELs in CeD patients even after 20 years on a GFD suggesting the events are permanent. This demonstrates the impact of chronic inflammation can be overwhelming for naturally occurring tissue-resident lymphocytes which exhibit extreme stability and longevity in healthy patients studied up to the age of 60 years.

Given the TCR$\gamma\delta^+$ IEL comapartment is occupied by a naturally occurring subset in the steady state, our study does not provide comprehensive data on the stability of induced T_{RM} in the context of chronic inflammation. Given our identification of a CDR3 motif in the active disease state, we may be able to shed light on this question by studying the dynamics of H-J1$^+$ clones after gluten-challenge. However, a major caveat is it will be difficult to decipher the origin of re-expanded clones bearing H-J1$^+$ TCRs as they may originate from newly primed cells upon the re-introduction of gluten. A single cell approach would be much more powerful here as the likelihood of both the CDR3γ and CDR3δ of H-J1$^+$ associated TCRs being encoded for by the exact same DNA sequence in two T cells with different clonal origins is unlikely. Therefore, the stability of induced T_{RM} in the context of chronic inflammation is

yet to be fully elucidated.

4.3.2 Model for turnover of TCR$\gamma\delta^+$ IELs in CeD

By integrating the data we generated on the function and TCR repertoire of TCR$\gamma\delta^+$ IELs in health and disease with what is known about lymphocyte trafficking dynamics[89,139,142] and immunity in general, we propose here a model by which the turnover of TCR$\gamma\delta^+$ IELs takes place in CeD.

The heterogeneity we observe in potential CeD patients provides a unique window into the events that precede the full blown turnover of the TCR$\gamma\delta^+$ IEL compartment. V$\delta1^+$ IELs are expanded in potential CeD patients, similarly to what we observe in the active and GFD states. A critical difference is the compartment displays evidence of transition in potential CeD patients with some patients having lost all BTNL3/8 reactive IELs while other patients exhibit expansions of NCR$^+$ IELs with intact BTNL3/8 reactivity. We propose that the naturally occurring tissue-resident V$\delta1^+$ IEL compartment responds to the initial break in tolerance to gluten by expanding in an attempt to potentially stave off effects of inflammation. This observation is actually in line with the hypothesis put forward by Hayday[31,90] that the expansion of TCR$\gamma\delta^+$ IELs is in an attempt to stave off infiltrating killer cells and that eventually a tipping point is reached and full blown disease ensues. Importantly, Hayday and colleagues identified BTNL molecules as selecting agents within the tissue for TCR$\gamma\delta^+$ IELs[20]. This advancement educates our model and we propose the observed loss of BTNL8 expression in a subset of potential CeD patients and in active CeD patients sets the stage for the eventual loss of the naturally occurring tissue-resident TCR$\gamma\delta^+$ IELs. As we show the entire TCR$\gamma\delta^+$ IEL compartment is biased towards BTNL3/8 reactivity, these cells most likely die in the absence of their ligand or alternatively are turned over by processes that are yet to be fully elucidated whereby infiltrating cells destined to become IEL sup-

plant them[89] or they egress out of the tissue as a result of extended periods of inflammation[137].

The celiac TCR$\gamma\delta^+$ IEL can originate from three primary sources. (i) The first is from within the tissue whereby low frequency clones, which are not BTNL3/8 reactive and that we do not detect because of limitations in the amount of material that can be collected and sequenced from humans, expand in response to *in situ* signals. (ii) The second is the non-specific recruitment of TCR$\gamma\delta^+$ T cells from the periphery by chemokine gradients[139] created within the inflamed celiac mucosa. (iii) The third is TCR$\gamma\delta^+$ T cells may be primed in Pp or mesenteric lymph nodes (MLN) in response to disease specific antigens and subsequently recruited to the gut to establish residence in the IEL compartment. We believe the first is the least likely given the homogenous nature of the TCR$\gamma\delta^+$ IEL compartment in the steady state. The sustained expansion of TCR$\gamma\delta^+$ IELs in the GFD state where inflammation has subsided is difficult to reconcile with the first option because in the absence of the in situ trigger that expanded these cells to begin with one would predict a contraction. A combination of the second and third options is most compatible with the combined data we observe in potential CeD patients, active CeD patients, and GFD CeD patients. We only observe evidence of antigen driven expansions in active CeD patients with the emergence of the H-J1 CDR3γ motif. This suggests the initial pool of TCR$\gamma\delta^+$ IELs that take over residence in place of the naturally occurring subset in potential CeD patients arise from peripheral cells recruited into the tissue. In the absence of a driving antigen we propose these cells establish residence in an antigen-independent manner as has been shown for the generation of bystander T_{RM} cells in mouse[10,11]. Bystander T_{RM} cells originated from cells with an effector or memory phenotype (antigen experienced)[10,11] and we show a significant proportion of V$\delta1^+$ and V$\delta1^-$ T cells can be found in peripheral blood with this phenotype. Next comes the event that results in the clonal expansion of H-J1 bearing T cells in active CeD patients. These cells may expand locally in the tissue in response to the induction of a celiac specific ligand or they may be de novo primed in Pp or MLNs with

subsequent recruitment into the tissue. Support for the latter comes from our data showing that dominant clonal expansions bearing the H-J1 motif could be found in the blood of active CeD patients. Interestingly, patients with subdominant H-J1$^+$ clones in the intestine had dominant H-J1$^+$ clones in the blood. Finally, the absence of expanded H-J1 bearing TCRs in the GFD state coupled with the observed high diversity of TCRs would fit with a model whereby the active CeD ligand is lost upon resolution of inflammation resulting in a redistribution of the repertoire. The high diversity of TCRs in GFD patients coupled with the absence of an active TCR signaling transcriptional signature, which was observed in active CeD patients, would then provoke the suggestion that GFD IELs lack a ligand. Resident cells in the GFD state may be maintained indefinitely in the absence of antigen or the IEL compartment may undergo steady state turnover as was proposed for mouse IELs[89].

More nuanced features of the TCR repertoire that are not easily fit into a general model need to be considered. The preferential expansion of Vδ1$^+$ IELs in CeD is difficult to reconcile. Upon the loss of the naturally occurring subset, our data do not provide much insight into why Vδ1 expressing T cells would be preferentially recruited to the inflamed tissue in the absence of selection, especially when considering Vδ1$^+$ T cells make up a small fraction of TCR$\gamma\delta^+$ T cells in the blood. We also did not find any Vδ1 associated CDR3 motifs in active CeD patients with clonal expansions carrying the Vγ-chain H-J1 CDR3 so if the Vδ1 chain plays a role in recognition of the celiac ligand this must depend on CDR1 and CDR2 encoded regions. Interestingly, Vδ1 is the most widely used δ-chain in steady state IELs as well. The fact that Vδ1$^-$ IELs showed equal reactivity to BTNL3/8 in the steady state makes this bias difficult to reconcile if BTNL3/8 molecules are to be considered the sole ligand in the steady state. The inherent Vδ1$^+$ bias amongst IELs may then be a explained by a constitutively expressed (health and disease) gut-specific self ligand that biases towards the selection of Vδ1 bearing TCRs. Alternatively, the bias may be the result of Vδ1$^-$ specificities and their associated ligands being enriched elsewhere in the body. For instance, it has been shown that human

V$\delta 2^+$ T cells can recognize phosphoantigens[143] and peripheral blood V$\delta 2^+$ T cells play a role in *Mycobacterium* infections[144] suggesting they may exert effector functions outside of tissues. In mouse, V$\delta 1^+$ cells are enriched in skin with their cognate ligand Skint1[19]. A comprehensive analysis of chemokine receptor expression on human peripheral V$\delta 1^+$ and V$\delta 1^-$ T cells may shed light on which subset expresses the pre-requisite set of receptors that would favor recruitment into the inflamed gut.

Our data have made it possible to generate testable hypothesis about the mechanisms at play in the turnover of tissue-resident TCR$\gamma\delta^+$ IELs in CeD.

4.3.3 Implications for human disease

It has been estimated that up to 1.6 million Americans adhere to a GFD without having been diagnosed with CeD[145]. Moreover, analysis of serologies and intestinal biopsies in the absence of gluten ingestion will show up normal and the current standard of care for diagnosing CeD involves prolonged gluten challenge followed by biopsy to observe the development of villous atrophy. The data we present on *ex vivo* profilling of NCR expression on V$\delta 1^+$ IELs could be used as diagnostic tool for patients on a GFD. The loss of NCR$^+$ V$\delta 1^+$ IELs when combined with the expansion of V$\delta 1^+$ IELs is a robust readout and holds up in patients on a GFD for up to 20 years. Additionally, analysis of the ILC compartment revleaded that NCR expression on these cells was lost in active CeD patients but recovered on a GFD. This data could then be used to potentially decipher whether or not a patient complaining of symptoms claiming to be on a GFD actually had contaminating exposure to gluten. These analysis could be readily applied by equipped hospitals as they rely on commercially available antibodies and flow cytometry. Similar technical approaches are currently used to determine whether patients have refractory celiac disease.

The loss of naturally occurring tissue-resident lymphocytes may occur in other chronic inflammatory conditions. Our data from human colon showed NCR^+ $V\delta1^+$ IELs are well represented and other studies have shown colon IEL exhibit BTNL3/8 reactivity with *TRGV4* usage[20]. It would then be easily testable in diseases such as Crohn's disease and ulcerative colitis as human samples can be readily obtained for study. Based on our model, the critical event proceeding the turnover of this innate compartment has to involve the modulation of BTNL3/8 expression. Interestingly, BTNL8 transcripts were shown to be significantly reduced in patients with ulcerative colitis[120] making it a good candidate for us to test our model.

The permanent loss of the naturally occurring $TCR\gamma\delta^+$ IEL subset in CeD leaves the afflicted region of the small intestine without a unique subset that cannot be compensated for by $TCR\alpha\beta^+$ IELs as these cells do not express NKp44 or NKp46. Patients with CeD have an increased risk to develop small intestinal adenocarcinomas but whether or not the loss of innate $TCR\gamma\delta^+$ IELs contributes to this is speculative.

CHAPTER 5

FUTURE DIRECTIONS

A series of intersting and independent questions have arisen as a consequence of uncovering the turnover of TCR$\gamma\delta^+$ IELs in CeD. The two most intersting are what do $\gamma\delta$ T cells in CeD see and what are the mechanisms by which the observed turnover takes place? A discussion of these questions will be the topic of this chapter.

5.1 Identifying the celiac ligand

The potential for a ligand that selects TCR$\gamma\delta^+$ IELs stems from our observation that clonal expansions in patients with active CeD were found to carry a shared CDR3γ characterized by a non-germline encoded (nucleotides generated during recombination process) H amino acid that was found adjacent to the J-segment 1 (H-J1). This CDR3γ motif was not associated with particular *TRGV* gene usage as we found overlapping CDR3s bearing the H-J1 between active CeD patients that used variable *TRGV* gene segments. Analysis of the repertoires of V$\delta1^+$ and V$\delta1^-$ IELs revealed that this H-J1 enrichment was only associated with Vδ1 bearing TCRs. Therefore, the TCR that is most likely to recognize a celiac ligand is a V$\delta1^+$H-J1$^+$ TCR. A final consideration is that H is a unique amino acid in that it can change conformations based on pH. pH could be play a role in recognition *in vivo* with inflammation and villous atrophy most likely altering the physiology of the gut microenvironment. Therefore, pH will need to be factored in when designing experiments to assess reactivity. In an attempt to study the reactivity of TCRs from active CeD patients to BTNL3/8, we have already generated V$\delta1^+$H-J1$^+$ T cell clones from two clonally expanded TCRs found in two unique active CeD patients. As was shown for BTNL3/8 assays, these T cell clones can be used in *in vitro* as well as *ex vivo* screening assays with potential ligands with assessment of induction of Nur77 via flow cytometry as a readout for TCR engament. In an attempt to develop a

more sensitive assay we will also transduce our TCRs into an NFAT-luciferase reporter line[146].

The series of observations that H-J1 bearing clones are not expanded in potential CeD patients, are clonally expanded in active CeD patients, and are no longer expanded in GFD CeD patients would fit with ligand expression being limited to the active state of disease. One set of ligands that would fit with these criteria is the variety of stress induced molecules that can be expressed by epithelial cells. The non-germline encoded nature of the H in the H-J1 motif would predict that such a ligand ought to be capable of presenting a variety of antigens as it is unlikely that the evolution of a ligand-TCR relationship between a stress induced molecule such as MIC-A, which is incapable of presenting variable antigens[147], would depend on random events during recombination for recognition. In an attempt to narrow down our search we investigated the transcript expression of a variety of molecules whose expression might be altered in CeD and with known capacity to present variable antigens (*CD1a, CD1b, CD1c, CD1d, MR1, HLA-E, HLA-F, HLA-G*) from whole biopsies of healthy individuals and patients in different stages of CeD. In line with our hypothesis, the expression of *HLA-E*, *HLA-F*, and *HLA-G* transcripts was significantly increased in active CeD patients relative to both controls and GFD-treated CeD patients (Fig. 5.1). Therefore, these three molecules make reasonable candidates for testing of reactivity with our H-J1 TCR clones in *in vitro* assays. The observations made by Davis and colleagues that Vδ1$^+$ T cells with a shared CDR3 motif can be found in blood six days after gluten-challenge[106], although difficult to explain as previously discussed, provoke the obvious choice of gluten as a potential antigen for Vδ1$^+$H-J1$^+$ IELs. This makes HLA-E a particular intersting choice as it has been shown that gliadin peptides can stabilize expression of HLA-E[148]. If gluten based peptides are not implicated (independent of what molecule they are presented on) one could use biopsies from active CeD patients as a source of potential antigen. Fractionating extracts and flowing them over columns coated with H-J1 bearing TCRs in an attempt to see if something sticks could be a viable strategy.

Additional tools that could be used are TCR tetramers from the H-J1 expressing clones. These tetramers could be used to stain epithelial cell fractions from patients or histology slides in an attempt to see if the ligand is expressed on the surface of epithelial cells from CeD patients. H-J1 T cell clones could also be co-cultured with the epithelial cell fractions to asses the presence of a ligand. As it can be challenging to get enough CeD patients in a time window conducive for high throughput screening, an alternative approach may be to incubate healthy biopsies (which are more readily available) with an array of inflammatory cytokines that are known to be up-regulated in CeD such as IL-15[84] and IFN-γ which have the potential to induce expression of stress ligands such as HLA-E[101]. One could then design experiments where the potential ligand is off or on to asses the reactivity of tetramers or T cell clones. Another approach could also be to generate a CRISPR/Cas KO library from a variety of cell lines with the potential to express a variety of ligands (either known or those that can be induced) and use the NFAT-Luciferease reporter for more high-throughput screening.

The hunt for the ligand will be challenging but we have put forward a compelling set of arguments that narrow down the candidates for the initial set of experiments. Ultimately, the identification of such a ligand could give great insights into the activities of these cells in CeD as well as provide additional evidence for alternative specificities for TCR$\gamma\delta^+$ T cells that could aid in better understanding how these cells function in immunity.

5.2 Mechanisms underlying the turnover of tissue-resident lymphocytes

Perhaps the most intriguing questions that arise from our work and other studies are those that relate to lymphocyte trafficking dynamics into and out of tissues. A survey of the

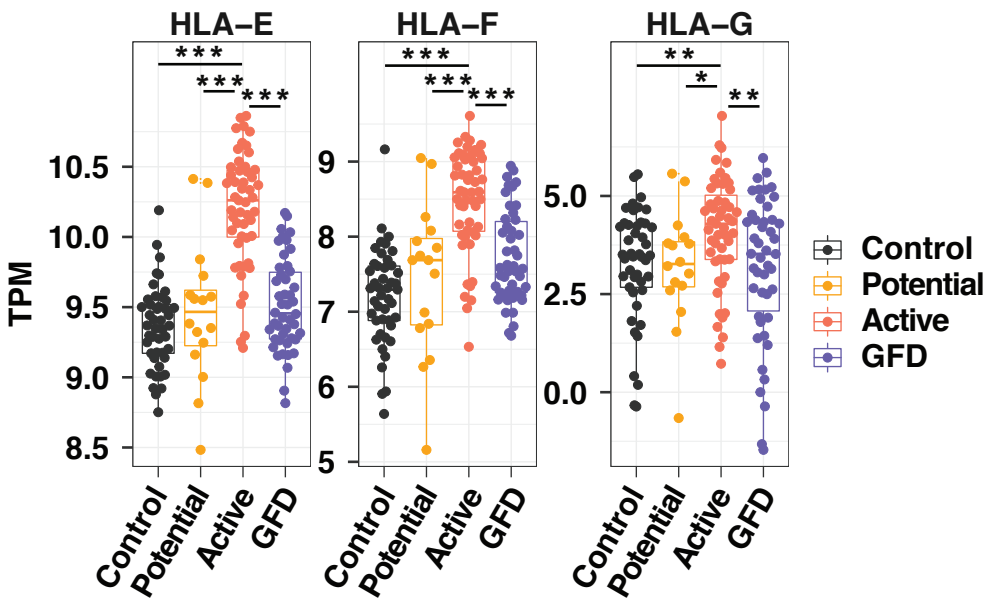

Figure 5.1: Expression of HLA-E, HLA-F, and HLA-G is enriched in active CeD
Whole biopsy RNA was isolated from patients and subjected to RNA-sequencing. Data for individual genes is represented as Transcripts Per Kilobase Million (TPM). Data is summarized in box plots displaying the first and third quartiles. *p<0.05, **p<0.01, ***p<0.001; Kruskal-Wallis rank sum test followed by Dunns test for multiple comparisons.

literature shows the majority of work has focused on characterizing how T cells get into and out of lymph nodes as well as how lymphocytes leave the blood and enter tissues[139,142], but the data becomes less clear with regards to lymphocyte egress from tissues and especially in the context of chronic inflammation. A handful of studies suggest that CCR7 expression may be required for egress of lymphocytes out of tissues and into lymph[135,136] but these studies rely on artificial models where lymphocytes are either injected into the tissue or recruited there by adjuvant. Furthermore, they only demonstrate that it is possible for cells to take the route from tissue to lymph but that does not mean that lymphocytes that actually establish residence maintain any capacity to egress from tissue. The reason the latter point is of interest is because we observe a loss of naturally occurring TCR$\gamma\delta^+$ IELs in CeD patients as well as the retraction of H-J1 bearing clones in active CeD patients and subsequent increased CDR3 diversity in GFD patients. Is the loss of this innate subset in part due to egress of cells in response to chronic inflammation? Do H-J1 cells simply die once

inflammation has subsided or are they actively excluded from the tissue? Is the increased diversity of cells in GFD patients a result of recycling of the IEL compartment? Also, it is known that lymphocyte infiltration as a whole goes down upon introduction of a GFD. Are all these events dependent on cell death *in situ* or is there a contribution of cell egress from tissues?

The mechanisms at play in the recruitment of new IELs into the tissue such as appears to be the case in CeD are also unclear. Are new cells being primed in secondary lymphoid organs or are they drawn in directly from the periphery? Work in mouse has suggested the IEL compartment is constantly being turned over with a steady influx of cells directly from the thymus driven by expression of $\alpha 4\beta 7$ or from cells that appear to be primed in Pp prior to routing back to the gut[89]. Which of these mechanisms is at play in CeD remains to be determined.

Some of the basic aspects of our proposed model require the development of new tools in order to be tested properly. It was shown that V$\gamma 7^+$ IELs in mouse are dependent on Btnl1 expression early in life and that induced expression later in life was not sufficient to recoup this population[20]. However, this study did not show what happens to this population when Btnl1 expression is taken away after the niche has been established. An inducible Btnl1 KO model would recreate the loss of BTNL8 expression later in life that we observe in CeD patients and allow for the testing of whether or not V$\gamma 7^+$ IELs can be maintained in the absence of their ligand and whether or not inflammation is required for the loss of cells to take place and if these cells are lost what cells take their place?

Another interesting question is whether immune responses that are genrerated in the gut at a given site can lead to protection elsewhere in the body. As described previously, data put forward by Davis and colleagues on the appearance of CD103$^+$ CD38$^+$ TCR$\gamma\delta^+$ T cells in the blood post gluten challenge[106] provokes the question of whether or not it is possible for T cells to leave the gut and find their way back into circulation after the initiation

of inflammation locally. Moreover, it has been suggested for ILC2s that populations that reside in the gut can contribute to immune response in the lungs[149]. And then there is the mysterious case of oral tolerance where it is known that the establishment of tolerance to a dietary antigen in the gut can protect against exposure to the same dietary antigen at peripheral sites[150]. Developing genetic tools in mousse that could allow for fate-mapping of cells that establish residence in the gut would provide a powerful tool as cells could then be easily traced throughout the body in response to various triggers. More data is needed to establish such models because gut exclusive markers for lymphocytes are still lacking.

BIBLIOGRAPHY

[1] J. M. Schenkel and D. Masopust, "Tissue-resident memory T cells.," *Immunity*, vol. 41, pp. 886–897, Dec. 2014.

[2] N. Zhang and M. J. Bevan, "Transforming growth factor-β signaling controls the formation and maintenance of gut-resident memory T cells by regulating migration and retention.," *Immunity*, vol. 39, pp. 687–696, Oct. 2013.

[3] K. L. Cepek, S. K. Shaw, C. M. Parker, G. J. Russell, J. S. Morrow, D. L. Rimm, and M. B. Brenner, "Adhesion between epithelial cells and T lymphocytes mediated by E-cadherin and the alpha E beta 7 integrin.," *Nature*, vol. 372, pp. 190–193, Nov. 1994.

[4] C. N. Skon, J.-Y. Lee, K. G. Anderson, D. Masopust, K. A. Hogquist, and S. C. Jameson, "Transcriptional downregulation of S1pr1 is required for the establishment of resident memory CD8+ T cells.," *Nature Immunology*, vol. 14, pp. 1285–1293, Dec. 2013.

[5] L. L. Lanier, D. W. Buck, L. Rhodes, A. Ding, E. Evans, C. Barney, and J. H. Phillips, "Interleukin 2 activation of natural killer cells rapidly induces the expression and phosphorylation of the Leu-23 activation antigen.," *The Journal of experimental medicine*, vol. 167, pp. 1572–1585, May 1988.

[6] L. R. Shiow, D. B. Rosen, N. Brdicková, Y. Xu, J. An, L. L. Lanier, J. G. Cyster, and M. Matloubian, "CD69 acts downstream of interferon-alpha/beta to inhibit S1P1 and lymphocyte egress from lymphoid organs.," *Nature*, vol. 440, pp. 540–544, Mar. 2006.

[7] S. Sugahara, T. Shimizu, Y. Yoshida, T. Aiba, S. Yamagiwa, H. Asakura, and T. Abo, "Extrathymic derivation of gut lymphocytes in parabiotic mice.," *Immunology*, vol. 96, pp. 57–65, Jan. 1999.

[8] G. Gasteiger, X. Fan, S. Dikiy, S. Y. Lee, and A. Y. Rudensky, "Tissue residency of innate lymphoid cells in lymphoid and nonlymphoid organs.," *Science*, vol. 350, pp. 981–985, Nov. 2015.

[9] H. Peng, X. Jiang, Y. Chen, D. K. Sojka, H. Wei, X. Gao, R. Sun, W. M. Yokoyama, and Z. Tian, "Liver-resident NK cells confer adaptive immunity in skin-contact inflammation.," *Journal of Clinical Investigation*, vol. 123, pp. 1444–1456, Apr. 2013.

[10] L. K. Beura, J. S. Mitchell, E. A. Thompson, J. M. Schenkel, J. Mohammed, S. Wijeyesinghe, R. Fonseca, B. J. Burbach, H. D. Hickman, V. Vezys, B. T. Fife, and D. Masopust, "Intravital mucosal imaging of CD8+ resident memory T cells shows tissue-autonomous recall responses that amplify secondary memory.," *Nature Immunology*, vol. 19, pp. 173–182, Feb. 2018.

[11] S. L. Park, A. Zaid, J. L. Hor, S. N. Christo, J. E. Prier, B. Davies, Y. O. Alexandre, J. L. Gregory, T. A. Russell, T. Gebhardt, F. R. Carbone, D. C. Tscharke, W. R. Heath, S. N. Mueller, and L. K. Mackay, "Local proliferation maintains a stable pool of tissue-resident memory T cells after antiviral recall responses.," *Nature Immunology*, vol. 19, pp. 183–191, Feb. 2018.

[12] A. Zaid, L. K. Mackay, A. Rahimpour, A. Braun, M. Veldhoen, F. R. Carbone, J. H. Manton, W. R. Heath, and S. N. Mueller, "Persistence of skin-resident memory T cells within an epidermal niche," *Proceedings of the National Academy of Sciences of the United States of America*, vol. 111, pp. 5307–5312, Apr. 2014.

[13] D. P. Hoytema van Konijnenburg, B. S. Reis, V. A. Pedicord, J. Farache, G. D. Victora, and D. Mucida, "Intestinal Epithelial and Intraepithelial T Cell Crosstalk Mediates a Dynamic Response to Infection.," *Cell*, vol. 171, pp. 783–794.e13, Nov. 2017.

[14] X. Jiang, R. A. Clark, L. Liu, A. J. Wagers, R. C. Fuhlbrigge, and T. S. Kupper, "Skin infection generates non-migratory memory CD8+ T(RM) cells providing global skin immunity.," *Nature*, vol. 483, pp. 227–231, Feb. 2012.

[15] X. Fan and A. Y. Rudensky, "Hallmarks of Tissue-Resident Lymphocytes," *Cell*, vol. 164, pp. 1198–1211, Mar. 2016.

[16] A. M. Mowat and W. W. Agace, "Regional specialization within the intestinal immune system.," *Nature Reviews Immunology*, vol. 14, pp. 667–685, Oct. 2014.

[17] T. Kenna, L. Golden-Mason, S. A. Porcelli, Y. Koezuka, J. E. Hegarty, C. O'Farrelly, D. G. Doherty, and L. G. Mason, "NKT cells from normal and tumor-bearing human livers are phenotypically and functionally distinct from murine NKT cells.," *Journal of immunology (Baltimore, Md. : 1950)*, vol. 171, pp. 1775–1779, Aug. 2003.

[18] Y. Cui, K. Franciszkiewicz, Y. K. Mburu, S. Mondot, L. Le Bourhis, V. Premel, E. Martin, A. Kachaner, L. Duban, M. A. Ingersoll, S. Rabot, J. Jaubert, J.-P. De Villartay, C. Soudais, and O. Lantz, "Mucosal-associated invariant T cell-rich congenic mouse strain allows functional evaluation.," *Journal of Clinical Investigation*, vol. 125, pp. 4171–4185, Nov. 2015.

[19] S. D. Barbee, M. J. Woodward, G. Turchinovich, J.-J. Mention, J. M. Lewis, L. M. Boyden, R. P. Lifton, R. Tigelaar, and A. C. Hayday, "Skint-1 is a highly specific, unique selecting component for epidermal T cells.," *Proceedings of the National Academy of Sciences*, vol. 108, pp. 3330–3335, Feb. 2011.

[20] R. Di Marco Barros, N. A. Roberts, R. J. Dart, P. Vantourout, A. Jandke, O. Nussbaumer, L. Deban, S. Cipolat, R. Hart, M. L. Iannitto, A. Laing, B. Spencer-Dene, P. East, D. Gibbons, P. M. Irving, P. Pereira, U. Steinhoff, and A. Hayday, "Epithelia Use Butyrophilin-like Molecules to Shape Organ-Specific $\gamma\delta$ T Cell Compartments.," *Cell*, vol. 167, pp. 203–218.e17, Sept. 2016.

[21] B. D. McDonald, J. J. Bunker, I. E. Ishizuka, B. Jabri, and A. Bendelac, "Elevated T cell receptor signaling identifies a thymic precursor to the TCR$\alpha\beta$(+)CD4(-)CD8β(-) intraepithelial lymphocyte lineage.," *Immunity*, vol. 41, pp. 219–229, Aug. 2014.

[22] A. Bandeira, T. Mota-Santos, S. Itohara, S. Degermann, C. Heusser, S. Tonegawa, and A. Coutinho, "Localization of / T cells to the intestinal epithelium is independent of normal microbial colonization.," *The Journal of experimental medicine*, vol. 172, pp. 239–244, July 1990.

[23] D. Masopust, V. Vezys, A. L. Marzo, and L. Lefrancois, "Preferential localization of effector memory cells in nonlymphoid tissue.," *Science*, vol. 291, pp. 2413–2417, Mar. 2001.

[24] M. A. Cooper, T. A. Fehniger, and M. A. Caligiuri, "The biology of human natural killer-cell subsets.," *Trends in Immunology*, vol. 22, pp. 633–640, Nov. 2001.

[25] P. H. Kruse, J. Matta, S. Ugolini, and E. Vivier, "Natural cytotoxicity receptors and their ligands.," *Immunology and Cell Biology*, vol. 92, pp. 221–229, Mar. 2014.

[26] A. Bendelac, O. Lantz, M. E. Quimby, J. W. Yewdell, J. R. Bennink, and R. R. Brutkiewicz, "CD1 recognition by mouse NK1+ T lymphocytes.," *Science*, vol. 268, pp. 863–865, May 1995.

[27] T. Kawano, J. Cui, Y. Koezuka, I. Toura, Y. Kaneko, K. Motoki, H. Ueno, R. Nakagawa, H. Sato, E. Kondo, H. Koseki, and M. Taniguchi, "CD1d-restricted and TCR-mediated activation of valpha14 NKT cells by glycosylceramides.," *Science*, vol. 278, pp. 1626–1629, Nov. 1997.

[28] E. Treiner, L. Duban, S. Bahram, M. Radosavljevic, V. Wanner, F. Tilloy, P. Affaticati, S. Gilfillan, and O. Lantz, "Selection of evolutionarily conserved mucosal-associated invariant T cells by MR1.," *Nature*, vol. 422, pp. 164–169, Mar. 2003.

[29] L. Kjer-Nielsen, O. Patel, A. J. Corbett, J. Le Nours, B. Meehan, L. Liu, M. Bhati, Z. Chen, L. Kostenko, R. Reantragoon, N. A. Williamson, A. W. Purcell, N. L. Dudek, M. J. McConville, R. A. J. O'Hair, G. N. Khairallah, D. I. Godfrey, D. P. Fairlie, J. Rossjohn, and J. McCluskey, "MR1 presents microbial vitamin B metabolites to MAIT cells.," *Nature*, vol. 491, pp. 717–723, Nov. 2012.

[30] S. N. Mueller and L. K. Mackay, "Tissue-resident memory T cells: local specialists in immune defence," *Nature Reviews Immunology*, vol. 16, pp. 79–89, Dec. 2015.

[31] A. Hayday, E. Theodoridis, E. Ramsburg, and J. Shires, "Intraepithelial lymphocytes: exploring the Third Way in immunology.," *Nature Immunology*, vol. 2, pp. 997–1003, Nov. 2001.

[32] H. Cheroutre, F. Lambolez, and D. Mucida, "The light and dark sides of intestinal intraepithelial lymphocytes," *Nature Reviews Immunology*, vol. 11, pp. 445–456, June 2011.

[33] M. Kawaguchi, M. Nanno, Y. Umesaki, S. Matsumoto, Y. Okada, Z. Cai, T. Shimamura, Y. Matsuoka, M. Ohwaki, and H. Ishikawa, "Cytolytic activity of intestinal intraepithelial lymphocytes in germ-free mice is strain dependent and determined by T cells expressing gamma delta T-cell antigen receptors.," *Proceedings of the National Academy of Sciences*, vol. 90, pp. 8591–8594, Sept. 1993.

[34] S. Kuo, A. El Guindy, C. M. Panwala, P. M. Hagan, and V. Camerini, "Differential appearance of T cell subsets in the large and small intestine of neonatal mice.," *Pediatric research*, vol. 49, pp. 543–551, Apr. 2001.

[35] Y. Umesaki, H. Setoyama, S. Matsumoto, and Y. Okada, "Expansion of alpha beta T-cell receptor-bearing intestinal intraepithelial lymphocytes after microbial colonization in germ-free mice and its independence from thymus.," *Immunology*, vol. 79, pp. 32–37, May 1993.

[36] N. Cerf-Bensussan, D. Guy-Grand, B. Lisowska-Grospierre, C. Griscelli, and A. K. Bhan, "A monoclonal antibody specific for rat intestinal lymphocytes.," *Journal of immunology (Baltimore, Md. : 1950)*, vol. 136, pp. 76–82, Jan. 1986.

[37] N. Cerf-Bensussan, A. Jarry, N. Brousse, B. Lisowska-Grospierre, D. Guy-Grand, and C. Griscelli, "A monoclonal antibody (HML-1) defining a novel membrane molecule present on human intestinal lymphocytes.," *European journal of immunology*, vol. 17, pp. 1279–1285, Sept. 1987.

[38] J. Shires, E. Theodoridis, and A. C. Hayday, "Biological insights into TCRgammadelta+ and TCRalphabeta+ intraepithelial lymphocytes provided by serial analysis of gene expression (SAGE).," *Immunity*, vol. 15, pp. 419–434, Sept. 2001.

[39] A. M. Fahrer, Y. Konigshofer, E. M. Kerr, G. Ghandour, D. H. Mack, M. M. Davis, and Y.-h. Chien, "Attributes of $\gamma\delta$ intraepithelial lymphocytes as suggested by their transcriptional profile," *Proceedings of the National Academy of Sciences*, vol. 98, no. 18, pp. 10261–10266, 2001.

[40] S. Melgar, A. Bas, S. Hammarström, and M.-L. Hammarström, "Human small intestinal mucosa harbours a small population of cytolytically active CD8+ alphabeta T lymphocytes.," *Immunology*, vol. 106, pp. 476–485, Aug. 2002.

[41] G. Boll, A. Rudolphi, S. Spiess, and J. Reimann, "Regional specialization of intraepithelial T cells in the murine small and large intestine.," *Scandinavian journal of immunology*, vol. 41, pp. 103–113, Feb. 1995.

[42] K. W. Beagley, K. Fujihashi, A. S. Lagoo, S. Lagoo-Deenadaylan, C. A. Black, A. M. Murray, A. T. Sharmanov, M. Yamamoto, J. R. McGhee, and C. O. Elson, "Differences in intraepithelial lymphocyte T cell subsets isolated from murine small versus large intestine.," *Journal of immunology (Baltimore, Md. : 1950)*, vol. 154, pp. 5611–5619, June 1995.

[43] V. Camerini, C. Panwala, and M. Kronenberg, "Regional specialization of the mucosal immune system. Intraepithelial lymphocytes of the large intestine have a different phenotype and function than those of the small intestine.," *Journal of immunology (Baltimore, Md. : 1950)*, vol. 151, pp. 1765–1776, Aug. 1993.

[44] C. Lundqvist, V. Baranov, S. Hammarström, L. Athlin, and M. L. Hammarström, "Intra-epithelial lymphocytes. Evidence for regional specialization and extrathymic T cell maturation in the human gut epithelium.," *International Immunology*, vol. 7, pp. 1473–1487, Sept. 1995.

[45] K. A. Casey, K. A. Fraser, J. M. Schenkel, A. Moran, M. C. Abt, L. K. Beura, P. J. Lucas, D. Artis, E. J. Wherry, K. Hogquist, V. Vezys, and D. Masopust, "Antigen-Independent Differentiation and Maintenance of Effector-like Resident Memory T Cells in Tissues," *Journal of immunology (Baltimore, Md. : 1950)*, vol. 188, pp. 4866–4875, May 2012.

[46] A. Jarry, N. Cerf-Bensussan, N. Brousse, F. Selz, and D. Guy-Grand, "Subsets of CD3+ (T cell receptor alpha/beta or gamma/delta) and CD3- lymphocytes isolated from normal human gut epithelium display phenotypical features different from their counterparts in peripheral blood.," *European journal of immunology*, vol. 20, pp. 1097–1103, May 1990.

[47] M. Latthe, L. Terry, and T. T. MacDonald, "High frequency of CD8 alpha alpha homodimer-bearing T cells in human fetal intestine.," *European journal of immunology*, vol. 24, pp. 1703–1705, July 1994.

[48] G. Verstichel, D. Vermijlen, L. Martens, G. Goetgeluk, M. Brouwer, N. Thiault, Y. Van Caeneghem, S. De Munter, K. Weening, S. Bonte, G. Leclercq, T. Taghon, T. Kerre, Y. Saeys, J. Van Dorpe, H. Cheroutre, and B. Vandekerckhove, "The checkpoint for agonist selection precedes conventional selection in human thymus.," *Science immunology*, vol. 2, Feb. 2017.

[49] D. Guy-Grand, B. Cuénod-Jabri, M. Malassis-Seris, F. Selz, and P. Vassalli, "Complexity of the mouse gut T cell immune system: identification of two distinct natural killer T cell intraepithelial lineages.," *European journal of immunology*, vol. 26, pp. 2248–2256, Sept. 1996.

[50] L. Lefrancois, "Phenotypic complexity of intraepithelial lymphocytes of the small intestine.," *Journal of immunology (Baltimore, Md. : 1950)*, vol. 147, pp. 1746–1751, Sept. 1991.

[51] D. Mucida, M. M. Husain, S. Muroi, F. van Wijk, R. Shinnakasu, Y. Naoe, B. S. Reis, Y. Huang, F. Lambolez, M. Docherty, A. Attinger, J.-W. Shui, G. Kim, C. J. Lena, S. Sakaguchi, C. Miyamoto, P. Wang, K. Atarashi, Y. Park, T. Nakayama, K. Honda, W. Ellmeier, M. Kronenberg, I. Taniuchi, and H. Cheroutre, "Transcriptional reprogramming of mature CD4 helper T cells generates distinct MHC class II-restricted cytotoxic T lymphocytes.," *Nature Immunology*, vol. 14, pp. 281–289, Mar. 2013.

[52] B. S. Reis, A. Rogoz, F. A. Costa-Pinto, I. Taniuchi, and D. Mucida, "Mutual expression of the transcription factors Runx3 and ThPOK regulates intestinal CD4+ T cell immunity," *Nature Immunology*, vol. 14, pp. 271–280, Jan. 2013.

[53] C. Atuma, V. Strugala, A. Allen, and L. Holm, "The adherent gastrointestinal mucus gel layer: thickness and physical state in vivo.," *American journal of physiology. Gastrointestinal and liver physiology*, vol. 280, pp. G922–9, May 2001.

[54] M. E. V. Johansson, M. Phillipson, J. Petersson, A. Velcich, L. Holm, and G. C. Hansson, "The inner of the two Muc2 mucin-dependent mucus layers in colon is devoid of bacteria.," *Proceedings of the National Academy of Sciences of the United States of America*, vol. 105, pp. 15064–15069, Sept. 2008.

[55] B. Meresse, Z. Chen, C. Ciszewski, M. Tretiakova, G. Bhagat, T. N. Krausz, D. H. Raulet, L. L. Lanier, V. Groh, T. Spies, E. C. Ebert, P. H. Green, and B. Jabri, "Coordinated induction by IL15 of a TCR-independent NKG2D signaling pathway converts CTL into lymphokine-activated killer cells in celiac disease.," *Immunity*, vol. 21, pp. 357–366, Sept. 2004.

[56] A. C. Hayday, H. Saito, S. D. Gillies, D. M. Kranz, G. Tanigawa, H. N. Eisen, and S. Tonegawa, "Structure, organization, and somatic rearrangement of T cell gamma genes.," *Cell*, vol. 40, pp. 259–269, Feb. 1985.

[57] M. B. Brenner, J. McLean, D. P. Dialynas, J. L. Strominger, J. A. Smith, F. L. Owen, J. G. Seidman, S. Ip, F. Rosen, and M. S. Krangel, "Identification of a putative second T-cell receptor.," *Nature*, vol. 322, pp. 145–149, July 1986.

[58] J. M. Lewis, M. Girardi, S. J. Roberts, S. D Barbee, A. C. Hayday, and R. E. Tigelaar, "Selection of the cutaneous intraepithelial $\gamma\delta$+ T cell repertoire by a thymic stromal determinant," *Nature Immunology*, vol. 7, pp. 843–850, July 2006.

[59] M. Bonneville, R. L. O'Brien, and W. K. Born, "$\gamma\delta$ T cell effector functions: a blendof innate programming and acquiredplasticity," *Nature Publishing Group*, vol. 10, pp. 467–478, June 2010.

[60] Y. Chowers, W. Holtmeier, J. Harwood, E. Morzycka-Wroblewska, and M. F. Kagnoff, "The V delta 1 T cell receptor repertoire in human small intestine and colon.," *The Journal of experimental medicine*, vol. 180, pp. 183–190, July 1994.

[61] W. Holtmeier, Y. Chowers, A. Lumeng, E. Morzycka-Wroblewska, and M. F. Kagnoff, "The delta T cell receptor repertoire in human colon and peripheral blood is oligoclonal irrespective of V region usage.," *Journal of Clinical Investigation*, vol. 96, pp. 1108–1117, Aug. 1995.

[62] W. Holtmeier, M. Pfänder, A. Hennemann, T. M. Zollner, R. Kaufmann, and W. F. Caspary, "The TCR-delta repertoire in normal human skin is restricted and distinct from the TCR-delta repertoire in the peripheral blood.," *The Journal of investigative dermatology*, vol. 116, pp. 275–280, Feb. 2001.

[63] S. Ravens, C. Schultze-Florey, S. Raha, I. Sandrock, M. Drenker, L. Oberdörfer, A. Reinhardt, I. Ravens, M. Beck, R. Geffers, C. von Kaisenberg, M. Heuser, F. Thol, A. Ganser, R. Förster, C. Koenecke, and I. Prinz, "Human $\gamma\delta$ T cells are quickly reconstituted after stem-cell transplantation and show adaptive clonal expansion in response to viral infection.," *Nature Immunology*, vol. 18, pp. 393–401, Apr. 2017.

[64] M. S. Davey, C. R. Willcox, S. P. Joyce, K. Ladell, S. A. Kasatskaya, J. E. McLaren, S. Hunter, M. Salim, F. Mohammed, D. A. Price, D. M. Chudakov, and B. E. Willcox, "Clonal selection in the human Vδ1 T cell repertoire indicates $\gamma\delta$ TCR-dependent adaptive immune surveillance.," *Nature Communications*, vol. 8, p. 14760, Mar. 2017.

[65] J. L. Harden, D. Hamm, N. Gulati, M. A. Lowes, and J. G. Krueger, "Deep Sequencing of the T-cell Receptor Repertoire Demonstrates Polyclonal T-cell Infiltrates in Psoriasis," *F1000Research*, Aug. 2015.

[66] C. A. Janeway, B. Jones, and A. Hayday, "Specificity and function of T cells bearing gamma delta receptors.," *Immunology today*, vol. 9, pp. 73–76, Mar. 1988.

[67] E. J. Adams, Y.-h. Chien, and K. C. Garcia, "Structure of a $\gamma\delta$ T cell receptor in complex with the nonclassical MHC T22," *Science*, vol. 308, no. 5719, pp. 227–231, 2005.

[68] A. P. Uldrich, J. Le Nours, D. G. Pellicci, N. A. Gherardin, K. G. McPherson, R. T. Lim, O. Patel, T. Beddoe, S. Gras, J. Rossjohn, and D. I. Godfrey, "CD1d-lipid antigen recognition by the $\gamma\delta$ TCR," *Nature Immunology*, vol. 14, pp. 1137–1145, Sept. 2013.

[69] A. M. Luoma, C. D. Castro, t. Mayassi Toufic, L. A. Bembinster, L. Bai, D. Picard, B. Anderson, L. Scharf, J. E. Kung, L. V. Sibener, P. B. Savage, B. Jabri, A. Bendelac, and E. J. Adams, "Crystal structure of Vδ1 T cell receptor in complex with CD1d-sulfatide shows MHC-like recognition of a self-lipid by human $\gamma\delta$ T cells.," *Immunity*, vol. 39, no. 6, pp. 1032–1042, 2013.

[70] W. K. Born, M. Kemal Aydintug, and R. L. O'Brien, "Diversity of $\gamma\delta$ T-cell antigens," *Cellular and Molecular Immunology*, vol. 10, pp. 13–20, Oct. 2012.

[71] Y.-h. Chien, C. Meyer, and M. Bonneville, "$\gamma\delta$T Cells: First Line of Defense and Beyond," *Annual Review of Immunology*, vol. 32, pp. 121–155, Mar. 2014.

[72] P. Vantourout and A. Hayday, "Six-of-the-best: unique contributions of $\gamma\delta$ T cells to immunology," *Nature Reviews Immunology*, vol. 13, pp. 88–100, Jan. 2013.

[73] M. M. Nielsen, D. A. Witherden, and W. L. Havran, "$\gamma\delta$ T cells in homeostasis and host defence of epithelial barrier tissues.," *Nature Reviews Immunology*, vol. 17, pp. 733–745, Dec. 2017.

[74] A. S. Ismail, K. M. Severson, and S. Vaishnava, "$\gamma\delta$ intraepithelial lymphocytes are essential mediators of host–microbial homeostasis at the intestinal mucosal surface," in *Proceedings of the ...*, 2011.

[75] S. J. Roberts, A. L. Smith, A. B. West, L. Wen, R. C. Findly, M. J. Owen, and A. C. Hayday, "T-cell alpha beta + and gamma delta + deficient mice display abnormal but distinct phenotypes toward a natural, widespread infection of the intestinal epithelium.," *Proceedings of the National Academy of Sciences*, vol. 93, pp. 11774–11779, Oct. 1996.

[76] R. Boismenu and W. L. Havran, "Modulation of epithelial cell growth by intraepithelial gamma delta T cells.," *Science*, vol. 266, pp. 1253–1255, Nov. 1994.

[77] K. L. Edelblum, L. Shen, C. R. Weber, A. M. Marchiando, B. S. Clay, Y. Wang, I. Prinz, B. Malissen, A. I. Sperling, and J. R. Turner, "Dynamic migration of $\gamma\delta$ intraepithelial lymphocytes requires occludin.," *Proceedings of the National Academy of Sciences of the United States of America*, vol. 109, pp. 7097–7102, May 2012.

[78] V. Chennupati, T. Worbs, X. Liu, F. H. Malinarich, S. Schmitz, J. D. Haas, B. Malissen, R. Förster, and I. Prinz, "Intra- and intercompartmental movement of gammadelta T cells: intestinal intraepithelial and peripheral gammadelta T cells represent exclusive nonoverlapping populations with distinct migration characteristics.," *The Journal of Immunology*, vol. 185, pp. 5160–5168, Nov. 2010.

[79] M. Emoto, O. Neuhaus, Y. Emoto, and S. H. Kaufmann, "Influence of beta 2-microglobulin expression on gamma interferon secretion and target cell lysis by intraepithelial lymphocytes during intestinal Listeria monocytogenes infection.," *Infection and immunity*, vol. 64, pp. 569–575, Feb. 1996.

[80] V. Abadie, L. M. Sollid, L. B. Barreiro, and B. Jabri, "Integration of Genetic and Immunological Insights into a Model of Celiac Disease Pathogenesis," *Annual Review of Immunology*, vol. 29, pp. 493–525, Apr. 2011.

[81] B. Jabri and L. M. Sollid, "Tissue-mediated control of immunopathology in coeliac disease," *Nature Reviews Immunology*, vol. 9, pp. 858–870, Dec. 2009.

[82] G. J. Tack, W. H. M. Verbeek, M. W. J. Schreurs, and C. J. J. Mulder, "The spectrum of celiac disease: epidemiology, clinical aspects and treatment," *Nature Reviews Gastroenterology & Hepatology*, vol. 7, pp. 204–213, Mar. 2010.

[83] S. Husby, S. Koletzko, I. R. Korponay-Szabó, M. L. Mearin, A. Phillips, R. Shamir, R. Troncone, K. Giersiepen, D. Branski, C. Catassi, M. Lelgeman, M. Mäki, C. Ribes-Koninckx, A. Ventura, K. P. Zimmer, ESPGHAN Working Group on Coeliac Disease Diagnosis, ESPGHAN Gastroenterology Committee, and European Society for Pediatric Gastroenterology, Hepatology, and Nutrition, "European Society for Pediatric Gastroenterology, Hepatology, and Nutrition guidelines for the diagnosis of coeliac disease.." J Pediatr Gastroenterol Nutr, Jan. 2012.

[84] M. Setty, V. Discepolo, V. Abadie, S. Kamhawi, T. Mayassi, A. Kent, C. Ciszewski, M. Maglio, E. Kistner, G. Bhagat, C. Semrad, S. S. Kupfer, P. H. Green, S. Guandalini, R. Troncone, J. A. Murray, J. R. Turner, and B. Jabri, "Distinct and Synergistic Contributions of Epithelial Stress and Adaptive Immunity to Functions of Intraepithelial

Killer Cells and Active Celiac Disease.," *Gastroenterology*, vol. 149, pp. 681–91.e10, Sept. 2015.

[85] M. N. Marsh and C. J. Heal, "Evolutionary Developments in Interpreting the Gluten-Induced Mucosal Celiac Lesion: An Archimedian Heuristic.," *Nutrients*, vol. 9, Feb. 2017.

[86] T. S. Halstensen, H. Scott, and P. Brandtzaeg, "Intraepithelial T cells of the TcR $/^+$ $CD8^-$ and $V1/J1^+$ phenotypes are increased in coeliac disease.," *Scandinavian journal of immunology*, vol. 30, pp. 665–672, Dec. 1989.

[87] T. Kutlu, N. Brousse, C. Rambaud, F. Le Deist, J. Schmitz, and N. Cerf-Bensussan, "Numbers of T cell receptor (TCR) β+ but not of TcR + intraepithelial lymphocytes correlate with the grade of villous atrophy in coeliac patients on a long term normal diet.," *Gut*, vol. 34, pp. 208–214, Feb. 1993.

[88] E. Savilahti, A. Arato, and M. Verkasalo, "Intestinal / receptor-bearing T lymphocytes in celiac disease and inflammatory bowel diseases in children. Constant increase in celiac disease.," *Pediatric research*, vol. 28, pp. 579–581, Dec. 1990.

[89] D. Guy-Grand, P. Vassalli, G. Eberl, P. Pereira, O. Burlen-Defranoux, F. Lemaitre, J. P. Di Santo, A. A. Freitas, A. Cumano, and A. Bandeira, "Origin, trafficking, and intraepithelial fate of gut-tropic T cells.," *The Journal of experimental medicine*, vol. 210, pp. 1839–1854, Aug. 2013.

[90] A. C. Hayday, "[gamma][delta] cells: a right time and a right place for a conserved third way of protection.," *Annual Review of Immunology*, vol. 18, pp. 975–1026, 2000.

[91] G. Pineton de Chambrun, L. Peyrin-Biroulet, M. Lémann, and J.-F. Colombel, "Clinical implications of mucosal healing for the management of IBD.," *Nature Reviews Gastroenterology & Hepatology*, vol. 7, pp. 15–29, Jan. 2010.

[92] D. M. da Fonseca, T. W. Hand, S.-J. Han, M. Y. Gerner, A. G. Zaretsky, A. L. Byrd, O. J. Harrison, A. M. Ortiz, M. Quinones, G. Trinchieri, J. M. Brenchley, I. E. Brodsky, R. N. Germain, G. J. Randolph, and Y. Belkaid, "Microbiota-Dependent Sequelae of Acute Infection Compromise Tissue-Specific Immunity," *Cell*, vol. 163, pp. 354–366, Oct. 2015.

[93] T. Goodman and L. Lefrancois, "Expression of the gamma-delta T-cell receptor on intestinal CD8+ intraepithelial lymphocytes.," *Nature*, vol. 333, pp. 855–858, June 1988.

[94] M. Bonneville, C. A. Janeway, K. Ito, W. Haser, I. Ishida, N. Nakanishi, and S. Tonegawa, "Intestinal intraepithelial lymphocytes are a distinct set of gamma delta T cells.," *Nature*, vol. 336, pp. 479–481, Dec. 1988.

[95] J. M.-L. Tjon, J. van Bergen, and F. Koning, "Celiac disease: how complicated can it get?," *Immunogenetics*, vol. 62, pp. 641–651, July 2010.

[96] B. Lebwohl, D. S. Sanders, and P. H. R. Green, "Coeliac disease.," *Lancet (London, England)*, vol. 391, pp. 70–81, Jan. 2018.

[97] D. A. Witherden, K. Ramirez, and W. L. Havran, "Multiple Receptor-Ligand Interactions Direct Tissue-Resident $\gamma\delta$ T Cell Activation.," *Frontiers in immunology*, vol. 5, p. 602, 2014.

[98] F. Sallusto, D. Lenig, R. Förster, M. Lipp, and A. Lanzavecchia, "Two subsets of memory T lymphocytes with distinct homing potentials and effector functions.," *Nature*, vol. 401, pp. 708–712, Oct. 1999.

[99] J. J. C. Thome, N. Yudanin, Y. Ohmura, M. Kubota, B. Grinshpun, T. Sathaliyawala, T. Kato, H. Lerner, Y. Shen, and D. L. Farber, "Spatial Map of Human T Cell Compartmentalization and Maintenance over Decades of Life," *Cell*, vol. 159, pp. 814–828, Nov. 2014.

[100] B. Meresse, G. Malamut, and N. Cerf-Bensussan, "Celiac Disease: An Immunological Jigsaw," *Immunity*, vol. 36, pp. 907–919, June 2012.

[101] B. Meresse, S. A. Curran, C. Ciszewski, G. Orbelyan, M. Setty, G. Bhagat, L. Lee, M. Tretiakova, C. Semrad, E. Kistner, R. J. Winchester, V. Braud, L. L. Lanier, D. E. Geraghty, P. H. Green, S. Guandalini, and B. Jabri, "Reprogramming of CTLs into natural killer-like cells in celiac disease.," *The Journal of experimental medicine*, vol. 203, pp. 1343–1355, May 2006.

[102] B. Jabri and V. Abadie, "IL-15 functions as a danger signal to regulate tissue-resident T cells and tissue destruction.," *Nature Reviews Immunology*, vol. 15, pp. 771–783, Dec. 2015.

[103] Y. Xu, V. Olman, and D. Xu, "Clustering gene expression data using a graph-theoretic approach: an application of minimum spanning trees.," *Bioinformatics (Oxford, England)*, vol. 18, pp. 536–545, Apr. 2002.

[104] D. M. W. Zaiss, W. C. Gause, L. C. Osborne, and D. Artis, "Emerging functions of amphiregulin in orchestrating immunity, inflammation, and tissue repair.," *Immunity*, vol. 42, pp. 216–226, Feb. 2015.

[105] N. Colaert, K. Helsens, L. Martens, J. Vandekerckhove, and K. Gevaert, "Improved visualization of protein consensus sequences by iceLogo.," *Nature Methods*, vol. 6, pp. 786–787, Nov. 2009.

[106] A. Han, E. W. Newell, J. Glanville, N. Fernandez-Becker, C. Khosla, Y.-h. Chien, and M. M. Davis, "Dietary gluten triggers concomitant activation of CD4+ and CD8+ $\alpha\beta$ T cells and $\gamma\delta$ T cells in celiac disease.," *Proceedings of the National Academy of Sciences of the United States of America*, vol. 110, pp. 13073–13078, Aug. 2013.

[107] A. Fabregat, S. Jupe, L. Matthews, K. Sidiropoulos, M. Gillespie, P. Garapati, R. Haw, B. Jassal, F. Korninger, B. May, M. Milacic, C. D. Roca, K. Rothfels, C. Sevilla, V. Shamovsky, S. Shorser, T. Varusai, G. Viteri, J. Weiser, G. Wu, L. Stein, H. Hermjakob, and P. D'Eustachio, "The Reactome Pathway Knowledgebase.," *Nucleic Acids Research*, vol. 46, pp. D649–D655, Jan. 2018.

[108] J. F. Ashouri and A. Weiss, "Endogenous Nur77 Is a Specific Indicator of Antigen Receptor Signaling in Human T and B Cells.," *Journal of immunology (Baltimore, Md. : 1950)*, vol. 198, pp. 657–668, Jan. 2017.

[109] P. Vantourout, A. Laing, M. J. Woodward, I. Zlatareva, L. Apolonia, A. W. Jones, A. P. Snijders, M. H. Malim, and A. C. Hayday, "Heteromeric interactions regulate butyrophilin (BTN) and BTN-like molecules governing $\gamma\delta$ T cell biology.," *Proceedings of the National Academy of Sciences of the United States of America*, vol. 115, pp. 1039–1044, Jan. 2018.

[110] K. Früh and Y. Yang, "Antigen presentation by MHC class I and its regulation by interferon gamma.," *Current Opinion in Immunology*, vol. 11, pp. 76–81, Feb. 1999.

[111] C. Nathan, "From transient infection to chronic disease," *Science*, vol. 350, pp. 161–161, Oct. 2015.

[112] P. H. R. Green and C. Cellier, "Celiac disease.," *New England Journal of Medicine*, vol. 357, pp. 1731–1743, Oct. 2007.

[113] S. Picelli, O. R. Faridani, A. K. Björklund, G. Winberg, S. Sagasser, and R. Sandberg, "Full-length RNA-seq from single cells using Smart-seq2.," *Nature Protocols*, vol. 9, pp. 171–181, Jan. 2014.

[114] G. Trynka, K. A. Hunt, N. A. Bockett, J. Romanos, V. Mistry, A. Szperl, S. F. Bakker, M. T. Bardella, L. Bhaw-Rosun, G. Castillejo, E. G. de la Concha, R. C. de Almeida, K.-R. M. Dias, C. C. van Diemen, P. C. A. Dubois, R. H. Duerr, S. Edkins, L. Franke, K. Fransen, J. Gutierrez, G. A. R. Heap, B. Hrdlickova, S. Hunt, L. Plaza Izurieta, V. Izzo, L. A. B. Joosten, C. Langford, M. C. Mazzilli, C. A. Mein, V. Midah, M. Mitrovic, B. Mora, M. Morelli, S. Nutland, C. Núñez, S. Onengut-Gumuscu, K. Pearce, M. Platteel, I. Polanco, S. Potter, C. Ribes-Koninckx, I. Ricaño-Ponce, S. S. Rich, A. Rybak, J. L. Santiago, S. Senapati, A. Sood, H. Szajewska, R. Troncone, J. Varadé, C. Wallace, V. M. Wolters, A. Zhernakova, Spanish Consortium on the Genetics of Coeliac Disease (CEGEC), PreventCD Study Group, Wellcome Trust Case Control Consortium (WTCCC), B. K. Thelma, B. Cukrowska, E. Urcelay, J. R. Bilbao, M. L. Mearin, D. Barisani, J. C. Barrett, V. Plagnol, P. Deloukas, C. Wijmenga, and D. A. van Heel, "Dense genotyping identifies and localizes multiple common and rare variant association signals in celiac disease.," *Nature Genetics*, vol. 43, pp. 1193–1201, Nov. 2011.

[115] S. Purcell, B. Neale, K. Todd-Brown, L. Thomas, M. A. R. Ferreira, D. Bender, J. Maller, P. Sklar, P. I. W. de Bakker, M. J. Daly, and P. C. Sham, "PLINK: a tool

set for whole-genome association and population-based linkage analyses.," *American journal of human genetics*, vol. 81, pp. 559–575, Sept. 2007.

[116] A. J. Monsuur, P. I. W. de Bakker, A. Zhernakova, D. Pinto, W. Verduijn, J. Romanos, R. Auricchio, A. Lopez, D. A. van Heel, J. B. A. Crusius, and C. Wijmenga, "Effective detection of human leukocyte antigen risk alleles in celiac disease using tag single nucleotide polymorphisms.," *PLoS ONE*, vol. 3, p. e2270, May 2008.

[117] L. Koskinen, J. Romanos, K. Kaukinen, K. Mustalahti, I. Korponay-Szabo, D. Barisani, M. T. Bardella, F. Ziberna, S. Vatta, G. Széles, Z. Pocsai, K. Karell, K. Haimila, R. Ádány, T. Not, A. Ventura, M. Mäki, J. Partanen, C. Wijmenga, and P. Saavalainen, "Cost-effective HLA typing with tagging SNPs predicts celiac disease risk haplotypes in the Finnish, Hungarian, and Italian populations.," *Immunogenetics*, vol. 61, pp. 247–256, Apr. 2009.

[118] D. A. Price, J. M. Brenchley, L. E. Ruff, M. R. Betts, B. J. Hill, M. Roederer, R. A. Koup, S. A. Migueles, E. Gostick, L. Wooldridge, A. K. Sewell, M. Connors, and D. C. Douek, "Avidity for antigen shapes clonal dominance in CD8+ T cell populations specific for persistent DNA viruses.," *The Journal of experimental medicine*, vol. 202, pp. 1349–1361, Nov. 2005.

[119] M. P. Lefranc, "IMGT, the international ImMunoGeneTics database(R)," *Nucleic Acids Research*, vol. 31, pp. 307–310, Jan. 2003.

[120] C. Lebrero-Fernández, U. A. Wenzel, P. Akeus, Y. Wang, H. Strid, M. Simrén, B. Gustavsson, L. G. Börjesson, S. L. Cardell, L. Öhman, M. Quiding-Järbrink, and A. Bas-Forsberg, "Altered expression of Butyrophilin (BTN) and BTN-like (BTNL) genes in intestinal inflammation and colon cancer.," *Immunity, inflammation and disease*, vol. 4, pp. 191–200, June 2016.

[121] J. Holst, A. L. Szymczak-Workman, K. M. Vignali, A. R. Burton, C. J. Workman, and D. A. A. Vignali, "Generation of T-cell receptor retrogenic mice.," *Nature Protocols*, vol. 1, no. 1, pp. 406–417, 2006.

[122] S. Gras, Z. Chen, J. J. Miles, Y. C. Liu, M. J. Bell, L. C. Sullivan, L. Kjer-Nielsen, R. M. Brennan, J. M. Burrows, M. A. Neller, R. Khanna, A. W. Purcell, A. G. Brooks, J. McCluskey, J. Rossjohn, and S. R. Burrows, "Allelic polymorphism in the T cell receptor and its impact on immune responses.," *The Journal of experimental medicine*, vol. 207, pp. 1555–1567, July 2010.

[123] N. L. Bray, H. Pimentel, P. Melsted, and L. Pachter, "Near-optimal probabilistic RNA-seq quantification.," *Nature Biotechnology*, vol. 34, pp. 525–527, May 2016.

[124] M. D. Robinson, D. J. McCarthy, and G. K. Smyth, "edgeR: a Bioconductor package for differential expression analysis of digital gene expression data.," *Bioinformatics (Oxford, England)*, vol. 26, pp. 139–140, Jan. 2010.

[125] M. E. Ritchie, B. Phipson, D. Wu, Y. Hu, C. W. Law, W. Shi, and G. K. Smyth, "limma powers differential expression analyses for RNA-sequencing and microarray studies.," *Nucleic Acids Research*, vol. 43, p. e47, Apr. 2015.

[126] X. Brochet, M. P. Lefranc, and V. Giudicelli, "IMGT/V-QUEST: the highly customized and integrated system for IG and TR standardized V-J and V-D-J sequence analysis," *Nucleic Acids Research*, vol. 36, pp. W503–W508, May 2008.

[127] M. Smithson and J. Verkuilen, "A better lemon squeezer? Maximum-likelihood regression with beta-distributed dependent variables.," *Psychological Methods*, vol. 11, no. 1, pp. 54–71, 2006.

[128] S. Ferrari and F. Cribari-Neto, "Beta Regression for Modelling Rates and Proportions," *Journal of Applied Statistics*, vol. 31, pp. 799–815, Aug. 2004.

[129] Y. Benjamini and Y. Hochberg, "Controlling the False Discovery Rate: A Practical and Powerful Approach to Multiple Testing on JSTOR," *Journal of the Royal Statistical Society Series B ...*, 1995.

[130] D. Maddelein, N. Colaert, I. Buchanan, N. Hulstaert, K. Gevaert, and L. Martens, "The iceLogo web server and SOAP service for determining protein consensus sequences," *Nucleic Acids Research*, vol. 43, pp. W543–W546, June 2015.

[131] M. R. Dunne, L. Elliott, S. Hussey, N. Mahmud, J. Kelly, D. G. Doherty, and C. F. Feighery, "Persistent changes in circulating and intestinal $\gamma\delta$ T cell subsets, invariant natural killer T cells and mucosal-associated invariant T cells in children and adults with coeliac disease.," *PLoS ONE*, vol. 8, no. 10, p. e76008, 2013.

[132] A. Regnault, A. Cumano, P. Vassalli, D. Guy-Grand, and P. Kourilsky, "Oligoclonal repertoire of the CD8 alpha alpha and the CD8 alpha beta TCR-alpha/beta murine intestinal intraepithelial T lymphocytes: evidence for the random emergence of T cells.," *The Journal of experimental medicine*, vol. 180, pp. 1345–1358, Oct. 1994.

[133] S. P. Balk, E. C. Ebert, R. L. Blumenthal, F. V. McDermott, K. W. Wucherpfennig, S. B. Landau, and R. S. Blumberg, "Oligoclonal expansion and CD1 recognition by human intestinal intraepithelial lymphocytes.," *Science*, vol. 253, pp. 1411–1415, Sept. 1991.

[134] C. Van Kerckhove, G. J. Russell, K. Deusch, K. Reich, A. K. Bhan, H. DerSimonian, and M. B. Brenner, "Oligoclonality of human intestinal intraepithelial T cells.," *The Journal of experimental medicine*, vol. 175, pp. 57–63, Jan. 1992.

[135] S. K. Bromley, S. Y. Thomas, and A. D. Luster, "Chemokine receptor CCR7 guides T cell exit from peripheral tissues and entry into afferent lymphatics," *Nature Immunology*, vol. 6, pp. 895–901, Aug. 2005.

[136] G. F. Debes, C. N. Arnold, A. J. Young, S. Krautwald, M. Lipp, J. B. Hay, and E. C. Butcher, "Chemokine receptor CCR7 required for T lymphocyte exit from peripheral tissues," *Nature Immunology*, vol. 6, pp. 889–894, Aug. 2005.

[137] M. N. Brown, S. R. Fintushel, M. H. Lee, S. Jennrich, S. A. Geherin, J. B. Hay, E. C. Butcher, and G. F. Debes, "Chemoattractant receptors and lymphocyte egress from extralymphoid tissue: changing requirements during the course of inflammation.," *The Journal of Immunology*, vol. 185, pp. 4873–4882, Oct. 2010.

[138] B. Jabri, N. P. de Serre, C. Cellier, K. Evans, C. Gache, C. Carvalho, J. F. Mougenot, M. Allez, R. Jian, P. Desreumaux, J. F. Colombel, C. Matuchansky, H. Cugnenc, M. Lopez-Botet, E. Vivier, A. Moretta, A. I. Roberts, E. C. Ebert, D. Guy-Grand, N. Brousse, J. Schmitz, and N. Cerf-Bensussan, "Selective expansion of intraepithelial lymphocytes expressing the HLA-E-specific natural killer receptor CD94 in celiac disease.," *Gastroenterology*, vol. 118, pp. 867–879, May 2000.

[139] A. D. Luster, R. Alon, and U. H. von Andrian, "Immune cell migration in inflammation: present and future therapeutic targets," *Nature Immunology*, vol. 6, pp. 1182–1190, Dec. 2005.

[140] B. S. Sheridan, P. A. Romagnoli, Q.-M. Pham, H.-H. Fu, F. Alonzo, W.-D. Schubert, N. E. Freitag, and L. Lefrançois, "$\gamma\delta$ T cells exhibit multifunctional and protective memory in intestinal tissues.," *Immunity*, vol. 39, pp. 184–195, July 2013.

[141] M. S. Davey, C. R. Willcox, A. T. Baker, S. Hunter, and B. E. Willcox, "Recasting Human Vδ1 Lymphocytes in an Adaptive Role.," *Trends in Immunology*, vol. 39, pp. 446–459, June 2018.

[142] J. G. Cyster and S. R. Schwab, "Sphingosine-1-phosphate and lymphocyte egress from lymphoid organs.," *Annual Review of Immunology*, vol. 30, pp. 69–94, 2012.

[143] P. Constant, F. Davodeau, M. A. Peyrat, Y. Poquet, G. Puzo, M. Bonneville, and J. J. Fournié, "Stimulation of human gamma delta T cells by nonpeptidic mycobacterial ligands.," *Science*, vol. 264, pp. 267–270, Apr. 1994.

[144] Y. Shen, D. Zhou, L. Qiu, X. Lai, M. Simon, L. Shen, Z. Kou, Q. Wang, L. Jiang, J. Estep, R. Hunt, M. Clagett, P. K. Sehgal, Y. Li, X. Zeng, C. T. Morita, M. B. Brenner, N. L. Letvin, and Z. W. Chen, "Adaptive immune response of Vgamma2Vdelta2+ T cells during mycobacterial infections.," *Science*, vol. 295, pp. 2255–2258, Mar. 2002.

[145] A. Rubio-Tapia, J. F. Ludvigsson, T. L. Brantner, J. A. Murray, and J. E. Everhart, "The prevalence of celiac disease in the United States.," *The American Journal of Gastroenterology*, vol. 107, pp. 1538–44– quiz 1537– 1545, Oct. 2012.

[146] J. Glanville, H. Huang, A. Nau, O. Hatton, L. E. Wagar, F. Rubelt, X. Ji, A. Han, S. M. Krams, C. Pettus, N. Haas, C. S. L. Arlehamn, A. Sette, S. D. Boyd, T. J. Scriba, O. M. Martinez, and M. M. Davis, "Identifying specificity groups in the T cell receptor repertoire.," *Nature*, vol. 547, pp. 94–98, July 2017.

[147] V. Groh, S. Bahram, S. Bauer, A. Herman, M. Beauchamp, and T. Spies, "Cell stress-regulated human major histocompatibility complex class I gene expressed in gastrointestinal epithelium.," *Proceedings of the National Academy of Sciences*, vol. 93, pp. 12445–12450, Oct. 1996.

[148] G. Terrazzano, M. Sica, C. Gianfrani, G. Mazzarella, F. Maurano, B. De Giulio, S. de Saint-Mezard, D. Zanzi, L. Maiuri, M. Londei, B. Jabri, R. Troncone, S. Auricchio, S. Zappacosta, and E. Carbone, "Gliadin regulates the NK-dendritic cell cross-talk by HLA-E surface stabilization.," *Journal of immunology (Baltimore, Md. : 1950)*, vol. 179, pp. 372–381, July 2007.

[149] Y. Huang, K. Mao, X. Chen, M.-A. Sun, T. Kawabe, W. Li, N. Usher, J. Zhu, J. F. Urban, W. E. Paul, and R. N. Germain, "S1P-dependent interorgan trafficking of group 2 innate lymphoid cells supports host defense.," *Science*, vol. 359, pp. 114–119, Jan. 2018.

[150] T. Worbs, U. Bode, S. Yan, M. W. Hoffmann, G. Hintzen, G. Bernhardt, R. Förster, and O. Pabst, "Oral tolerance originates in the intestinal immune system and relies on antigen carriage by dendritic cells," *Journal of Experimental Medicine*, vol. 203, pp. 519–527, Mar. 2006.